

Kalman Filter based Novel Centralized Dynamic
State Estimation in Multi-Machine Power System
Incorporating DFIGs

A Thesis Submitted to
Nirma University

In Partial Fulfillment of the Requirements for
The Degree of
Doctor of Philosophy

in
Technology and Engineering
by

Dishang D. Trivedi (11FTPHDE04)



Institute of Technology
Nirma University
Ahmedabad-382481
Gujarat, India
October 2017

Dedicated

To

Almighty

and

My family

Nirma University
Institute of Technology
Certificate

This is to certify that the thesis entitled "Kalman Filter based Novel Centralized Dynamic State Estimation in Multi-Machine Power System Incorporating DFIGs " has been prepared by Mr. Dishang D. Trivedi (11FTPHDE04) under my supervision and guidance. The thesis is his original work completed after careful research and investigation. The work of the thesis is of the standard expected of a candidate for Ph.D. Programme in Electrical Engineering and I recommend that it be sent for evaluation.

Date: 10/04/2018

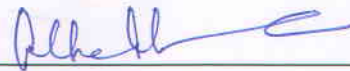


Prof.(Dr.) S. C. Vora
Research supervisor

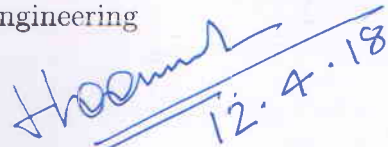
Forwarded By:



Prof.(Dr.) P. N. Tekwani
Head of the Department (EE)



Prof.(Dr.) Alka Mahajan
Dean, Faculty of Technology
and Engineering



Prof.(Dr.) D. A. Pujara
Dean, Faculty of Doctoral Studies
and Research

Executive Registrar

Abstract

The omnipresent, conventional synchronous generators are playing a pivotal role since many years to meet ever increasing demand of electrical energy. A steep growth in energy requirements is now met by power generation mix of fossil fuel based and renewable energy based generators. The stochastic nature of renewable generations, expanding power networks, complex interactions among the system components and loads etc. impose need for superior monitoring and control at power system level for its stable operation. For efficient operation and control of the power system, it is essential for the energy management system (EMS) operator to have an accurate information about every generator's dynamic states and power system behaviour.

Diminishing fossil fuels and environment concerns advocated nations to gradually adopt renewable energy sources. Wind energy, better on multiple aspects among other renewable options, is dominating today in the power networks. Among wind energy generators, doubly fed induction generators (DFIGs) are widely accepted due to its operational flexibility, small converter size, better power control and low cost. The parallel operation of DFIGs (or wind farm) with pervasive synchronous generators brings in enhanced system dynamics. This condition strongly dictates dynamic state estimation (DSE), not only to infer information about synchronous generators but concurrently know the states of wind generator(s). The performance of DFIGs also dependent on the converter control circuitry and its feedback loop. This thesis is the record of work that appropriately models the generators and the network, suitable for the adoption by the Kalman filter based algorithms to perform the DSE. With the help of the availability of centralized measurement data, the states of all the generators in the multi-machine system can be established simultaneously. Subsequently, the dynamic states of the DFIG are used for its rotor power control under specific conditions.

The synchronous generators, usually considered as a voltage source in the literature are presented by relevant state-space model for stability analysis. On the other hand, widely accepted DFIG based wind generator is presented as current source state-space model. As the models of both the generators are far apart, it is necessitated to bring both on the same platform. The thesis contains the work that shows the possibility of model unification of both kind of generators. Employing traditional DFIG current-source state model, a current-source state model of synchronous generators is proposed and validated using standard software platform. Highlighting feature of the proposed mathematical model is its applicability to power system with no limits on number of synchronous generators and DFIGs. Considering modelling intricacies, the use of these models is recommended to achieve concurrent DSE in a multi-machine power system. Employing current source models of synchronous generators and with substantial penetration of DFIG in multi-machine system, approach for concurrent DSE of synchronous generator and DFIG is presented. The mathematical model is simulated in MATLAB / Simulink platform for the validation. The power system dynamic conditions realized in the MATLAB / Simulink model are then treated as the data available from the phasor measurement units (PMUs) (with and without noise). This is used for the extended Kalman filter (EKF) and unscented Kalman filter (UKF) based DSE algorithms. Centralized dynamic state estimator based on EKF and UKF are employed for the faithful state predictions for all the generators under power system dynamic conditions and results are presented.

Application of dynamic states in real time is equally important to achieve better control and operation of DFIG. This apparatus, normally operate in hostile condition whether on-shore or off-shore, can undergo internal sensor erratic operation. Under such conditions, use of dynamic states obtained using EKF, is proposed to have error-free, continuous and smooth operation of DFIG. The results are embodied in the thesis. As an offshoot of main work, comparative performance of EKF and UKF with different PMU measurement data update rates under discontinuous measurement is analysed. Additionally, use of weighted least square estimation (WLSE) algorithm as an alternate to load flow under bad measurement condition is deliberated with results.

Nirma University Institute of Technology Declaration

I, Mr Dishang D. Trivedi, registered as full time Research Scholar, bearing Registration Number 11FTPHDE04 for Doctoral Programme under the Faculty of Technology and Engineering of Nirma University do hereby declare that I have completed the course work, pre-synopsis and my research work as prescribed under R. Ph. D. 3.5.

I do hereby declare that the thesis submitted is original and is the outcome of the independent investigations / research carried out by me and contains no plagiarism. The research is leading to the discovery of new techniques already known. This work has not been submitted by any other University or Body in quest of a degree, diploma or any other kind of academic award.

I do hereby further declare that the text, diagrams or any other material taken from other sources (including but not limited to books, journals and web) have been acknowledged, referred and cited to the best of my knowledge and understanding.

Date: 10/04/2018



Dishang D. Trivedi


Dr. S. C. Vasa
10/Apr/2018

Acknowledgements

I would like to take this opportunity to devote this research work on “Kalman Filter based Novel Approach for Centralized Dynamic State Estimation for Multi-Machine Power System Incorporating DFIGs ” to the Almighty, God, for providing me an opportunity and strength to pursue a Ph.D at Institute of Technology, Nirma University.

Inmost of my heart, I am obligated to my guide Prof.(Dr.) S. C. Vora, without his precious guidance, consistent support and continuous motivation this research work would not have been possible. His words of wisdom, valuable suggestions and constant endeavor for pushing towards perfection have helped me emphatically during my research. His attention to each detail, minute observations and suggested altercations while approaching problems has helped me greatly. I look forward to his continued valuable guidance in future.

I would like to express my sincere regards to Prof. Vivek Pandya, PDPU, Gandhinagar and Prof.(Dr.) P. N. Tekwani, Head of department, EE, IT,NU for their invaluable suggestions and useful feedback during Research Progress Committee meetings.

My sincere thanks to Prof.(Dr.) P. N. Tekwani as a Head of Department, Electrical Engineering Department, Institute of Technology, Nirma University and for all the support and giving freedom to do research independently in the department. I am gratified by the support from Dr. Ketan Kotecha, the then Director, IT, NU and Dr. Alka Mahajan, Director, IT, NU.

I am also thankful to office of Commissonerate of Technical Education(CTE), Gujarat state for giving me an opportunity to pursue my research at Electrical Engineering department, Institute of Technology, Nirma University.

With valuable support from Prof.(Dr.) M. C. Chudasama, Head of Electrical

Engineering department, L. D. College of Engineering, it becomes possible for me to reach at this juncture with no difficulties. My special thanks to him for his consistent support. I am grateful to all my colleagues of Electrical Engineering department, L. D. College of Engineering for their support. My gratitude to Dr. G. P. Vadodariya, Principal, L. D. College of Engineering for their inspiring support and co-operation during this journey.

My heartfelt thanks to Mr. Urmil B. Bhatt, then student, M. Tech. (EPS), EE, IT, NU for his contribution and precious support during this journey. I am thankful and feel indebted for his persistent help during research. Thanking a friend, Mr. Dhaval patel, then full time research scholar, EC Dept, IT, NU is a must for his support.

I am thankful to laboratory assistants of Electrical Engineering department, IT, NU Mr. Sajid Chouhan, Mr. Pratik Jani, Mr. Ghanshyam Patel and office assistant Mr. Ashish Gandhi for providing their timely support and help to complete technical and administrative tasks.

I am greatly thankful to Dr. A S Patel, Deputy Registrar, Nirma University and staff of ph.d. section Mrs. A. P. Prashya and Mr. Sachin Kikani for providing support and guidance during entire tenure of research.

My most sincere gratitude with high regards to Dinkerrai H. Trivedi, My Father and Shivangiben D. Trivedi, My utmost caring Mother for providing precious cornerstone at each stage of my life. Their persistent support and ethical values of life, they have inherited in me, helped me a lot to arrive at the final destination of one of the difficult journey of my life.

Finally, I want to thank my beloved wife Dhvani, for her eternal unconditional love, sacrifices, and support and also to my charmingly chaotic son Jayansh for gifting me moments which helped me to relax and regain strength for work. They both are the motivational force and inner core strength that helps me to stand firmly against ups and downs in past few years. I am also grateful to my sisters and my family members for their help during this journey.

Whole journey to this point was not an easy one. I thank all those mentioned and unmentioned, who have helped me, directly or indirectly on the way.

Dishang D. Trivedi
(11F7PHDE04)

Contents

Certificate	iv
Declaration	v
Abstract	vi
Acknowledgements	viii
List of Tables	xiii
List of Figures	xiv
Nomenclature and Abbreviations	xvii
1 Introduction	1
1.1 Dynamic state estimation in power system	2
1.2 Literature review	5
1.3 Motivation	12
1.4 Contribution of thesis	14
1.5 Outline of thesis	15
2 Coalesced Model of Synchronous Generator and DFIG	17
2.1 Introduction	17
2.2 Aspects of modelling	18
2.3 Simulation aspects for model validation	20
2.4 Discussion	24
2.4.1 State - space model as DFIG (base model)	24
2.4.2 State - space model as SG	25
2.5 Conclusions	26
3 Kalman Filters based Centralized Concurrent DSE	27
3.1 EKF based Centralized Concurrent Dynamic State Estimation in Multi-machine Power System	27
3.1.1 Intoduction	27
3.1.2 State-space current source models for EKF implementation	29
3.1.3 Case studies	40
3.2 UKF based centralized concurrent DSE of multi-machine system	47
3.2.1 UKF as a DSE tool	47
3.2.2 Simulation preliminaries	48

3.2.3	Simulation results and discussion	49
3.3	Observations on comparative performance of EKF and UKF	52
3.4	Conclusions	56
4	Application of EKF based DSE for DFIG under Faulty Current Sensor Measurements	58
4.1	Introduction	58
4.2	Mathematical Approach for DSE of DFIG	59
4.3	EKF implementation for DFIG	62
4.3.1	Discrete model of DFIG for EKF implementation	62
4.3.2	Simulation preliminaries and DSE of DFIG using EKF	63
4.4	Case studies and discussions	65
4.4.1	Case I: Current sensor measurement with noise	65
4.4.2	Case II: Current sensor measurement with outliers	68
4.4.3	Case III: Measurement unavailability due to current sensor failure	74
4.5	Conclusions	77
5	Conclusions	79
5.1	Future Scope	82
	Appendices	84
A	Comparative Analysis of EKF and UKF with Multiple Measurement Update Rate during Intermittent Measurement	84
A.1	Introduction	84
A.2	Test systems and simulations preliminaries	86
A.2.1	State representation and measurement aspects	86
A.2.2	Simulated anomalous measurement conditions	88
A.3	Case studies	89
A.3.1	Complete loss of measurement data	89
A.3.2	Partial loss of measurement data	92
A.4	Discussion	94
A.4.1	Case I – WSCC test system	94
A.4.2	Case II – IEEE 14 bus test system	96
A.5	Conclusions	97
B	WLSE Assisted Load Flow under Bad Measurement Conditions	99
B.1	Introduction	99
B.2	Brief on WLSE and bad data detection	100
B.2.1	Method of WLSE for static state estimation	101
B.2.2	Bad data detection	102
B.3	Case study	103
B.4	Results and discussion	104
B.5	Conclusion	106
C	Extended Kalman Filter(EKF) Algorithm	108
D	Unscented Kalman Filter (UKF) Algorithm	111

E Improved Coalesced Model of Synchronous Generator and DFIG	114
List of publications	118
Works Cited	120

List of Tables

2.1	Quantities to be considered for realization of different machines	26
3.1	Comparison of RMSE for EKF and UKF	53
3.2	Comparison of estimation time	55
3.3	Comparison of convergence time with different % of initialization error	56
A.1	Summary of anomalous measurement conditions for both test systems for all three measurement update rates (50 sa/s, 33 sa/s and 25 sa/s)	88
A.2	Comparison of EKF and UKF based estimators' performance for three measurement data unavailable conditions and measurement update time intervals	97
B.1	Results of WLSE and Load flow under without bad measurements . .	105
B.2	Comparative results of WLSE and Load flow under static condition when P_2 is corrupted with 0.37 p.u. of error	106
B.3	Comparative results of WLSE and Load flow under static condition when Q_6 is corrupted with 0.2 p.u. of error	107

List of Figures

2.1	DFIG connected to infinite bus (source : internet)	20
2.2	Current states i_{abc} under steady state (pre-fault) and dynamic condition (during fault) obtained using PSCAD model and proposed model respectively, for (a, b) DFIG, (c, d) SG	21
2.3	Variation of DFIG's different variables <i>viz.</i> v_{qs} , v_{dr} , P_{dfig} and Q_{dfig} under steady state (pre-fault) and dynamic condition (during fault) obtained using PSCAD model and proposed model respectively	23
2.4	Variation of SG's different variables <i>viz.</i> v_{qs} , v_{fd} , P_{sg} and Q_{sg} under steady state (pre-fault) and dynamic condition (during fault) obtained using PSCAD model and Proposed model respectively	24
3.1	WSCC 3-generator 9-bus test system, where synchronous gen. #2 is replaced with equally rated DFIG based wind farm	32
3.2	DFIG integrated with rest of WSCC 3-gen. 9-bus test system	37
3.3	Block diagram of MATLAB/Simulink implementation of WSCC system with DFIG	38
3.4	Implementation of WSCC with DFIG system in PSCAD/EMTDC	39
3.5	Currents i_{abc_1} , i_{abc_2} and i_{abc_3} under steady state and dynamic condition obtained using MATLAB model and PSCAD model for (a, b) synchronous generator #1, (c, d) DFIG and (e, f) synchronous generator #3	40
3.6	Active and reactive power measurements with 1% SD Gaussian noise	41
3.7	Actual and estimated i_{ds_1} under steady-state and transient condition for synchronous generator #1 showing initial convergence of estimation algorithm	42
3.8	Actual and estimated i_{qs_1} , i_{fd_1} , i_{D_1} under steady-state and transient condition for synchronous generator # 1	43
3.9	Actual and estimated i_{ds_2} , i_{qs_2} , i_{dr_2} , i_{qr_2} under steady-state and fault condition for DFIG	43
3.10	Actual and estimated i_{ds_3} , i_{qs_3} , i_{fd_3} , i_{D_3} under steady-state and fault condition for synchronous generator #3	44
3.11	WSCC 3-generator 9-bus system in steady state with sudden 50% reduction in output active power of DFIG wind farm	45
3.12	Swing generator #1 current states - actual and estimated, due to output active power reduction in DFIG	46
3.13	DFIG current states - actual and estimated, due to output active power reduction in DFIG	46

3.14	Synchronous generator #3 current states - actual and estimated, due to output active power reduction in DFIG	47
3.15	WSCC three-generator nine-bus test system, where synchronous gen. #2 is replaced with equally rated DFIG based wind farm	49
3.16	Actual and estimated i_{ds1} under steady-state and transient condition for synchronous generator #1 showing initial convergence of estimation algorithm	50
3.17	Actual and estimated i_{qs1}, i_{fd1}, i_{D1} under steady-state and transient condition for synchronous generator#1	50
3.18	Actual and estimated $i_{ds2}, i_{qs2}, i_{dr2}, i_{qr2}$ under steady-state and fault condition for DFIG	51
3.19	Actual and estimated $i_{ds3}, i_{qs3}, i_{fd3}, i_{D3}$ under steady-state and fault condition for synchronous generator #3	51
4.1	Rotor side converter (RSC) control circuit for DPC	60
4.2	(a) Change in output active and (b) change in output reactive power, under dynamic condition	64
4.3	(a) Active power and (b) reactive power, with and without noise	64
4.4	(a) i_{ds} actual and i_{ds-est} estimated using EKF algorithm (b) i_{qs} actual and i_{qs-est} estimated using EKF algorithm	65
4.5	(a) i_{dr} actual and i_{dr-est} estimated using EKF algorithm (b) i_{qr} actual and i_{qr-est} estimated using EKF algorithm	66
4.6	(a) Effect of noise on i_{dr} (b) noisy i_{dr} is replaced with i_{dr-est}	66
4.7	(a) Effect of noise on i_{qr} (b) noisy i_{qr} is replaced with i_{qr-est}	67
4.8	a) Effect of noisy i_{dr} and i_{qr} on P_r (b) P_r after noisy currents replaced with i_{dr-est} and i_{qr-est}	68
4.9	(a) Effect of noisy i_{dr} and i_{qr} on Q_r (b) Q_r after noisy currents replaced with i_{dr-est} and i_{qr-est}	69
4.10	(a) Effect of outliers on i_{dr} (b) i_{dr} with outliers replaced with i_{dr-est}	69
4.11	(a) Effect of outliers on i_{qr} (b) i_{qr} with outliers replaced with i_{qr-est}	70
4.12	(a)-(b) Effect of i_{dr} and i_{qr} having outliers on P_r and Q_r , (c)-(d) P_r and Q_r after measurement with outliers replaced with i_{dr-est} and i_{qr-est}	70
4.13	(a)-(b) Effect of i_{dr} and i_{qr} having outliers on P and Q , (c)-(d) P and Q after measurement with outliers replaced with i_{dr-est} and i_{qr-est}	72
4.14	(a) Effect of outliers during dynamic condition on i_{dr} (b) i_{dr} with outliers replaced with i_{dr-est}	72
4.15	(a) Effect of outliers during dynamic condition on i_{qr} (b) i_{qr} with outliers replaced with i_{qr-est}	73
4.16	(a)-(b) Effect of i_{dr} and i_{qr} having outliers on P_r and Q_r , (c)-(d) P_r and Q_r after measurement with outliers replaced with i_{dr-est} and i_{qr-est}	74
4.17	(a)-(b) i_{dr} and i_{qr} measurement unavailability for 0.5 s and 1.4 s duration, (c)-(d) i_{dr} and i_{qr} when unavailable measurements are replaced with i_{dr-est} and i_{qr-est}	75
4.18	Flowchart showing application of DSE under measurement data unavailability	75
4.19	(a)-(b) P_r and Q_r measurement unavailability for 0.5 s and 1.4 s duration, (c)-(d) P_r and Q_r when unavailable measurements are replaced with i_{dr-est} and i_{qr-est}	76

A.1	WSCC- three generator nine bus test system (Anderson and Fouad).	89
A.2	Performance of EKF and UKF in estimation of variations in speed of generator 2 (ω_2) (WSCC system), measurement update interval of 0.02 s and all measurements missing for (a) 3 cycles, (b) 4 cycles and (c) 5 cycles duration	90
A.3	Performance of EKF and UKF in estimation of variations in speed of generator 2 (ω_2) (WSCC system), measurement update interval of 0.03 s and all measurements missing for (a) 3 cycles, (b) 4 cycles and (c) 5 cycles duration	91
A.4	Performance of EKF and UKF in estimation of variations in speed of generator 2 (ω_2) (WSCC system), measurement update interval of 0.04 s and all measurements missing for (a) 3 cycles, (b) 4 cycles and (c) 5 cycles duration	91
A.5	IEEE 14 bus test system (courtesy: internet source).	92
A.6	Performance of EKF and UKF in estimation of variations in speed of generator 2 (ω_2) (IEEE 14 bus system), measurement update interval of 0.02 s and all measurements missing for (a) 3 cycles, (b) 4 cycles and (c) 5 cycles duration	93
A.7	Performance of EKF and UKF in estimation of variations in speed of generator 2 (ω_2) (IEEE 14 bus system), measurement update interval of 0.03 s and all measurements missing for (a) 3 cycles, (b) 4 cycles and (c) 5 cycles duration	93
A.8	Performance of EKF and UKF in estimation of variations in speed of generator 2 (ω_2) (IEEE 14 bus system), measurement update interval of 0.04 s and all measurements missing for (a) 3 cycles, (b) 4 cycles and (c) 5 cycles duration	94
A.9	Performance of EKF and UKF in estimation of variations in speed of generator 2 (ω_2) (WSCC system), measurement update interval of 0.02 s and two measurements missing for (a) 3 cycles, (b) 4 cycles and (c) 5 cycles duration	95
A.10	Performance of EKF and UKF in estimation of variations in speed of generator 2 (ω_2) (IEEE 14 bus system), measurement update interval of 0.02 s and two measurements missing for (a) 3 cycles, (b) 4 cycles and (c) 5 cycles duration	95
B.1	Algorithm for WLSE backed load flow	104
E.1	Instantaneous currents of DFIG (Gen.# 2) (a)–(b) i_{abc} , (b)–(c) stator direct axis current– i_{ds} , (c)–(d) stator quadrature axis current – i_{qs}	115
E.2	WSCC 3-gen. 9-bus system with SG (Gen. #2) on PSCAD/EMTDC platform	116
E.3	Instantaneous currents of SG (Gen.# 2) (a)–(b) i_{abc} , (b)–(c) stator direct axis current– i_{ds} , (c)–(d) stator quadrature axis current – i_{qs}	116

Nomenclature and Abbreviations

Nomenclature

v_s, v_r	Stator and rotor voltage
i_s, i_r	Stator and rotor current
v_{fd}, i_{fd}	Field winding voltage and current of synchronous generator
V_D, i_D	Damper winding voltage and current of synchronous generator
i_{ds}, i_{qs}	Direct and quadrature axis stator currents
i_{dr}, i_{qr}	Direct and quadrature axis rotor currents
v_{ds}, v_{qs}	Direct and quadrature axis stator voltages
v_{dr}, v_{qr}	Direct and quadrature axis rotor voltages
λ	Stator or rotor flux linkage
R_s, R_r	Stator and rotor resistance
L_s, L_r, L_m	Stator, rotor and magnetizing inductance
ω_s, ω_r	Synchronous speed and rotor speed
P_s, Q_s	Stator active and reactive power
P_r, Q_r	Rotor active and reactive power
P	Output active power
Q	Output reactive power
$\hat{i}_{dr}^+ = i_{dr-est}$	Estimated i_{dr}
$\hat{i}_{qr}^+ = i_{qr-est}$	Estimated i_{qr}
P_{r-est}, Q_{r-est}	Estimated rotor active and reactive power

Subscripts

d	Synchronous frame direct axis component
q	Synchronous frame quadrature axis component

Superscripts

$-$	<i>Priori</i>
$+$	<i>Posteriori</i>
$\hat{}$	<i>Estimated signal</i>
$*$	Reference signal

Abbreviations

SSE	Static state estimation
DSE	Dynamic State Estimation
PMU	Phasor measurement unit
EKF	Extended Kalman filter
UKF	Unscented Kalman filter
WLSE	Weighted least square error
WSCC	Western system coordination council
DFIG	Doubly fed induction generator

SG	Synchronous generator
GSC	Grid side converter
RSC	Rotor side converter
RTU	Remote terminal unit
SCADA	Supervisory control and data acquisition
PCC	Point of common coupling
SMIB	Single machine infinite bus
UT	Unscented transform
RMSE	Root mean square error
MPPT	Maximum power point tracking
LVRT	Low voltage ride through
SD	Standard deviation
FRT	Fault ride through

Chapter 1

Introduction

Consistently increasing demand of energy has pushed power networks to operate nearly close to their transmission and generation threshold limits. To meet ever increasing demand of energy, power networks have undergone manifold expansion in past decades. Geographically widespread power system requires elaborated specifications, complex modelling, and multiple tools to evaluate performance parameters, system stability, reliability etc. The time and frequency domain analysis, mathematical tools and techniques, are the key to offer insights in the behaviour of the system. Power system stability during and after network disturbances, at present, is monitored by SCADA and technologically enhanced tool like PMUs. These tools provide situational awareness, which is then supported with local and global power grid controllers.

Erstwhile approach to obtain steady state analysis of power network was to employ load flow studies. It becomes ineffective with exponential increase in complexity and operational aspects of network. Apart from higher derivative efforts due to enlarged power network, delay in measurement availability using RTUs has also contributed substantially for increased time consumed by load flow calculation. Hence, during process of load flow calculation, which provides useful information regarding present state of power network, assumption of quasi-static nature of power system is a precondition. The SSE using Static state estimators, based on least square estimation etc., offered an advantage of providing information about important states, which can be similar to load flow results. For static state estimation, measurements data are collected through RTUs, which is an important component of SCADA structure.

For large systems, due to slow measurement update rates of RTUs, it became very difficult for static state estimator to offer information regarding fast changing power system dynamics.

These conditions made it imperative to have knowledge of critical states of power network in real time i.e. with changing dynamics. Consideration of ‘quasi-static-ness’ of power network becomes obsolete in such conditions. Maintaining stability and reliability of power network, under increased fast changing dynamics, warrants for faster and accurate monitoring and control, not available using SSE. The DSE emerges as the need of the hour. For the DSE, fast and accurate measurements are prerequisites and these become feasible due to technological advancements in measurement and communication technology like PMU and faster communication protocols.

Moreover, slackening of fossil fuels and environmental constraints encourages for more and more inclusion of renewable energy sources. Over the past few years, there is a rise in generation mix (i.e. of conventional and renewable) to fulfill the demand. Benefit of clean energy from renewable energy has come with disadvantages of its stochastic nature, which further increases system complexity and dynamics of power network. Such expanding power networks incorporate more generation - load dynamics. Already needed DSE to capture the dynamics of power network equipped with conventional power sources, it is now much sought after due to integration of renewable energy sources. Hence, it becomes essential to have DSE that can simultaneously provide information regarding crucial states of ubiquitous conventional generators and rapidly penetrating renewable energy sources. Prior information regarding dynamic states of conventional and renewable generators may be helpful to EMS operator to achieve rapid monitoring and control in power network.

1.1 Dynamic state estimation in power system

Focussing on the comprehensive discussion on state estimation, an immediate classification indicates ‘Static’ and ‘Dynamic’ state estimation. The SSE plays a pivotal role in power system as a back-up to load flow and offer initial information for power system security assessment. LSE and its variant WLSE are the popular tools for SSE.

Consequently, need of DSE arose which can provide real time information of

crucial dynamic states and their future trends to power system operator.

Pre-requisite for DSE of power system is systematic mathematical modelling of highly complex and non-linear power system including that of various power system components. Power system mathematical representation is inherently non-linear in nature, requires DSE tools which can incorporate these non-linearities. Apart from that, DSE tool must be capable enough to provide accurate dynamic state estimates of power system at rapid rate to EMS operator. For DSE to be performed at high rate, it becomes imperative to provide measurements to DSE tool at much faster rate. Conventional SCADA system provides measurements to EMS operator at electrically long time interval. Obtaining measurement at slow rate fails to capture fast changing dynamics of power system which lasts only for few cycles. Measurement availability to dynamic state estimator at slower rate does not allow for DSE and hence, difficulty in implementing DSE based analysis and protection.

With practical implementation of PMU in early 90s, the concept of fast and accurate measurement availability is materialized. PMUs supported with a Global Positioning System (GPS) reference clock can provide the needed high-speed synchronized sampling with $1 \mu\text{s}$ accuracy. PMUs using multiple time sources, including non-GPS references used coherently calibrated and working group, can give data rates up to 120 samples/s and above. The availability of measurement data from PMUs opens new era of possibilities of DSE for widely spread power system.

Since the conceptualization of power system state estimation in 1970 to till date voluminous approaches have been adopted by researchers to obtain information regarding crucial states under the dynamic condition. Kalman filter based tool *viz.* EKF, which works on the principle of linearization (using Jacobian matrices), has emerged as a prominent tool for DSE implementation. EKF has been used comprehensively on large scale to achieve accurate DSE of different states, incorporating expedient mathematical modelling, for multi-synchronous-machine power systems (Ghahremani and Kamwa, “Dynamic State Estimation in Power System by Applying the Extended Kalman Filter With Unknown Inputs to Phasor Measurements” “Local and Wide-Area PMU-Based Decentralized Dynamic State Estimation in Multi-Machine Power Systems” Huang, Schneider, and Nieplocha Bila Tebianian and Jeyasurya). The usage of EKF has been proposed to achieve accurate estimation of syn-

chronous generators' states and parameters. The usage of EKF is further extended for parameter calibration. Furthermore, application of EKF is suggested to alleviate the problem of bad data in measurements. With widespread acceptance of EKF for DSE in power system, some of constraints also emerges *viz.* linearization error for highly non-linear system and more calculation time in achieving estimates for large power systems. Hence, the new approach based on Kalman filter is proposed which is UKF. UKF used UT for state prediction and so eliminating the need of jacobian calculation as well as linearization error. Many researcher have successfully implemented UKF to obtain DSE for dynamic states of large multi-synchronous-machine power system (Valverde and Terzija Wang, Gao, and Meliopoulos). Performance of UKF has been investigated with high noise content in measurement data as well as for other anomalous measurement conditions and its responses are fine. At the same time, UKF suffers constraint of higher calculation time for reasonably small system as compared to EKF. However, area of comparative performance of EKF and UKF under intermittent measurement condition along with different measurement data update rate suggests space to explore.

Among all renewable energy sources, wind energy is one of the widely accepted energy source. Wind energy technology has observed considerable technological advancements *viz.* fixed speed induction generator to variable speed induction generator to full rated converter (FRC) supported induction / synchronous generators. DFIG has received wider acceptance in recent times due to its capability to operate in wide speed range, lower rating of power electronic converters and flexibility of power control in all four quadrants.

Large penetration of wind energy sources, especially DFIGs, warrants for information regarding variations in its dynamic states to an EMS operator for ingenious system monitoring, protection as well as corrective controls. Hence, DSE of DFIG assumes a great significance. Using EKF as a DSE tool and employing comprehensive state-space model, accurate dynamic states are achieved for DFIG based SMIB under steady state and dynamic conditions (Bourdoulis and Alexandridis Shahriari et al.). For large multi-machine system, comprising of conventional SGs and DFIGs, productive state estimation for dynamic states of only DFIG is described in literature (S. Yu, "Realization of State-Estimation-Based DFIG Wind Turbine Control Design in

Hybrid Power Systems Using Stochastic Filtering Approaches” S. Yu, “State Estimation of Doubly Fed Induction Generator Wind Turbine in Complex Power Systems”). The rapidly increasing penetration of DFIGs results in its parallel operation with conventional SGs and hence, necessitates defining integrated mathematical model. Such integrated model can be implemented for concurrent DSE of all types of generators by centralized dynamic state estimator. Simultaneous availability of dynamic states can open up new dimensions of wide grid monitoring and control of conventional and renewable energy sources.

After obtaining information regarding dynamic states of all the types of energy sources, it becomes essential to utilize these for a control operation. On-shore and off-shore hostile working environment of DFIGs can cause possibility of erroneous operation of reasonably sensitive internal sensors *viz.* current, voltage and speed sensors. It becomes worthy to explore domain of application of DSE, under erroneous sensor output conditions, replacing the estimated outcome for improved operation.

1.2 Literature review

The power system state estimation equips user with the intricate details of the system and its component states - measurable and non-measurable. The investigations related to state estimation has been explored on various dimensions - on issues in estimation, modelling requirements, tools for estimation, practicability of the estimated states and its applications. The static and dynamic state estimations offer judgement on system trends, behaviour and intuitive idea of stability. For a vast electrical grid involving multi-machines and dynamic loads, at present there is no immediate substitute to state estimation.

F. C. Schweppe *et. al.* first introduced the concept of power system state estimation (SE) and employed WLSE technique to obtain power system static states (Schweppe and Wildes). Initially SE was used to achieve power system states *viz.* voltage magnitudes and bus angles. Application of SE is then proposed for different power system operations like network contingency analysis and security enhancement (Schweppe and Rom Schweppe). In same era, real time tracking of states in power system using dynamic state estimator was proposed by (Debs and Larson) in 1970. Considering quasi-static nature, model of power system is proposed and faithful

tracking of states is presented using real time measurement in (Debs and Larson). A variable-dimension and stage-invariant Kalman filter based approach to estimate flux linkages of field and amortisseur windings of the synchronous generators is presented in (Miller and Lewis). Currents and voltages of field and armature with rotor angles of each generator are taken as measurements for successful state estimation (Miller and Lewis). Nishiya *et.al.* presented a Kalman filter algorithm based DSE. The paper shows the estimation of bus voltages and angles, which takes care of anomalies in bad data, change in network topology as well as sudden variation in states of network (Nishiya, Hasegawa, and Koike). Novel algorithm for real-time forecasting and filtering the state vector using exponential smoothing and least-square estimation technique is presented in (da Silva, Filho, and de Queiroz) and its performance is compared with Kalman filtering technique. DSE using EKF for the system having nonlinear measurement functions is discussed in (Mandal, Sinha, and Roy). Mandal *et. al* proposed hierarchical scheme for dynamic estimation (HSDE), in which dynamic state estimation of large system is done by creating small subsystems (through partitioning of large system). It leads to DSE of large system imbibing non-linearities of measurement functions (Sinha and Mandal). Comparative analysis of different techniques in estimating a significant parameter of power system *i.e.* frequency is investigated in (Subudhi et al.).

Primary requirement to obtain DSE in power system is faster and accurate measurements. With the implementations of PMUs, it has become possible for system operator to avail measurement at faster rate and with higher accuracy than conventional RTUs. The PMU enables the estimation of dynamic states in real time, based on wide area measurement, due to synchronized sampling at higher rates. PMU with typical sampling rate of ten through 120 samples/s, synchronized with the GPS clock, offers consistent capturing of power system measurements under normal and abnormal conditions (Zhou et al.). Reviewing impact of PMU usage on DSE algorithm's performance starts with the fact that measurement data accuracy as well as measurement data update rate are important factors for DSE. Inclusion of PMUs as a measurement tool, in addition to SCADA, show improvements in state estimation algorithms' performance and capabilities (Jain and Shivakumar, "Impact of PMU in dynamic state estimation of power systems" "Power system tracking and dynamic

state estimation”). Kalman filter based estimator is applied for multi-area angle and frequency estimation using PMU measurements in (Vahidnia et al.). In a large system, small areas are formed by group of coherent generators in (Vahidnia et al.). State estimation co-ordinated with load forecasting using Kalman filtering and discretized mathematical model is presented in (Blood, Krogh, and Ilic). Using mixed integer programming and PMU assisted measurements DSE estimation approach is proposed in (Aminifar et al.). It proposes simultaneous operation of discarding erroneous predicted values and offering accurate DSE of multi-machine systems under dynamic conditions (Aminifar et al.).

In recent times, EKF algorithm has emerged as one of widely used tools for DSE in power system (Simon). Using model decoupling, PMU data (real power, reactive power, bus voltage and angle) are treated as inputs as well as measurements alternatively. Real time EKF based estimation of synchronous generator’s dynamic states as well as estimation of generator’s parameters (i.e. mechanical power, transient reactance, moment of inertia and damping factor) is presented in (Fan and Wehbe). Real time estimation using Robust EKF (REKF) method, which has better performance than EKF, is proposed for estimation of harmonic states of power system by (Kumar, Das, and Sharma). With lesser number of measurements than EKF, REKF is shown to estimate states better under bad data condition in IEEE-14 bus system (Kumar, Das, and Sharma). For single-machine-infinite-Bus (SMIB) system and WSCC 3-generator 9-bus test system, performance of EKF based estimator under the conditions of sudden load change and three phase-to-ground fault is analyzed with anomalous measurement conditions in (Huang, Schneider, and Nieplocha). Improved EKF using second order Euler method for EKF with multi-step prediction is offered and its performance in case of topological error, parametric error and composite error has been demonstrated with measurement update interval of 0.04s using 16-machine 68-bus system in (Huang et al., “Estimating power system dynamic states using extended Kalman Filter”).

It was Huang *et. al.* (“Estimating power system dynamic states using extended Kalman Filter”) to suggest possibility of analyzing performance of EKF in case of measurement data unavailability. To estimate dynamic states of a single-machine infinite bus (SMIB) system, Ghahremani and Kamwa showed the use of EKF algorithm

to simultaneously estimate the synchronous generator (SG) states and unknown inputs using EKF-UI approach (Ghahremani and Kamwa, “Dynamic State Estimation in Power System by Applying the Extended Kalman Filter With Unknown Inputs to Phasor Measurements”). Using simulation results from POWERWORLD simulator platform, EKF based dynamic state estimation for dynamic states of synchronous generators *viz.* δ , ω , E'_d and E'_q is presented using WSCC 3-generator 9-bus system in (Tebianian and Jeyasurya). Possible application of dynamic states to activate turbine governor control is discussed in (Tebianian and Jeyasurya). Generator dynamic models are validated using disturbance recorded as PMU data is proposed in (Huang et al., “Generator dynamic model validation and parameter calibration using phasor measurements at the point of connection”). Proposed method uses EKF method for automatic parameter calibration by sensing change is estimated and actual parameters (“Generator dynamic model validation and parameter calibration using phasor measurements at the point of connection”). In (Deshmukh, Natarajan, and Pahwa), performance of EKF is deliberated in terms of error alongwith missing measurement representation as communication packet drops. In (Deshmukh, Natarajan, and Pahwa) estimated state error depends on boundedness of state error covariance matrix and initial estimation error. For different standard multi-machine systems, using local measurements *viz.* active power, reactive power, voltage phasor and frequency, EKF and EKF-UI approach are presented to realize wide area power system stabilizer (WA-PSS) and system integrated protection scheme (SIPS) (Ghahremani and Kamwa, “Local and Wide-Area PMU-Based Decentralized Dynamic State Estimation in Multi-Machine Power Systems”).

For application to large power system, EKF has some drawbacks like higher computation time due to Jacobian calculation and more suitability to linear system due to propagating linearization error (Julier, Uhlmann, and Durrant-Whyte). UKF based DSE using unscented transform (UT) is proposed and its application and advantages over EKF are well illustrated in literature (Julier, Uhlmann, and Durrant-Whyte). UKF’s application for estimation of power (i.e. active and reactive power, apparent power, power factor) and frequency using instantaneous power as an input signal to algorithm is discussed in (Valverde and Terzija). Successful estimation of round rotor and salient pole rotor synchronous generators’ parameters and states

with novel square root unscented Kalman filter (SRUKF) approach is discussed in (Huang, Li, and Yan). Approach of UKF for DSE in standard multi-machine power systems *viz.* WSCC 3-generator 9-bus system and IEEE 14-bus system is presented in (Wang, Gao, and Meliopoulos) under steady and transient conditions. UKF based de-centralized DSE is offered using local measurements from PMUs (Singh and Pal). Collection of measurements locally makes estimation procedure fast, accurate and easy to implement (Singh and Pal). DSE at distribution network level, with integration of renewable energy, is described in (Nguyen et al.). The performance of UKF is investigated at 18-bus distribution network level and validated with real time digital simulator (RTDS) platform (Nguyen et al.). Performance of Kalman filter based algorithms (EKF and UKF) heavily depends on quality of measurement data e.g. content and nature of noise in measurement (Huang, Schneider, and Nieplocha Valverde and Terzija S. Yu, “Realization of State-Estimation-Based DFIG Wind Turbine Control Design in Hybrid Power Systems Using Stochastic Filtering Approaches” S. Yu, “State Estimation of Doubly Fed Induction Generator Wind Turbine in Complex Power Systems”) and availability of measurement data e.g. discontinuity in measurement and measurement data update rate (Huang, Schneider, and Nieplocha). Hence, it becomes important to analyze performance of EKF and UKF in anomalous measurement conditions with various measurement data update rates.

The power generation, mix of fossil fuel based and renewable power sources is the reality today. The stochastic nature of renewable generations imposes need for superior monitoring at system level for the stable operation of grid. Increasing penetration of wind power to conventional power system has raised concerns regarding aspects of power system e.g. system frequency and inertia control, reactive power contributions, system stability etc. (Singh and Singh). In such and other conditions, for efficient operation and control of a power system, it is essential for EMS operator to have an accurate information about every machine’s dynamic states. On-shore and off-shore wind generation is one of the major renewable penetrating segment. Among various types of wind generators, DFIGs are gaining popularity due to high energy efficiency, low mechanical stress on the wind turbine, relatively low power rating of converters and flexible control of power (Feijo, Cidrs, and Carrillo). Reason for increasing avenues of research in DSE for DFIG states is its highly nonlinear

model, involving complex equivalent circuit and existence of converters along with their controllers (Khedher, Khemiri, and Mimouni). With the increasing presence of DFIG, its modelling and DSE become imperative. The performance of 3rd order and 5th order state-space model of DFIG under dynamic, transient condition is elaborated for SMIB system in (Ekanayake, Holdsworth, and Jenkins). Mathematical models of DFIG with different control strategies are presented in (Mishra et al. Wu et al., “Small signal stability analysis and optimal control of a wind turbine with doubly fed induction generator” “Decentralized Nonlinear Control of Wind Turbine With Doubly Fed Induction Generator” Abdelhafidh et al.). Eigenvalue sensitivity analysis and its impact on FRT capability of DFIG can be found in (Yang et al., “Oscillatory Stability and Eigenvalue Sensitivity Analysis of A DFIG Wind Turbine System” “Advanced Control Strategy of DFIG Wind Turbines for Power System Fault Ride Through”). Transient current analysis for DFIG based SMIB system is performed in (Senjyu et al.). Equations are derived for induction generator before and during fault conditions, and dependence of short circuit current on phase angle, at the occurrence of fault, is also explained in (Senjyu et al.). Transient model of DFIG, considering rotor dynamics, shows significant role of rotor converter for DPC control in (Kim, Moon, and Nam) and the results are compared with the simulation. Nature of variation of DFIG currents is explained using MATLAB/Simulink model in (Kim, Moon, and Nam). Comparative analysis of different state-space models of DFIG is proposed in (Jiang et al.). State-space model of DFIG comprised of modelling of all elements *viz.* drive mass train, pitch controller, rotor side controller, grid side controller and induction generator is presented and compared with other available models in (Jiang et al.). State-space modelling approach suitable for variable and fixed speed induction generators is presented in (Ugalde-Loo, Ekanayake, and Jenkins) and its eigenvalues are derived. Using motoring conventions for operation, proposed model’s performance is shown to meet grid code requirements. (Ugalde-Loo, Ekanayake, and Jenkins). Instead of conventional stator flux oriented control, DFIG model is presented for direct power control using non-linear detailed model in (Bourdoulis and Alexandridis). The direct power control offers independence from flux measurement. With the help of state space model of DFIG with reference to stationary axis *viz.* α and β , DSE of stator and rotor current i_α and i_β , rotor speed ω_r and its position, θ with augmented

integrals of i_α and i_β is conceptualized using EKF for SMIB system in (Malakar, Tripathy, and Krishnaswamy).

Application of EKF for DSE of DFIG using 15th order detailed non-linear model is comprehensively presented in (Shahriari et al.). Robustness of EKF algorithm, for DFIG based SMIB system, is verified under the conditions of wind velocity variations, different measurement noises and 3-phase-to-ground short circuit condition. It is to be noted that for checking the robustness, the measurements are obtained using PMU (Shahriari et al.). Estimation of states of DFIG *viz.* $i_{dr}, i_{qr}, i_{ds}, i_{qs}, \omega_r$ and a parameter J (moment of inertia) using ensemble Kalman filter (EnKF) is described in (Fan et al.). Fan et. al. gave insight to parameter calibration along with estimation of parameter (Fan et al.). Application of EKF for estimation of parameters of DFIG *viz.* stator and rotor resistances, leakage and mutual inductances, is proposed in (Abdelrahem, Hackl, and Kennel).

Sensitivity of EnKF algorithm to different measurement noise levels, initial state and parametric errors are discussed in (Fan et al.). Comparative analysis of particle filter (PF), EKF and UKF based dynamic state estimator along with bad data detection algorithm are proposed in (S. Yu, “Realization of State-Estimation-Based DFIG Wind Turbine Control Design in Hybrid Power Systems Using Stochastic Filtering Approaches” S. Yu, “State Estimation of Doubly Fed Induction Generator Wind Turbine in Complex Power Systems”) for DFIG states. For such estimation, measurement data are understood to be available using local PMU. The literature reviewed thus far, presents the DSE either for synchronous machine or for the asynchronous machine, but not both at a time. Hence, it is desirable to have mathematical model of generators *viz.* conventional and renewable, using which an EMS operator establish dynamic states of all type of generators.

Widely used DFIG’s complex operation is mainly controlled by back-to-back converters and supported by sensor and control circuitry. Performance of DFIG largely depends on condition of network to which it is connected, as well as on faithful operation of its own internal elements *viz.* back-to-back converters, voltage, current and speed measurement devices. Hence, it becomes imperative to analyze effect of faulty operation of sensors and/or control circuitry on operation of DFIG. Check on possibility to utilize DSE under such faulty condition will be an archetype. Solution

to fault in internal circuit of DFIG i.e. fault in back-to-back converter is narrated using Fourier supported analysis in (Giaourakis, Safacas, and Tsotoulidis). Solution to faulty speed measurement using fuzzy based sliding mode observer (FSMO) control of DFIG is proposed in (BELFEDAL, ALLAOUI, BELABBAS, et al.). FSMO approach estimates the speed of DFIG for control and eliminates requirement of speed sensor (BELFEDAL, ALLAOUI, BELABBAS, et al.). After detection of fault in sensors, reconfiguration of closed loop control using bank of observers is proposed in (Rothenhagen and Fuchs). Bunch of observers generate residual signal after fault detection and reconfiguration using estimated variables by observers is proposed in (Rothenhagen and Fuchs). To overcome effect of fault(s) in current sensors, hardware approach with field programmable gate array (FPGA) based grid side converter control is proposed in (Karimi et al.). Using state- space based model of DFIG, coherent current sensor observer is proposed in (Li et al.) using MATLAB/Simulink platform. Robust observer presents substitute to current sensor under dynamic and transient condition, but differs from actual quantity (Li et al.). El-hagry and Eskander presented estimation of i_{ds} , i_{qs} , i_{qr} and ω_r (rotor speed) using EKF over sub-to-super synchronous speed range of DFIG while employing i_{ds} , ω_r and capacitor charging current i_{dc} as measurement variables (EL-Hagry and Eskander). Further, estimated i_{ds} , i_{qs} , i_{qr} and ω_r of DFIG are used to derive v_{ds} , v_{qs} , v_{dr} and v_{qr} . These derived variables are consequently proposed in the control loop to obtain control parameters which regulate rotor voltage and rotor position of DFIG (EL-Hagry and Eskander). Usually, process of DSE provides information pertaining to crucial dynamic states much earlier if the same state is collected using measurement sensors. Hence, when information of crucial dynamic states, whether measurable or unmeasurable, is available at one time stamp ahead, then it would be beneficial to use this information for better monitoring and control of DFIG based wind generators.

1.3 Motivation

The SSE in power system has a limitation i.e. inability to capture fast changing dynamics of states. This is attributed to quasi-static nature and overall state estimation duration is electrically large. Hence, for better system monitoring and control, DSE becomes inevitable. With integration of renewable sources, power system dynamics

further becomes prone to volatility and may behave abruptly.

The DSE of synchronous generator connected to SMIB and in multi-machine system is successfully depicted in literature. Incidentally, SMIB connected DFIG's dynamic state estimation is described in literature. For a DFIG farm connected in a multi-synchronous generator power system, literature indicates feasibility of estimation of DFIG dynamic states alone. Research possibilities exist in untouched domain of centralized concurrent DSE to apply in power system which can give information of dynamic states of conventional and renewable energy generators simultaneously. Such centralized concurrent DSE needs mathematical modelling of power system, especially of generators suitable to use for centralized DSE. With appropriate modelling, wide area measurement system (WAMS) supported by PMUs offer an opportunity to use these fast and accurate measurement to have centralized simultaneous DSE of all kind of generators. Changes in machine dynamics introduced by the power network shall also be faithfully recognized by DSE algorithm with an appropriate inclusion of power system network model.

A multi-machine system contains induction generator based renewable sources with conventional energy sources. It is noted that, state-space model of SGs as voltages source (Kundur, Balu, and Lauby) and DFIGs as current source do not permit their implementation for concurrent DSE of both types of generators centrally. Necessity arises to have a state-space mathematical model which can be implemented for EKF and UKF for simultaneous DSE of all generators. A correlated mathematical approach is the pre-requisite for implementation of centralized concurrent DSE of DFIG and synchronous generators in multimachine power system.

Not only the estimation of states serves the purpose, its real time application for better control and uninterrupted operation of DFIG under specific sensor condition is an avenue to work upon. Employing the DSE results can be a possible solution to faulty sensor issue and it can help in obtaining desired improvised control and operation of renewable energy source and for power network as a whole.

The trending tools in power system measurements have made measurement data reliable, accurate and offer insignificant transmission delay. A condition of total or partial measurement data loss may arise or a scenario may happen where the measurement data received are corrupted. It could be unintentional and / or due to

malfunction of communication link, manual error, or shortcoming in communication set up (Force). It becomes essential to check performance of widely accepted DSE tools i.e. EKF and UKF under condition of missing measurement packet at different measurement update rates.

1.4 Contribution of thesis

Objective #1: Establish base for the modelling of multi-machine power system involving different types of generators. Conventionally, the mathematical models of SGs and induction generators are significantly different, the former is usually represented as a voltage source and the later as a current source. It is essential to create a common mathematical platform so as to implement Kalman filter based algorithms. The objective is to study the available models, re-visit them and to arrive at common generator model for both the types of generators. The novel model is arrived at, tested and the implementation is presented.

Objective #2: To obtain the power system dynamics and DSE, employ the cylindrical rotor synchronous generator model (derived from DFIG base model), in coordination with the power system network model. It is imperative to assess the validity of the models used under the cases of faults at the generator terminals and faults in the power system. The validated mathematical model of the power system as an entity be employed with the algorithms of EKF and UKF algorithm for faithful, concurrent state estimation of all the measurable and non-measurable states using P and Q as the measurement data. The model, dynamics and DSE results are presented in the thesis. A performance analysis of EKF and UKF algorithms is highlighted.

Objective #3: Estimation of states helps in observing system stability and predicting upcoming issues. At the same time utilizing obtained states, as a real time application for DFIG operation be meaningful. The DFIG rotor current is measured by current sensor and the rotor power control loop uses the measured current as a feedback. Under the scenario of erratic measurement output from the current sensor, the DSE results be employed. Algorithm is used to detect erroneous sensor output conditions and use of dynamic states is suggested to replace the measurement for better control and desired operation of DFIG. The discussion and results are presented in the thesis.

An associated supplementary work describes the applicability of EKF and UKF under limited certain measurement update rates. This is presented in **Appendix A**. It is also proposed to use of static states achieved using WLSE as a back-up of load flow under bad data measurement conditions. Insight and analysis is presented in the thesis as **Appendix B**.

1.5 Outline of thesis

Chapter 2 gives insight to a novel current source model representation of synchronous generator and DFIGs. The state-space model of DFIG is used as base model to propose a novel approach to represent SG as current source state-space model. State-space models of machines have been implemented using MATLAB/Simulink environment. The validation of proposed models with standard software platform *viz.* PSCAD/EMTDC platform is described in this chapter.

Chapter 3 depicts the use of proposed current source model of SGs with DFIG for centralized concurrent dynamic state estimation. A state-space model is implemented for standard WSCC 3-generator 9-bus system (Anderson and Fouad Sauer, Pai, and Chow). Modification in this standard WSCC system is adopted to simulate large penetration of wind power. With the help of proposed model, obtaining centralized DSE of dynamic states of DFIG and SGs using PMU measurements forms the core part of this chapter. Successful DSE is achieved using both the tools of DSE *viz.* EKF and UKF under dynamic conditions. Comparative performance aspects of both DSE tools are presented at the end of chapter.

Chapter 4 shows the application of accurate dynamic states of DFIG achieved using EKF for erroneous current sensor conditions. Three different erroneous current sensor conditions are considered. Algorithm is used to detect the mal-operations of current sensor. Successful application of dynamic states is displayed under faulty current sensor conditions and hence, better control and continuous operation of DFIG is attained.

Chapter 5 concludes the thesis with summary of contributions and outlines ideas for the further research. This chapter is followed by work citation and appendices.

Appendices comprises of discussion on supplementary work and the typical algorithmic procedures for EKF and UKF. As a part of initial learning, the offshoot work is presented in **Appendix A**. It deals with comparative analysis of EKF and UKF having various measurement update rates under different intermittent measurement conditions. This is analyzed using two standard test systems *viz.* WSCC 3-generator 9-bus system (Sauer, Pai, and Chow Anderson and Fouad) and IEEE-14 bus test system (Pai and Chatterjee Christie). Next appendix (**Appendix B**) undertakes the SSE using WLSE method for standard WSCC test system. The estimated states are employed as a back-up to load flow results under bad data measurement conditions. The significant procedural steps of EKF and UKF form **Appendix C** and **Appendix D** respectively. Improvement to coalesced model of SG and DFIG presented in Chapter # 2, is briefly conveyed in **Appendix E** using multi-machine approach with corresponding results.

Chapter 2

Coalesced Model of Synchronous Generator and DFIG

2.1 Introduction

In present scenario, multi-machine coherent power system involves abundance of energy sources normally represented by either voltage or current sources. The synchronous generator typically conferred as voltage source in multi-machine power system. Continuously increasing penetration of wind energy source has made wind generators to operate in parallel with synchronous generators, normally pervasive in power system. Under the constant power output condition (at constant speed) with stable grid voltage, the widely accepted wind generator - doubly fed induction generator (DFIG) functions as the current source and accordingly mathematically represented. State-space modelling approach is ubiquitously accepted to analyze stability aspects of power system under dynamic conditions. To investigate stability aspects of power network occupied with conventional synchronous generators (SGs) and sizable penetration of DFIG based wind generators (DFIGs), it becomes indispensable to represent both generators by state-space model built on common platform i.e. either as voltage sources or as current sources.

Unified presentation of SGs and DFIGs offers opportunities to enhance centralized monitoring and control of power network. One significant aspect of enhanced monitoring and control of power network operation is dynamic state estimation which avails information regarding crucial dynamic states of power network under transient

conditions. To enact centralized DSE of multi-machine power system incorporating DFIG, an approach of current-source model presentation of synchronous generator forms the core of work presented. In addition to better monitoring, it offers an opportunity to perform a stability analysis quickly. The SGs, when represented by current source model, can be easily integrated in parallel with multi-machine system possessing renewable sources. The SG current source state-space model is quite involving and can be obtained by systematically restructuring the state model equations appearing in (Kundur, Balu, and Lauby).

2.2 Aspects of modelling

Traditionally, DFIG is presented as current-source model. Hence, mathematical state-space model of DFIG is adopted from (Fan et al.). The voltage (2.1, 2.2) and flux linkage (2.3) equations employed for DFIG form the basis and this modelling approach and its versatility is to be used for simulation of synchronous generator. The equations from (Fan et al.) are represented here as under.

$$\begin{aligned} v_{ds} &= R_s i_{ds} - \omega_s \lambda_{qs} + \frac{d\lambda_{ds}}{dt} \\ v_{qs} &= R_s i_{qs} + \omega_s \lambda_{ds} + \frac{d\lambda_{qs}}{dt} \end{aligned} \quad (2.1)$$

$$\begin{aligned} v_{dr} &= R_r i_{dr} - (\omega_s - \omega_r) \lambda_{qr} + \frac{d\lambda_{dr}}{dt} \\ v_{qr} &= R_r i_{qr} + (\omega_s - \omega_r) \lambda_{dr} + \frac{d\lambda_{qr}}{dt} \end{aligned} \quad (2.2)$$

$$\begin{aligned} \lambda_{ds} &= L_s i_{ds} + L_m i_{dr} \\ \lambda_{qs} &= L_s i_{qs} + L_m i_{qr} \\ \lambda_{dr} &= L_r i_{dr} + L_m i_{ds} \\ \lambda_{qr} &= L_r i_{qr} + L_m i_{qs} \end{aligned} \quad (2.3)$$

The current state equations i_{ds}, i_{qs}, i_{dr} and i_{qr} for DFIG are given as (2.4)

$$\begin{bmatrix} \dot{i}_{ds} \\ \dot{i}_{qs} \\ \dot{i}_{dr} \\ \dot{i}_{qr} \end{bmatrix} = lc \begin{bmatrix} -R_s L_r i_{ds} + [\omega_r L_m^2 + \omega_s (L_s L_r - L_m^2)] i_{qs} + R_r L_m i_{dr} \\ + \omega_r L_r L_m i_{qr} + L_r v_{ds} - L_m v_{dr} \\ -[\omega_r L_m^2 + \omega_s (L_s L_r - L_m^2)] i_{ds} - R_s L_r i_{qs} - \omega_r L_r L_m i_{dr} \\ + R_r L_m i_{qr} + L_r v_{qs} - L_m v_{qr} \\ R_s L_m i_{ds} - \omega_r L_s L_m i_{qs} - R_r L_s i_{dr} + [\omega_s (L_s L_r - L_m^2) \\ - \omega_r L_s L_r] i_{qr} - L_m v_{ds} + L_s v_{dr} \\ R_s L_m i_{qs} + \omega_r L_s L_m i_{ds} - R_r L_s i_{qr} - [\omega_s (L_s L_r - L_m^2) \\ - \omega_r L_s L_r] i_{dr} - L_m v_{qs} + L_s v_{qr} \end{bmatrix} \quad (2.4)$$

where $lc = \frac{1}{L_s L_r - L_m^2}$ = leakage co-efficient.

The input vector \mathbf{u} is presented as (2.5)

$$[\mathbf{u}] = \begin{bmatrix} v_{ds} \\ v_{qs} \\ v_{dr} \\ v_{qr} \end{bmatrix} \quad (2.5)$$

A critical observation indicates that the terms employed in (2.1 - 2.5) for DFIG, are essentially used in synchronous generator as well, with same technical functionality but slightly different nomenclature. It is therefore possible to assign appropriate values and conditions to specific terms to realize both machines from the same set of equations. It is to be noted that the DFIG model selected is a basic (low order) model and other detailed models may be employed as offered in (Ekanayake, Holdsworth, and Jenkins), (Bourdoulis and Alexandridis).

2.3 Simulation aspects for model validation

To prove the authenticity of the proposed current source state-space model, it is desirable that the dynamic response of both machines as generators is to be obtained using the DFIG state model. The responses of quantities are compared with the standard established software responses. In this work, the proposed state equations are developed in MATLAB / Simulink, initialized as in single machine infinite bus (SMIB) case as shown in Fig. 2.1.

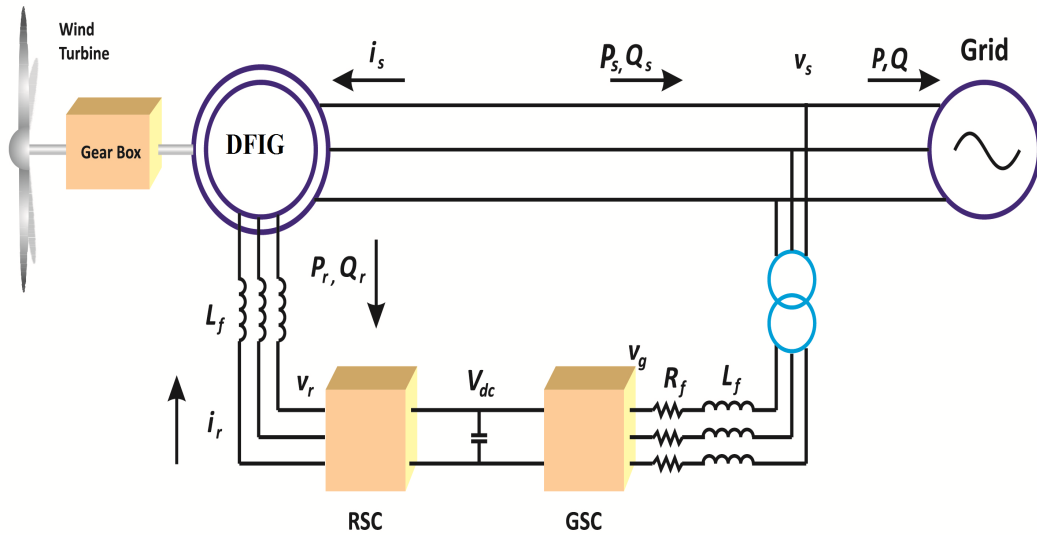


Figure 2.1: DFIG connected to infinite bus (source : internet)

The case is considered in which MATLAB/Simulink state-space model of DFIG is connected to infinite bus. In steady state, DFIG is supplying 4.7 MW of active power P at nearly unity power factor with value of Q given as 0.2 MVAR to grid. The machine rating, parameters are mentioned in **Appendix 2.1** (at end of the chapter). System frequency is set at 60 Hz. All quantities are prescribed in real, unless specified.

To simulate the dynamic condition, 3-phase-to-ground metallic short circuit fault is simulated at the point-of-common-coupling (PCC) at $t=1$ s. Fault persist for total simulation period of 2 s to observe the variation in terminal currents i_{abc} of DFIG. Variation in the current i_{abc} of DFIG for MATLAB/Simulink model and PSCAD model are shown in Fig.2.2(a) and Fig.2.2(b) respectively.

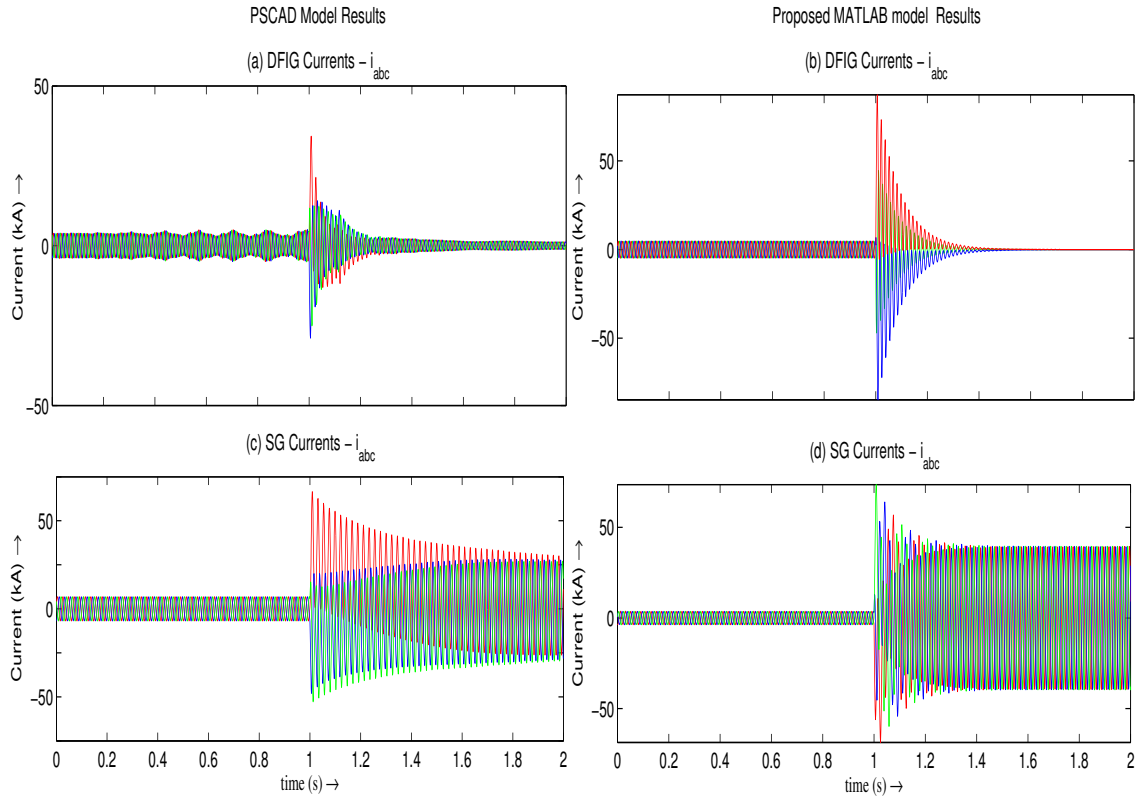


Figure 2.2: Current states i_{abc} under steady state (pre-fault) and dynamic condition (during fault) obtained using PSCAD model and proposed model respectively, for (a, b) DFIG, (c, d) SG

This work mainly focused on the coalesced model to analyze performance of induction generator (DFIG) and synchronous generator under dynamic conditions. On examining, except the slip, the asynchronous and synchronous machines have an inherent logical correspondence. Hence, the asynchronous machine current source state-space model can offer comparable attributes for synchronous machine. To validate the proposed idea of current-source model presentation of synchronous generator, state-space equation for synchronous generator is derived as shown in (2.6).

$$\begin{bmatrix} \dot{i}_{ds} \\ \dot{i}_{qs} \\ \dot{i}_{fd} \\ \dot{i}_D \end{bmatrix} = lc \begin{bmatrix} -R_s L_r i_{ds} + \omega_s L_s L_r i_{qs} + R_r L_m i_{fd} + \omega_s L_r L_m i_D + L_r v_{ds} \\ -L_m v_{fd} \\ -\omega_s L_s L_r i_{ds} - R_s L_r i_{qs} - \omega_s L_r L_m i_{fd} + R_r L_m i_D + L_r v_{qs} \\ -L_m v_D \\ R_s L_m i_{ds} - \omega_s L_s L_m i_{qs} - R_r L_s i_{fd} - \omega_s L_m^2 i_D - L_m v_{ds} \\ +L_s v_{fd} \\ \omega_s L_s L_m i_{ds} + R_s L_m i_{qs} + \omega_s L_m^2 i_{fd} - R_r L_s i_D - L_m v_{qs} \\ +L_s v_D \end{bmatrix} \quad (2.6)$$

where $lc = \frac{1}{L_s L_r - L_m^2} =$ leakage co-efficient.

To simulate second case, current source state-space MATLAB/Simulink model of synchronous generator using (2.6) is proposed. Rating and parametric equality have been maintained for suggested models of both generators. Analogous to the first case, cylindrical rotor SG based SMIB system is simulated with minor modifications in the base model of DFIG and subsequently, variation in output terminal current i_{abc} is observed during similar dynamic condition of persistent short-circuit fault. Dynamic responses of both generators are compared with the PSCAD / EMTDC results (Fig. 2.2)(c,d). The current direction, inward to the machine, is considered positive for both simulations.

For base case of DFIG, under the steady state condition and dynamic condition, comparative variation in voltages *viz.* stator q axis voltage- v_{qs} and rotor d axis voltage - v_{dr} achieved from PSCAD model and suggested MATLAB/Simulink model are shown in Fig.2.3(a,b) and Fig. 2.3(c,d) respectively.

Employing the current states i_{ds} , i_{qs} , i_{dr} and i_{qr} and input voltages v_{ds} , v_{qs} , v_{dr} and v_{qr} , the deviation in active power and reactive power of DFIG is obtained using

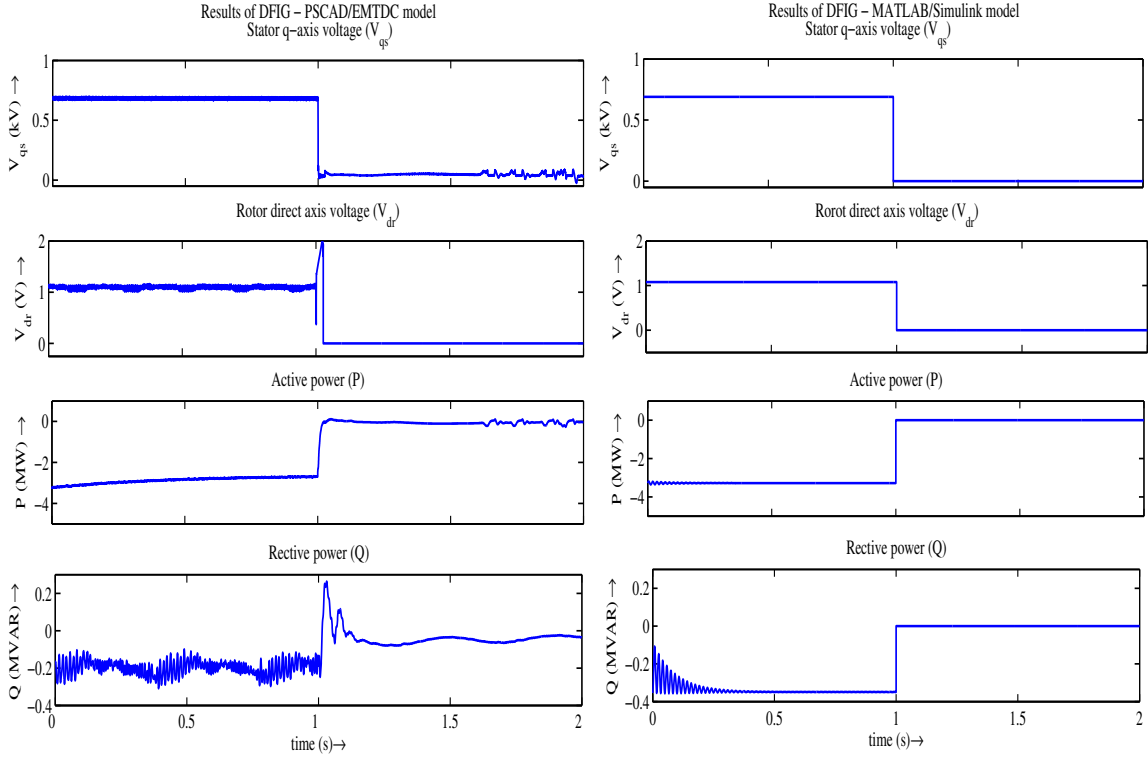


Figure 2.3: Variation of DFIG's different variables *viz.* v_{qs} , v_{dr} , P_{dfig} and Q_{dfig} under steady state (pre-fault) and dynamic condition (during fault) obtained using PSCAD model and proposed model respectively

equation (2.7).

$$\begin{aligned}
 P_{dfig} &= \frac{3}{2}(v_{ds}i_{ds} + v_{qs}i_{qs} + v_{dr}i_{dr} + v_{qr}i_{qr}) \\
 Q_{dfig} &= \frac{3}{2}(v_{qs}i_{ds} - v_{ds}i_{qs} + v_{qr}i_{dr} - v_{dr}i_{qr})
 \end{aligned} \tag{2.7}$$

Enforcing similarity of DFIG model validation with PSCAD/EMTDC for derived active and reactive power can be seen in Fig. 2.3 (e,f) and (g,h). Coherence in variation of active and reactive power proves analogy between models.

Similarly, to prove coherence of proposed MATLAB/Simulink current source model of synchronous generator with synchronous generator model on PSCAD/EMTDC platform, variation in parameters of significance- voltage parameters *viz.* v_{qs} and v_{fd} is shown in Fig.2.4.

For synchronous generator, the active power and reactive power variation is

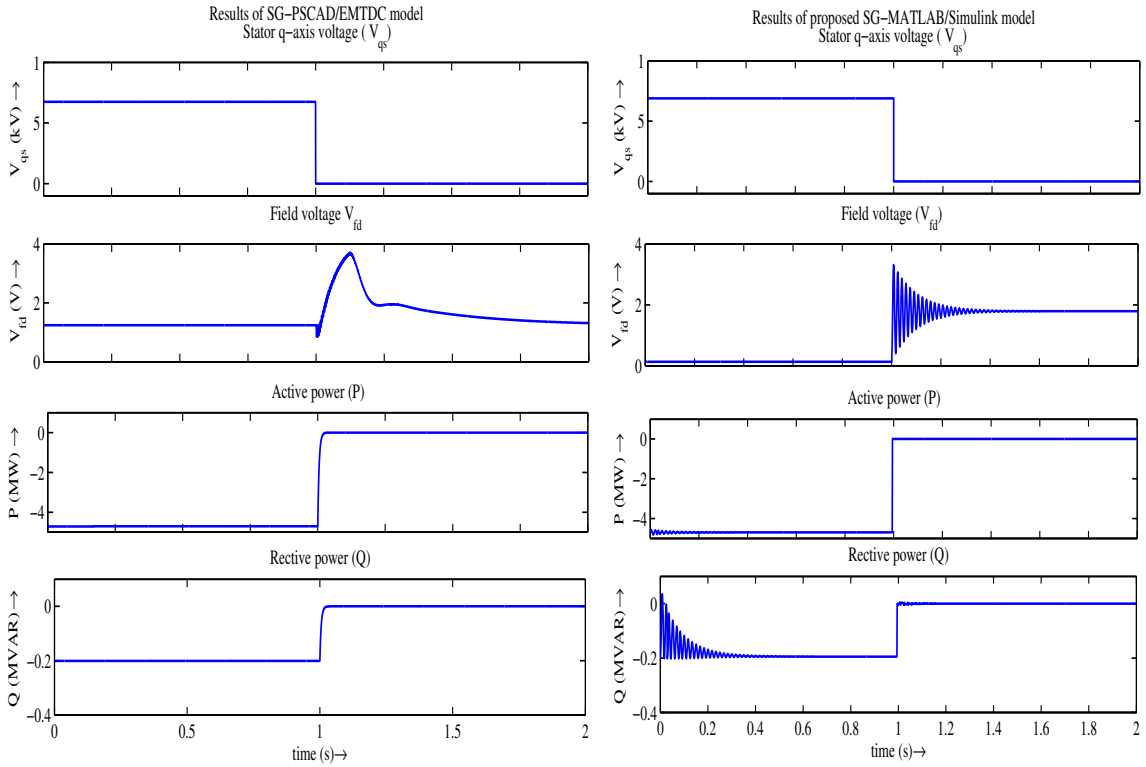


Figure 2.4: Variation of SG's different variables *viz.* v_{qs} , v_{fd} , P_{sg} and Q_{sg} under steady state (pre-fault) and dynamic condition (during fault) obtained using PSCAD model and Proposed model respectively

achieved using following equation.

$$\begin{aligned}
 P_{sg} &= \frac{3}{2}(v_{ds}i_{ds} + v_{qs}i_{qs}) \\
 Q_{sg} &= \frac{3}{2}(v_{qs}i_{ds} - v_{ds}i_{qs})
 \end{aligned} \tag{2.8}$$

Active power and reactive power variation for proposed current-source synchronous generator model using MATLAB/Simulink model and PSCAD/EMTDC model are displayed in Fig. 2.4(e,g) and Fig. 2.4(h,f) respectively.

2.4 Discussion

2.4.1 State - space model as DFIG (base model)

For DFIG based SMIB system, the state model is initialized using appropriate voltage inputs. The machine rating, parameters are mentioned in **Appendix 2.1**. The said parameters are employed to get the current response in PSCAD/EMTDC software. The current i_{abc} or its components i_{ds} , i_{qs} and i_{dr} , i_{qr} are the states, which demonstrate the variations under dynamic condition *viz.* 3-phase-to-ground short circuit fault at

the machine terminals. Such condition in the machine model is realized by changing the input voltage appropriately and the response is observed for i_{abc} in PSCAD as well as in MATLAB and is presented in Fig. 2.2(a) - 2.2(b) respectively. The pre-fault duration in figures refers the steady state response and thereafter, the fault at $t = 1s$ is duly responded. These results validate the model. The PSCAD response is depicted just around the fault, truncating its initialization issues. Needless to say that the trends of i_{ds}, i_{qs} and i_{dr}, i_{qr} are similar.

To emulate the crowbar resistance effect, the voltage v_{dr} and v_{qr} are reduced to zero using appropriate rate limiter, rather than a step change. The variations in the MATLAB model response magnitude are due to the fact that the step change in proposed models results in severe oscillations, which are normally limited by controllers and rate limiters in the standard software models. Changes observed in other significant parameters of DFIG *viz.* v_{qs}, v_{dr}, P_{dfig} and Q_{dfig} are in resemblance to variation of PSCAD/EMTDC model with modest assumption and modelling limitations (Fig. 2.3).

2.4.2 State - space model as SG

Absence of slip and effect of excitation is desired for SG . Using $\omega_r = \omega_s, v_{dr} = v_{fd}$ and $v_{qr} = v_D = \text{constant}$ (close to zero, based on initial condition) can offer equivalent SG performance. Although, the DFIG model does not reflect implementation of any controllers or rate limiters, it is interesting to observe that the AVR effect for SG is inherent in the equations being considered. The response of MATLAB state model and the PSCAD model results fulfill the validation requirements in the Fig. 2.2(c) - 2.2(d) for SG. It is important to note that i_{qr} and v_{qr} hold negligible importance for cylindrical rotor synchronous generator. However, in case of salient-pole rotor synchronous generator variation in i_{qr} and hence, v_{qr} can reflect its proximity to damper winding current and voltage respectively. Results shown in Fig. 2.4 provide strengthening support to prove proposed SG model operation analogous to SG model created on standard software platform of PSCAD/EMTDC. It may be further noted that the same model with proper sign changes can offer functionality of other induction machines also.

Table 2.1 refers summary of the quantities to be modified for realization of

synchronous machines, the DFIG model being a base machine (2.4).

Table 2.1: Quantities to be considered for realization of different machines

Machine	Quantities	Remark
SG	$\omega_r = \omega_s, v_{dr} = v_{fd},$ $v_{qr} = \text{Constant (close to zero, based on initial cond.)}$	v_{dr} will be derived from state $i_{dr}(i_{fd})$ in case of short circuit studies

2.5 Conclusions

Reducing variety of sources on one type and making use of the same state - space model for asynchronous and synchronous machines could make the power system analysis much simple, requires less computational memory and time. Presented work makes an effort to create the synchronous generator source type and state - model unification by employing the DFIG basic current source state model. Using appropriate values of input quantities, supported by proper initialization of state model, leads to use the same model as both machines by incorporating minor changes and logical attributes. The responses of states under steady and dynamic conditions as both machines are presented and validated using PSCAD model. These coalesced models offer their usage as two different machines for multi-machine power system stability analysis, state estimation, eigenvalue analysis etc..

Appendix 2.1

DFIG rated $MVA = 5$, rated line voltage 0.69 kV, rotor resistance (R_r) = 0.5779 m Ω , rotor inductance (L_r) = 1.1657 mH, mutual inductance (L_m) = 1.1138 mH, stator resistance (R_s) = 0.514 m Ω , stator inductance (L_s) = 1.1632 mH, frequency (f) = 60 Hz, synchronous speed (ω_s) = 377 rad/s, rotor speed (ω_r) = 410 rad/s, slip (s) = -0.088.

Chapter 3

Kalman Filters based Centralized Concurrent DSE

3.1 EKF based Centralized Concurrent Dynamic State Estimation in Multi-machine Power Sys- tem

3.1.1 Introduction

A steep growth in energy requirement is supplied today by power generation mix of fossil fuel based generators and renewable power generators. The stochastic nature of renewable generations imposes need for superior monitoring at system level for the stable operation. The PMU enables the estimation of dynamic states in real time, based on wide area measurement, due to higher sampling rates and synchronized sampling. PMU, with typical sampling rate ranging from 10 sa/s through 120 sa/s with the GPS clock synchronization, offers consistent capturing of power system measurements under normal as well as abnormal network conditions (Zhou et al.). To estimate the dynamic states of a single-machine infinite bus (SMIB) system, Ghahremani and Kamwa showed the use of EKF algorithm to simultaneously estimate the synchronous generator (SG) states and unknown inputs (Ghahremani and Kamwa, “Dynamic State Estimation in Power System by Applying the Extended Kalman Filter With Unknown Inputs to Phasor Measurements”). For multi-machine systems,

Huang et al. (Huang, Schneider, and Nieplocha Huang et al., “Estimating power system dynamic states using extended Kalman Filter” “Generator dynamic model validation and parameter calibration using phasor measurements at the point of connection”), Fan and Wehbe (Fan and Wehbe), Ghahremani and Kamwa (Ghahremani and Kamwa, “Local and Wide-Area PMU-Based Decentralized Dynamic State Estimation in Multi-Machine Power Systems”), Tebianian and Jeyasurya (Tebianian and Jeyasurya) have indicated plausible use of PMU data with the help of extended Kalman filter (EKF) for online state and parameter estimation of conventional synchronous generators.

Among various types of wind generators, DFIGs are gaining popularity due to high energy efficiency, low mechanical stress on the wind turbine, relatively low power rating of converters and flexible control of power. With the increasing presence of DFIG, its modelling and dynamic state estimation (DSE) becomes imperative. Another variant of Kalman filter *viz.* ensemble Kalman filter (EnKF) is used to estimate dynamic states and parameters of DFIG with noisy measurement and initial parametric error in (Fan et al.). Comparative analysis of particle filter (PF), EKF and unscented Kalman filter (UKF) based dynamic state estimator along with bad data detection algorithm are proposed for DFIG states in (S. Yu, “Realization of State-Estimation-Based DFIG Wind Turbine Control Design in Hybrid Power Systems Using Stochastic Filtering Approaches” S. Yu, “State Estimation of Doubly Fed Induction Generator Wind Turbine in Complex Power Systems”). For such estimation, measurement data are understood to be available using local PMU.

Research domain so far, presents the DSE either for synchronous machine or for the asynchronous machine, but not for both at a time. For a vastly spread power system, a fault in the system, sudden changes in wind generator output (e.g. wind speed change) or change in load demand impacts the generation from synchronous generators and their dynamics. These dynamics of course can be obtained simultaneously by the DSE approach, once the system model is integrated with the synchronous and asynchronous machine models on same platform. This work offers integration of different types of generators in power system and considers the availability of active and reactive power measurements centrally employing PMUs. In this section, this is employed in EKF based state estimator for concurrent DSE of conventional generators

as well as DFIG.

To present the case, a standard WSCC 9-bus test system has been selected. The standard test system is comprised of three synchronous generators of large capacity. For the sake of employing asynchronous generator, a synchronous generator at a P–V bus, bus #2, is replaced by a DFIG based wind farm of equivalent capacity (with modest assumption employed). Remaining two synchronous generators are cylindrical rotor machines. The P and Q controls of DFIG are adjusted such that its P_{out} and Q_{out} of DFIG are similar to the synchronous generator #2 of standard test system. Highlighting feature of the work is that the DFIG as well as the synchronous generators are represented as current sources, unlike usual case of synchronous generator as voltage source (Kundur, Balu, and Lauby). Availability of P and Q at generator buses of all generators as measurement data (e.g. from PMU) and using initial values of bus voltages (based on load flow study of standard test system) in state-space model offers the centralized faithful estimation using EKF for DSE of synchronous generators and DFIG (under dynamic and transient conditions).

3.1.2 State-space current source models for EKF implementation

- *State-space model of generators*

To implement EKF based DSE, state-space model of DFIG is integrated with state-space model of synchronous generators. Conventionally, DFIG is treated as current source and its mathematical model is adopted from (Ekanayake, Holdsworth, and Jenkins),(Fan et al.) as base model. The d and q axis voltages for any p^{th} DFIG generator are represented as:

$$\begin{aligned}
 v_{ds_p} &= R_{s_p} i_{ds_p} - \omega_s \lambda_{qs_p} + \frac{d\lambda_{ds_p}}{dt} \\
 v_{qs_p} &= R_{s_p} i_{qs_p} + \omega_s \lambda_{ds_p} + \frac{d\lambda_{qs_p}}{dt} \\
 v_{dr_p} &= R_{r_p} i_{dr_p} - (\omega_s - \omega_r) \lambda_{qr_p} + \frac{d\lambda_{dr_p}}{dt} \\
 v_{qr_p} &= R_{r_p} i_{qr_p} + (\omega_s - \omega_r) \lambda_{dr_p} + \frac{d\lambda_{qr_p}}{dt}
 \end{aligned} \tag{3.1}$$

In above equations λ terms represent flux linkages, $v_{ds_p}, v_{qs_p}, v_{dr_p}$ and v_{qr_p} are the stator and rotor voltages on synchronously rotating d and q axis, while ω_s and ω_r

are synchronous speed and rotor speed respectively. Components of stator and rotor flux linkages for DFIG are,

$$\begin{aligned}
 \lambda_{ds_p} &= L_{s_p} i_{ds_p} + L_{m_p} i_{dr_p} \\
 \lambda_{qs_p} &= L_{s_p} i_{qs_p} + L_{m_p} i_{qr_p} \\
 \lambda_{dr_p} &= L_{r_p} i_{dr_p} + L_{m_p} i_{ds_p} \\
 \lambda_{qr_p} &= L_{r_p} i_{qr_p} + L_{m_p} i_{qs_p}
 \end{aligned} \tag{3.2}$$

Using (3.1) and (3.2), state-space equations in form of stator and rotor currents for DFIG (asynchronous generator) are as follows :

$$\begin{bmatrix} \dot{i}_{ds_p} \\ \dot{i}_{qs_p} \\ \dot{i}_{dr_p} \\ \dot{i}_{qr_p} \end{bmatrix} = l_{c_p} \begin{bmatrix} -R_{s_p} L_{r_p} i_{ds_p} + [\omega_{r_p} L_{m_p}^2 + \omega_{s_p} (L_{s_p} L_{r_p} - L_{m_p}^2)] i_{qs_p} + R_{r_p} L_{m_p} i_{dr_p} \\ \quad + \omega_{r_p} L_{r_p} L_{m_p} i_{qr_p} + L_{r_p} v_{ds_p} - L_{m_p} v_{dr_p} \\ -[\omega_r L_{m_p}^2 + \omega_s (L_{s_p} L_{r_p} - L_{m_p}^2)] i_{ds_p} - R_{s_p} L_{r_p} i_{qs_p} - \omega_r L_{r_p} L_{m_p} i_{dr_p} \\ \quad - R_{r_p} L_{m_p} i_{qr_p} + L_{r_p} v_{qs_p} - L_{m_p} v_{qr_p} \\ R_{s_p} L_{m_p} i_{ds_p} - \omega_r L_{s_p} L_{m_p} i_{qs_p} - R_{s_p} L_{s_p} i_{dr_p} - L_{m_p} v_{ds_p} + L_{s_p} v_{dr_p} \\ \quad + [\omega_s (L_{s_p} L_{r_p} - L_{m_p}^2) - \omega_r L_{s_p} L_{r_p}] i_{qr_p} \\ \omega_r L_{s_p} L_{m_p} i_{ds_p} + R_{s_p} L_{m_p} i_{qs_p} - R_{s_p} L_{s_p} i_{qr_p} - L_{m_p} v_{qs_p} + L_{s_p} v_{qr_p} \\ \quad - [\omega_s (L_{s_p} L_{r_p} - L_{m_p}^2) - \omega_r L_{s_p} L_{r_p}] i_{dr_p} \end{bmatrix} \tag{3.3}$$

where, $l_{c_p} = \frac{1}{L_{s_p} L_{r_p} - L_{m_p}^2}$ = leakage co-efficient.

The basic eqns. (3.1,3.2) and the model of DFIG machine in (3.3) forms the basis to create current source model of synchronous generator. It is apparent that appropriately considering quantities like ω , i_D , i_{fd} , etc. in a mathematical model of DFIG, a synchronous machine can be easily realized. The derived state-space model of any

n^{th} synchronous generator as current source model is presented in (3.4).

$$\begin{bmatrix} \dot{i}_{dsn} \\ \dot{i}_{qsn} \\ \dot{i}_{fdn} \\ \dot{i}_{Dn} \end{bmatrix} = l_{c_n} \begin{bmatrix} -R_{s_n} L_{r_n} i_{dsn} + \omega_s L_{s_n} L_{r_n} i_{qsn} + R_{r_n} L_{m_n} i_{fdn} + \omega_s L_{r_n} L_{m_n} i_{Dn} \\ + L_{r_n} v_{dsn} - L_{m_n} v_{fdn} \\ -\omega_s L_{s_n} L_{r_n} i_{dsn} - R_{s_n} L_{r_n} i_{qsn} - \omega_s L_{r_n} L_{m_n} i_{fdn} - R_{r_n} L_{m_n} i_{Dn} \\ + L_{r_n} v_{qsn} - L_{m_n} v_{Dn} \\ R_{s_n} L_{m_n} i_{dsn} - \omega_s L_{s_n} L_{m_n} i_{qsn} - R_{s_n} L_{s_n} i_{fdn} - \omega_s L_{m_n}^2 i_{Dn} \\ - L_{m_n} v_{dsn} + L_{s_n} v_{fdn} \\ \omega_s L_{s_n} L_{m_n} i_{dsn} + R_{s_n} L_{m_n} i_{qsn} - R_{r_n} L_{s_n} i_{Dn} + \omega_s L_{m_n}^2 i_{fdn} \\ - L_{m_n} v_{qsn} + L_{s_n} v_{Dn} \end{bmatrix} \quad (3.4)$$

where, $l_{c_n} = \frac{1}{L_{s_n} L_{r_n} - L_{m_n}^2}$.

It is important to note that this model inherently comprises of AVR and a damper winding behaviour.

The standard test system, WSCC 3-generator 9-bus system (Anderson and Fouad),(Sauer, Pai, and Chow), is used as the base for simulation purposes. To demonstrate the large penetration of wind energy, as mentioned earlier, in WSCC 3-generator 9-bus system, a synchronous generator (Gen #2) is replaced with DFIG based wind farm of equivalent rating as shown in Fig.3.1. The other synchronous generators viz. Gen #1 (swing gen), Gen #3 and loads in the system are maintained.

- **Mathematical model for DSE using EKF**

For the DSE, the precise mathematical modelling of the power system components is very essential. For a power system, having inherent non-linear relationship between its state and measurements, it becomes necessary to imbibe these non-linearities in estimation process to have accurate estimation of power system state variables (Mandal, Sinha, and Roy). In the work that follows, a variant of Kalman filter approach - the discrete extended Kalman filter (EKF) is used for DSE. Vital mathematical steps for

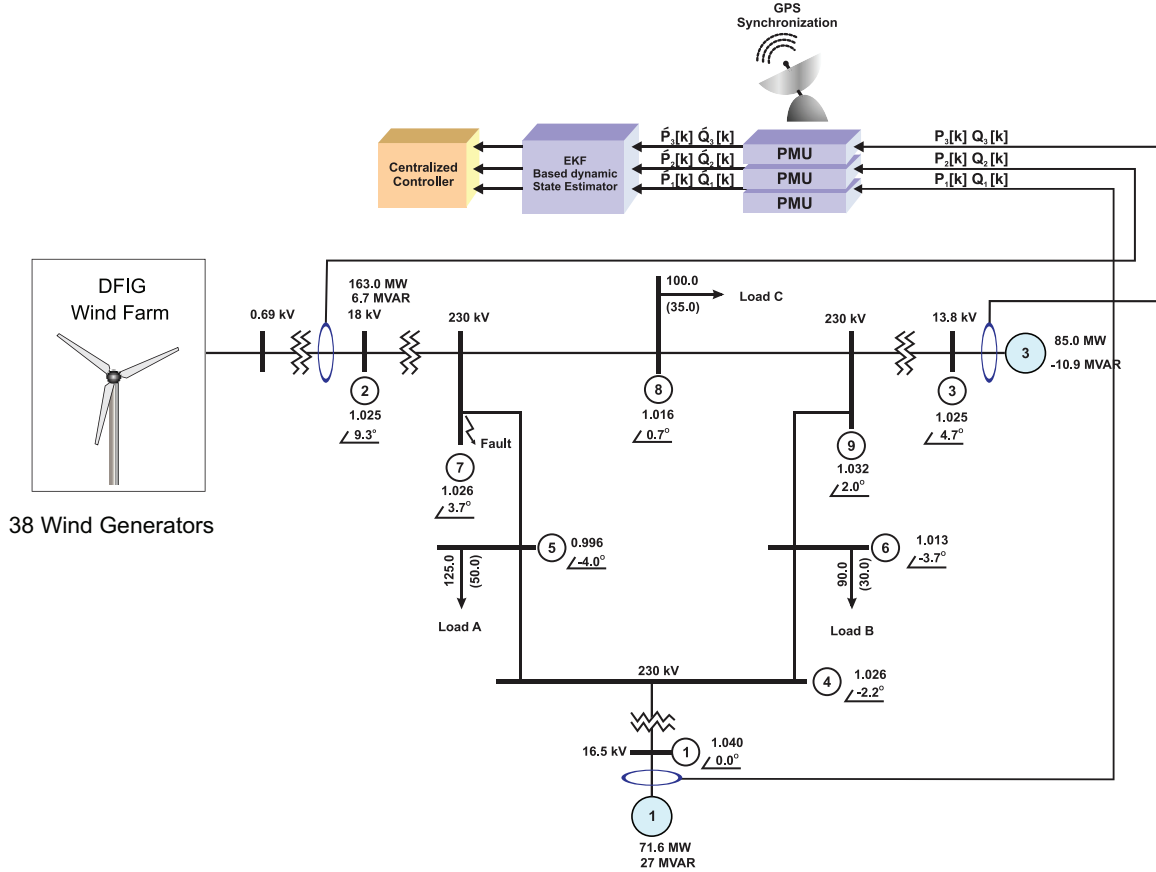


Figure 3.1: WSCC 3-generator 9-bus test system, where synchronous gen. #2 is replaced with equally rated DFIG based wind farm

discrete EKF are intricately treated in many literature (Ghahremani and Kamwa, “Dynamic State Estimation in Power System by Applying the Extended Kalman Filter With Unknown Inputs to Phasor Measurements” Wang, Gao, and Meliopoulos Huang, Schneider, and Nieplocha Simon) and is enumerated in **Appendix C**.

The fundamental state-space equation representation is required to be formulated for the implementation of EKF based DSE of a 9-bus test system i.e.

$$\dot{\mathbf{x}} = \mathbf{Ax} + \mathbf{Bu}. \quad (3.5)$$

It is derived based on the (3.3) - (3.4).

In the present 3-generator, 9-bus test system, Gen #1 and #3 are the conventional synchronous generators and Gen #2 is the asynchronous (DFIG) generator. In the following, four currents of each generator are the state, and hence the matrix dimension of \mathbf{x} is of 12×1 and \mathbf{A} is 12×12 . The sub-subscript to components in

vectors \mathbf{x} and \mathbf{u} refer to the generator number.

$$[\dot{\mathbf{x}}] = [\dot{i}_{ds1} \ \dot{i}_{qs1} \ \dot{i}_{fd1} \ \dot{i}_{D1} \ \dot{i}_{ds2} \ \dot{i}_{qs2} \ \dot{i}_{dr2} \ \dot{i}_{qr2} \ \dot{i}_{ds3} \ \dot{i}_{qs3} \ \dot{i}_{fd3} \ \dot{i}_{D3}]^T \quad (3.6)$$

and \mathbf{u} is comprised of input voltages and represented by,

$$[\mathbf{u}] = [v_{ds1} \ v_{qs1} \ v_{fd1} \ v_{D1} \ v_{ds2} \ v_{qs2} \ v_{dr2} \ v_{qr2} \ v_{ds3} \ v_{qs3} \ v_{fd3} \ v_{D3}]^T \quad (3.7)$$

The matrices \mathbf{A} and \mathbf{B} are apparently presented in (3.8), (3.9).

$$[\mathbf{A}]_{12 \times 12} = \begin{bmatrix} A_{11} & A_{12} & A_{13} & A_{14} & 0 & 0 & 0 & 0 & 0 & 0 & 0 & 0 \\ A_{21} & A_{22} & A_{23} & A_{24} & 0 & 0 & 0 & 0 & 0 & 0 & 0 & 0 \\ A_{31} & A_{32} & A_{33} & A_{34} & 0 & 0 & 0 & 0 & 0 & 0 & 0 & 0 \\ A_{41} & A_{42} & A_{43} & A_{44} & 0 & 0 & 0 & 0 & 0 & 0 & 0 & 0 \\ 0 & 0 & 0 & 0 & A_{55} & A_{56} & A_{57} & A_{58} & 0 & 0 & 0 & 0 \\ 0 & 0 & 0 & 0 & A_{65} & A_{66} & A_{67} & A_{68} & 0 & 0 & 0 & 0 \\ 0 & 0 & 0 & 0 & A_{75} & A_{76} & A_{77} & A_{78} & 0 & 0 & 0 & 0 \\ 0 & 0 & 0 & 0 & A_{85} & A_{86} & A_{87} & A_{88} & 0 & 0 & 0 & 0 \\ 0 & 0 & 0 & 0 & 0 & 0 & 0 & 0 & A_{99} & A_{910} & A_{911} & A_{912} \\ 0 & 0 & 0 & 0 & 0 & 0 & 0 & 0 & A_{109} & A_{1010} & A_{1011} & A_{1012} \\ 0 & 0 & 0 & 0 & 0 & 0 & 0 & 0 & A_{119} & A_{1110} & A_{1111} & A_{1112} \\ 0 & 0 & 0 & 0 & 0 & 0 & 0 & 0 & A_{129} & A_{1210} & A_{1211} & A_{1212} \end{bmatrix} \quad (3.8)$$

Non-zero elements of matrix $A_{12 \times 12}$ (3.8) are,

Elements of Generator # 1

$$A_{11} = A_{22} = -lc_1 R_{s1} L_{r1}, \quad A_{12} = -A_{21} = lc_1 \omega_s L_{s1} L_{r1},$$

$$A_{13} = A_{24} = lc_1 R_{r1} L_{m1}, \quad A_{14} = -A_{23} = lc_1 \omega_s L_{r1} L_{m1},$$

$$A_{31} = A_{42} = lc_1 R_{s1} L_{m1}, \quad A_{32} = -A_{41} = -lc_1 \omega_s L_{s1} L_{m1},$$

$$A_{33} = A_{44} = -lc_1 R_{s1} L_{s1}, \quad A_{34} = -A_{43} = -lc_1 \omega_s L_{s1} L_{r1}$$

Elements of Generator # 2

$$\begin{aligned}
A_{55} &= A_{66} = -lc_2 R_{s_2} L_{r_2}, & A_{56} &= -A_{65} = lc_2 [\omega_r L_{m_2}^2 + \omega_s (L_{s_2} L_{r_2} - L_{m_2}^2)], \\
A_{57} &= A_{68} = lc_2 R_{r_2} L_{m_2}, & A_{58} &= -A_{67} = lc_2 \omega_r L_{r_2} L_{m_2}, \\
A_{75} &= A_{86} = lc_2 R_{s_2} L_{m_2}, & A_{76} &= -A_{85} = -lc_2 \omega_r L_{s_2} L_{m_2}, \\
A_{77} &= A_{88} = -lc_2 R_{s_2} L_{s_2}, & A_{78} &= -A_{87} = lc_2 [\omega_s (L_{s_2} L_{r_2} - L_{m_2}^2) - \omega_r L_{s_2} L_{r_2}]
\end{aligned}$$

Elements of Generator # 3

$$\begin{aligned}
A_{99} &= A_{1010} = -lc_3 R_{s_3} L_{r_3}, & A_{910} &= -A_{109} = lc_3 \omega_s L_{s_3} L_{r_3}, \\
A_{911} &= A_{1012} = lc_3 R_{r_3} L_{m_3}, & A_{912} &= -A_{1011} = lc_3 \omega_s L_{r_3} L_{m_3}, \\
A_{1119} &= A_{1210} = lc_3 R_{s_3} L_{m_3}, & A_{1110} &= -A_{129} = -lc_3 \omega_s L_{s_3} L_{m_3}, \\
A_{1111} &= A_{1212} = -lc_3 R_{s_3} L_{s_3}, & A_{1112} &= -A_{1211} = -lc_3 \omega_s L_{s_3} L_{r_3}
\end{aligned}$$

In above, $lc_n = \frac{1}{L_{s_n} L_{r_n} - L_{m_n}^2}$; $n = 1, 2, 3$ are leakage co-efficients of three generators.

Matrix B is given by,

$$[\mathbf{B}]_{12 \times 12} = \begin{bmatrix}
B_{11} & 0 & B_{13} & 0 & 0 & 0 & 0 & 0 & 0 & 0 & 0 & 0 \\
0 & B_{22} & 0 & B_{24} & 0 & 0 & 0 & 0 & 0 & 0 & 0 & 0 \\
B_{31} & 0 & B_{33} & 0 & 0 & 0 & 0 & 0 & 0 & 0 & 0 & 0 \\
0 & B_{42} & 0 & B_{44} & 0 & 0 & 0 & 0 & 0 & 0 & 0 & 0 \\
0 & 0 & 0 & 0 & B_{55} & 0 & B_{57} & 0 & 0 & 0 & 0 & 0 \\
0 & 0 & 0 & 0 & 0 & B_{66} & 0 & B_{68} & 0 & 0 & 0 & 0 \\
0 & 0 & 0 & 0 & B_{76} & 0 & B_{78} & 0 & 0 & 0 & 0 & 0 \\
0 & 0 & 0 & 0 & 0 & B_{86} & 0 & B_{88} & 0 & 0 & 0 & 0 \\
0 & 0 & 0 & 0 & 0 & 0 & 0 & 0 & B_{99} & 0 & B_{911} & 0 \\
0 & 0 & 0 & 0 & 0 & 0 & 0 & 0 & 0 & B_{1010} & 0 & B_{1012} \\
0 & 0 & 0 & 0 & 0 & 0 & 0 & 0 & B_{119} & 0 & B_{1111} & 0 \\
0 & 0 & 0 & 0 & 0 & 0 & 0 & 0 & 0 & B_{1210} & 0 & B_{1212}
\end{bmatrix} \quad (3.9)$$

Matrix $B_{12 \times 12}$ (3.9) is comprised of following non-zero elements,

Elements of Generator# 1	Elements of Generator# 2
$B_{11} = B_{22} = lc_1 L_{r_1},$	$B_{55} = B_{66} = lc_2 L_{r_2},$
$B_{13} = B_{31} = B_{24} = B_{42} = -lc_1 L_{m_1}, \quad B_{57} = B_{75} = B_{68} = B_{86} = -lc_2 L_{m_2},$	
$B_{33} = B_{44} = lc_1 L_{s_1},$	$B_{77} = B_{88} = lc_2 L_{s_2}$
Elements of Generator# 3	
$B_{99} = B_{1010} = lc_3 L_{r_3},$	
$B_{911} = B_{119} = B_{1012} = B_{1210} = -lc_3 L_{m_3},$	
$B_{1111} = B_{1212} = lc_3 L_{s_3}$	

For EKF implementation, measurement matrix \mathbf{y} is constituted by output active and reactive power from all three generators. Measurement matrix \mathbf{y} comprised of active and reactive powers is given by (3.10).

$$\begin{aligned}
 [\mathbf{y}] &= \begin{bmatrix} P_1 \\ Q_1 \\ P_2 \\ Q_2 \\ P_3 \\ Q_3 \end{bmatrix} = \frac{3}{2} \begin{bmatrix} (v_{ds_1} i_{ds_1} + v_{qs_1} i_{qs_1}) \\ (v_{qs_1} i_{ds_1} - v_{ds_1} i_{qs_1}) \\ (v_{ds_2} i_{ds_2} + v_{qs_2} i_{qs_2} + v_{dr_2} i_{dr_2} + v_{qr_2} i_{qr_2}) \\ (v_{qs_2} i_{ds_2} - v_{ds_2} i_{qs_2} + v_{qr_2} i_{dr_2} - v_{dr_2} i_{qr_2}) \\ (v_{ds_3} i_{ds_3} + v_{qs_3} i_{qs_3}) \\ (v_{qs_3} i_{ds_3} - v_{ds_3} i_{qs_3}) \end{bmatrix} \quad (3.10)
 \end{aligned}$$

Here P_n and Q_n are the active power and reactive power output of generators; $n = 1, 2, 3$. As shown in Fig.3.1, all measurement data are centrally collected through various PMUs. Measurements are received at the sample rate of 0.001s.

Innate nature of EKF includes process of prediction and estimation along with filtering of noises *viz.* measurement noise and process noise. As per IEEE standard - 1159 noise content permitted up to 1% of voltage magnitude (“IEEE Recommended

Practice for Monitoring Electric Power Quality”). Characterization and quantification of PMU measurement noise is presented in (Brown et al.). Additive white Gaussian noise with various degree(s) of noise has been considered by researchers. References (Ghahremani and Kamwa, “Local and Wide-Area PMU-Based Decentralized Dynamic State Estimation in Multi-Machine Power Systems”) (Shi, Tylavsky, and Logic)(Zhou) use white Gaussian noise with zero mean and standard deviations of 0.2%, 2% and 3% respectively. In (Chen et al.) a standard deviation of 0.5% and 1% is considered for voltage and current data. Zero mean Gaussian noise distribution with standard deviation of 2% is considered in (Tripathy, Srivastava, and Singh).

To emulate the noise in measurements, all the P and Q measurements are corrupted with white Gaussian noise having zero mean and standard deviation of 1%. Further, a uniform process noise with standard deviation of 0.0001% and process noise covariance is presumed accordingly. Justifiable assumption of initial state error covariance of 1% of actual values is taken for proposed EKF approach. Under the steady state condition, active and reactive power generation of synchronous generators and DFIG are alike the standard WSCC 3-generator 9-bus test system. For EKF implementation, initialization of state variables is derived from the load flow results.

- ***Simulation Details***

Presented work studies DSE when the large quantum of wind based generation is fed in synchronous generator dominated grid. To replicate such renewable penetration situation, a synchronous generator (Gen. #2) in standard WSCC 3-generator 9-bus system is replaced with equivalent rating of DFIG based wind farm (Fig.3.1, 3.2 (Fan and Wehbe)). The wind farm is assumed to have large DFIG generators, of which 38 generators are running in parallel to provide the equivalent output power. Each generator is rated for 5 MVA, 0.69 kV and connected to system bus of 18 kV through the transformers. The machine rating, parameters of DFIG based wind generator are given in **Appendix 3.1** (at the end of chapter). It is assumed that the DFIG generators’ operation is coherent, the wind speed is constant for a simulation duration of 20s, the wind farm P and Q output is controllable. Each wind generator MPPT is considered to provide tracking of maximum power point and LVRT control is affected during the fault. These assumptions are justifiable, as the constant wind speed is

realistic for the simulation duration and as it is steady, the mechanical input to the DFIG is constant and hence the MPPT operation can be fixed. The system frequency is 60 Hz. All quantities are real, unless specified.

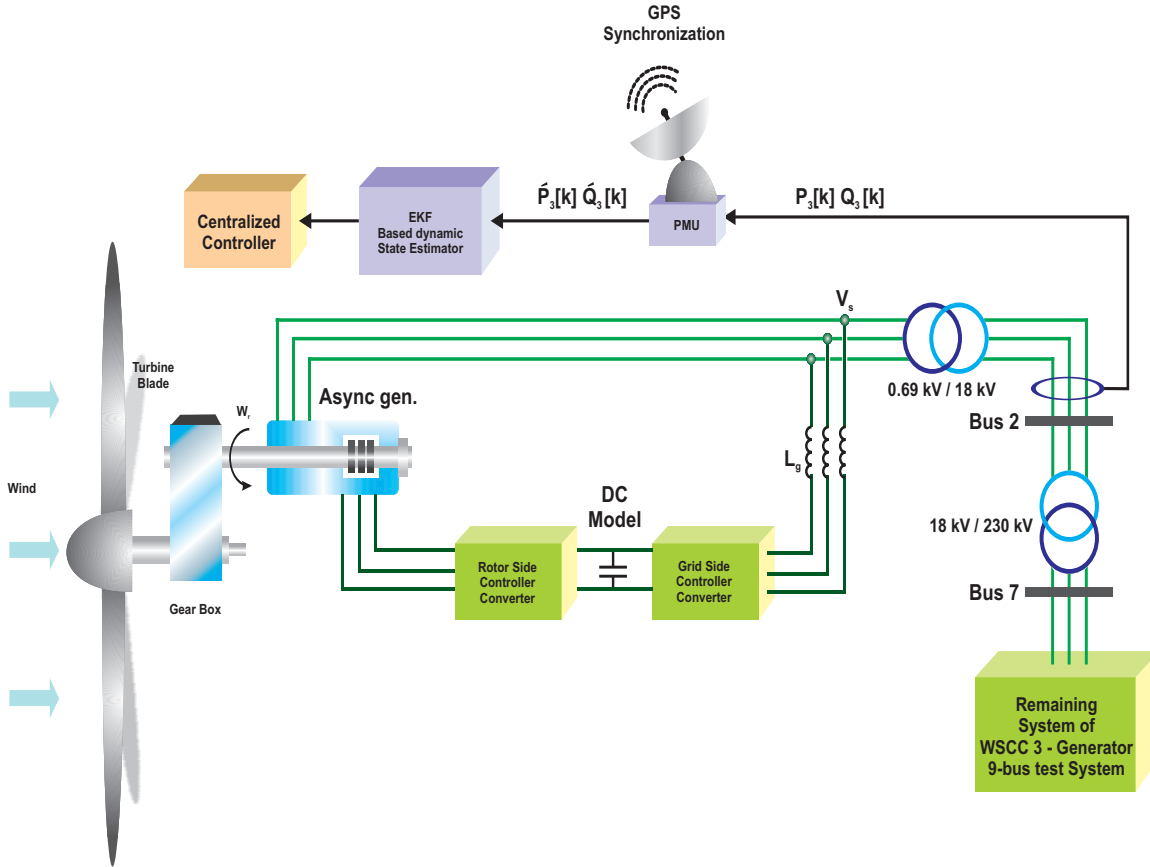


Figure 3.2: DFIG integrated with rest of WSCC 3-gen. 9-bus test system

Proposed state-space modelling, which represents all generators as current sources, is done using MATLAB/Simulink platform. Synchronous generators are modeled exhibiting the effect of excitation control. The modelling of turbine-governor system is not a part of the present work. In two-axis (d and q) representation of all generators, q axis leads d axis by 90° , and hence, a motoring convention is adopted through out the text. In modelling of DFIG, linearized operation of controllers is assumed. Focus of presented section is to show estimation of non-measurable states of generators, hence modelling of drive train and wind turbine and its control is not included here. The modelling of crowbar circuitry in suggested model is realized during the short circuit condition of the DFIG. The measurement data of P_n and Q_n are required for the EKF algorithm and hence to obtain them, PMUs are assumed to be available at bus #1, bus #2 and at bus #3.

The performance of integrated current source models of generators in a multi-

machine test system (created using MATLAB/Simulink platform) is validated with similar test system created on PSCAD/EMTDC platform. The indicative block diagram of state-space implementation of MATLAB/Simulink model is shown in Fig.3.3. Similarly to prove corroboration of MATLAB/Simulink model, similar model is built on standard PSCAD/EMTDC platform as shown in Fig. 3.4.

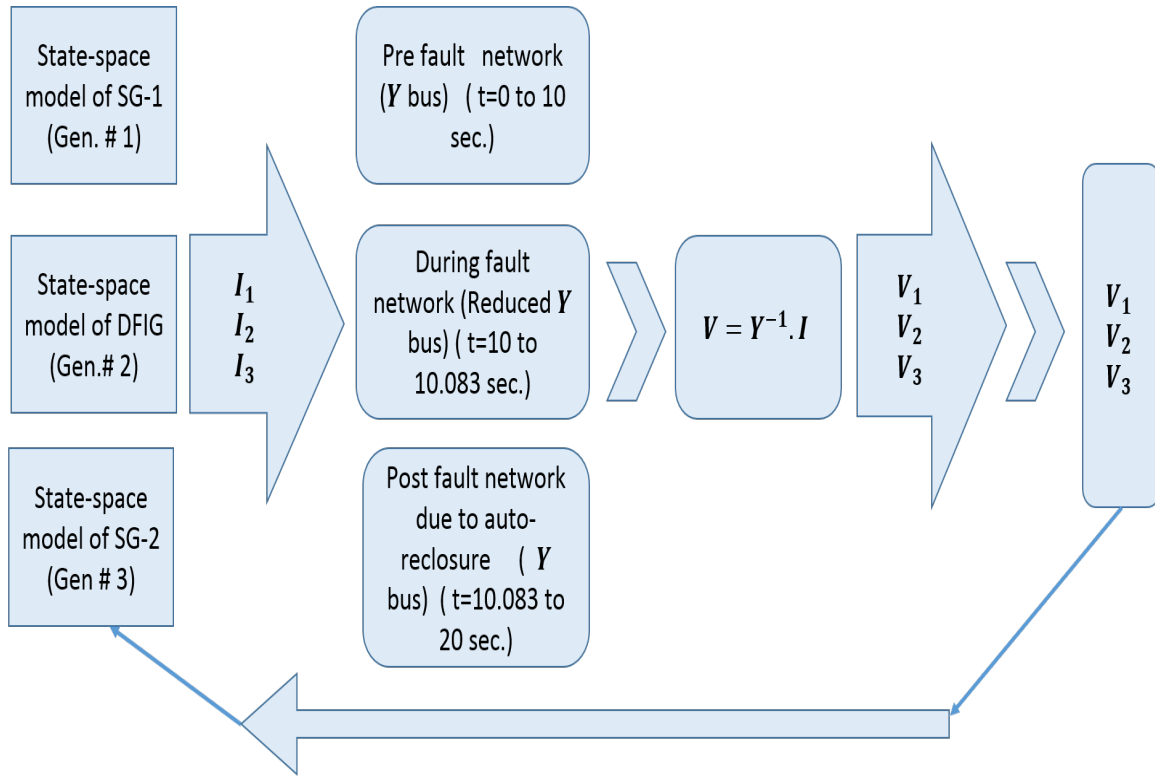


Figure 3.3: Block diagram of MATLAB/Simulink implementation of WSCC system with DFIG

The steady - state and transient conditions are simulated and various measurements are analyzed to ensure the correctness of the integration of current source generator models. It is observed that the active and reactive power, current and voltages obtained in both the systems are reasonably identical in waveshape and the magnitude mismatch is of only a few percentage. The periods before 10 s and after ~ 13 s indicate steady state behaviour for all the generators and the transient state exists between 10 s to 13 s. The results are presented, mainly focussed on transient state, for both the platforms *viz.* MATLAB/Simulink and PSCAD/EMTDC in Fig. 3.5 (for i_{abc_n}). This manifests the utility of the created MATLAB model and offers a feasibility of this model for the EKF based state estimation. Since the test system involves the participation of power system network (in terms of bus or line faults, parameter changes etc.), the generator terminal voltage variations are realized by using

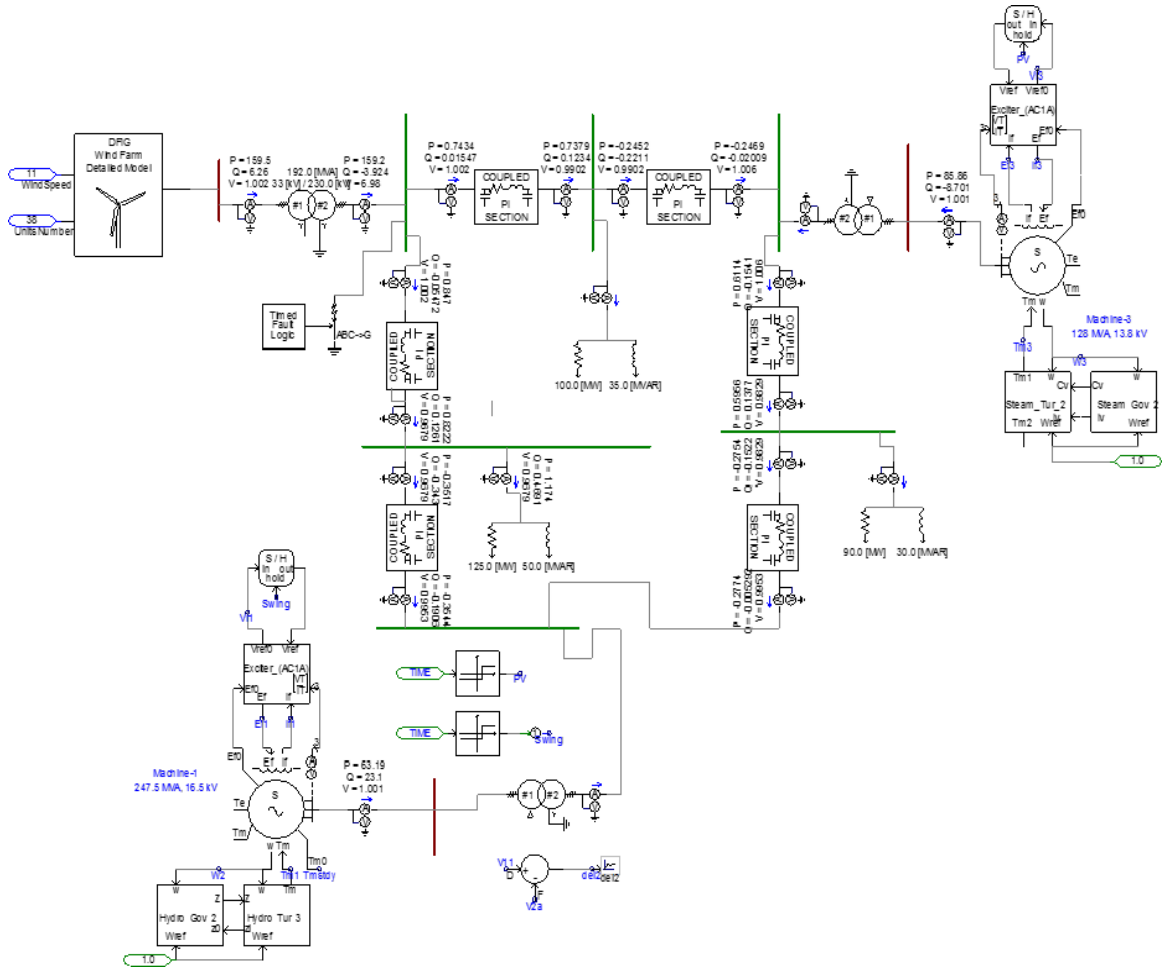


Figure 3.4: Implementation of WSCC with DFIG system in PSCAD/EMTDC

reduced Y_{bus} matrix as given below (Anderson and Fouad).

$$\begin{bmatrix} \mathbf{V} \\ \mathbf{V}_b \end{bmatrix} = \begin{bmatrix} \mathbf{Y}_{nn} & \mathbf{Y}_{nb} \\ \mathbf{Y}_{bn} & \mathbf{Y}_{bb} \end{bmatrix}^{-1} \begin{bmatrix} \mathbf{I} \\ 0 \end{bmatrix} \quad (3.11)$$

Here, $n=1..a$, a = number of generator buses ($a=3$ in this case), V_b is complex bus voltage where $b=1, 2..b$, b = total number of buses ($b=9$ in this case).

Hence, having knowledge of current vector \mathbf{I} , (3.12) can be derived using (3.11) to obtain the generators bus terminal voltage vector \mathbf{V} as,

$$\mathbf{V} = \mathbf{Y}_{reduced}^{-1} \cdot \mathbf{I}, \text{ where } \mathbf{Y}_{reduced} = (\mathbf{Y}_{nn} - \mathbf{Y}_{nb} \mathbf{Y}_{bb}^{-1} \mathbf{Y}_{bn})^{-1} \quad (3.12)$$

Based on this for presented case, the voltages (input) are fed back using $\mathbf{V} = [\mathbf{Z}_{reduced}] \mathbf{I} = [\mathbf{Y}_{reduced}]^{-1} \mathbf{I}$ as per the current changes due to fault conditions. This information is employed with the P and Q measurements available from all PMUs at the generator buses for the state estimation.

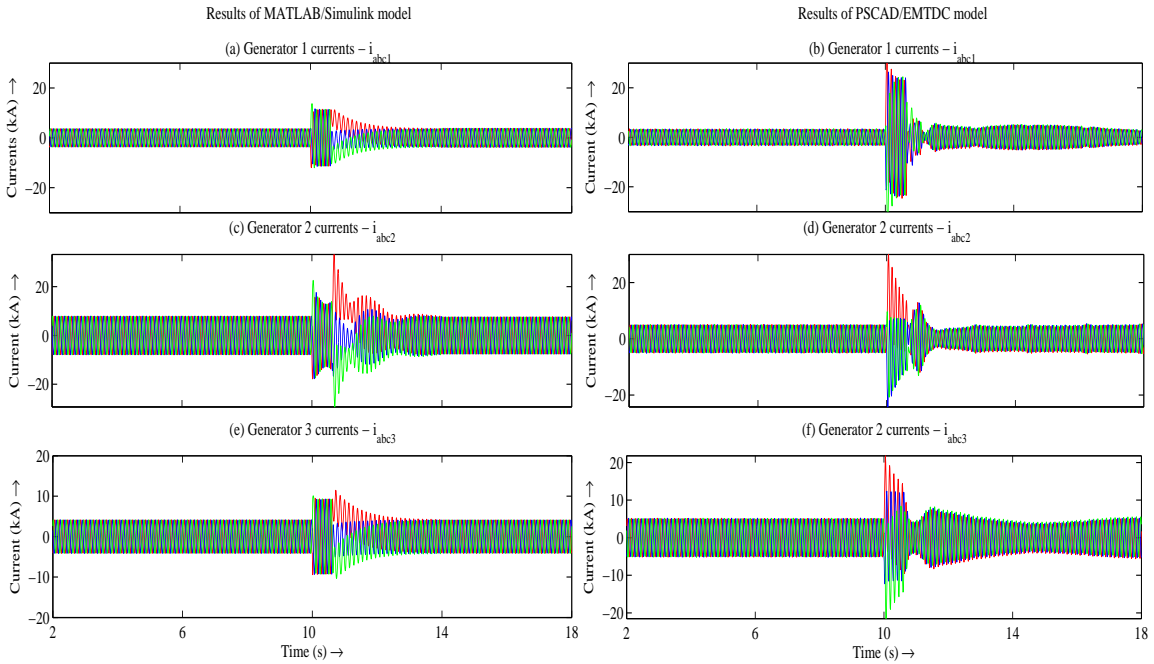


Figure 3.5: Currents i_{abc1} , i_{abc2} and i_{abc3} under steady state and dynamic condition obtained using MATLAB model and PSCAD model for (a, b) synchronous generator #1, (c, d) DFIG and (e, f) synchronous generator #3

3.1.3 Case studies

The mathematical model of a test system presented hereby involves asynchronous generator, synchronous generators and a bus network. The measurement data (corrupted with 1 % SD Gaussian noise, see Fig. 3.6) from generator buses are made available at a central data collector through PMUs. This results in implementation of model with discrete EKF based central state estimator. The striking feature of this work is the ability of centralized state estimator to simultaneously predict the dynamic states of all the generators during steady - state and in the events of transient conditions, either faults or other changes. Performance of this centralized dynamic state estimator is evaluated in this work for two specific cases *viz.* (1) a terminal fault near DFIG bus, 3-phase-to-ground fault at bus #7 and (2) a quick reduction in output active power of DFIG in the event of sudden reduction in wind speed. The states of all the generators are predicted and are discussed.

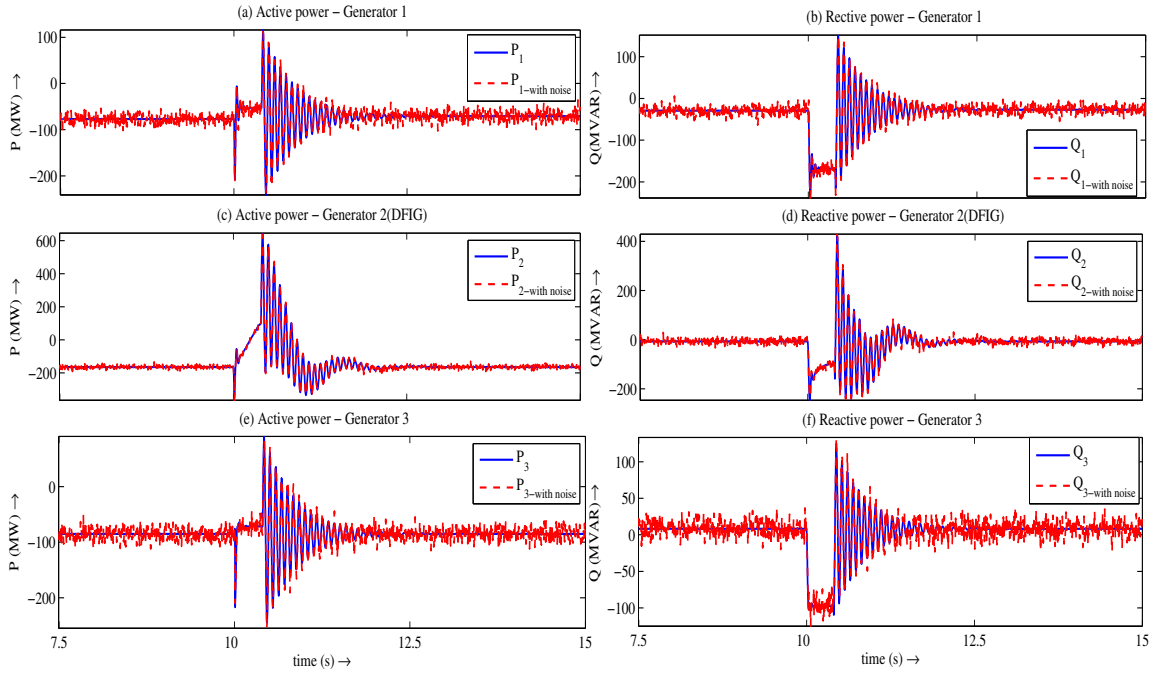


Figure 3.6: Active and reactive power measurements with 1% SD Gaussian noise

Case I: A short circuit fault near DFIG terminals

Usually, in a test system like SMIB or a multi-machine system, the state estimation of one synchronous generator is performed using Kalman approach (as in (Ghahremani and Kamwa, “Dynamic State Estimation in Power System by Applying the Extended Kalman Filter With Unknown Inputs to Phasor Measurements”). This case depicts the 3-phase-to-ground metallic short circuit fault near the induction generator bus and hence the consequent change in the bus network Y_{bus} . The fault persist only for 5 cycle duration (from $t = 10$ s) and circuit re-establishes subsequently. In the absence of current limiter circuits, oscillation in currents is observed at the instance of re-closure of breaker at the time of fault removal. It is to be noted that the DFIG behaves as a constant current source, not offering any change in its current output (voltage reduces to LVRT level, about 0.1 p.u.). Both the synchronous generator current output varies as per the new condition and the swing bus offers the most as compared to Gen. #3. All 12 current states are estimated using the P_n and Q_n as noisy measurements ($n = \text{gen. no.}$) and are depicted along with output three phase current variations. The d and q axis stator currents of synchronous generators ($i_{ds1}, i_{qs1}, i_{ds3}, i_{qs3}$) and field and damper winding currents ($i_{fd1}, i_{D1}, i_{fd3}, i_{D3}$) are successfully predicted during the network fault condition. Equally it is treated to observe the variations in DFIG states

viz. $i_{ds2}, i_{qs2}, i_{dr2}, i_{qr2}$ in Fig.3.9.

During transient condition, variation in actual state variables of Gen.# 1 i.e. $i_{ds1}, i_{qs1}, i_{fd1}, i_{D1}$ are shown in Figs. 3.7-3.8. The oscillations in attaining initial states, due to initial conditions observed in all the cases, however, quickly converges to actual states e.g. i_{ds1} as shown in Fig. 3.7(a-b) (MATLAB and PSCAD platform results). The period before 7.5 s and after ~ 15 s is the steady state behaviour of all the generators and the transient state in between, are presented for rest of the figures. These initial convergence are not depicted for rest of the cases to highlight the precise practicability of EKF algorithm during pre, during and post fault conditions. Estimation of rest of states of synchronous Gen #1 *viz.* i_{qs1}, i_{fd1}, i_{D1} are shown in Fig. 3.8(a-c).

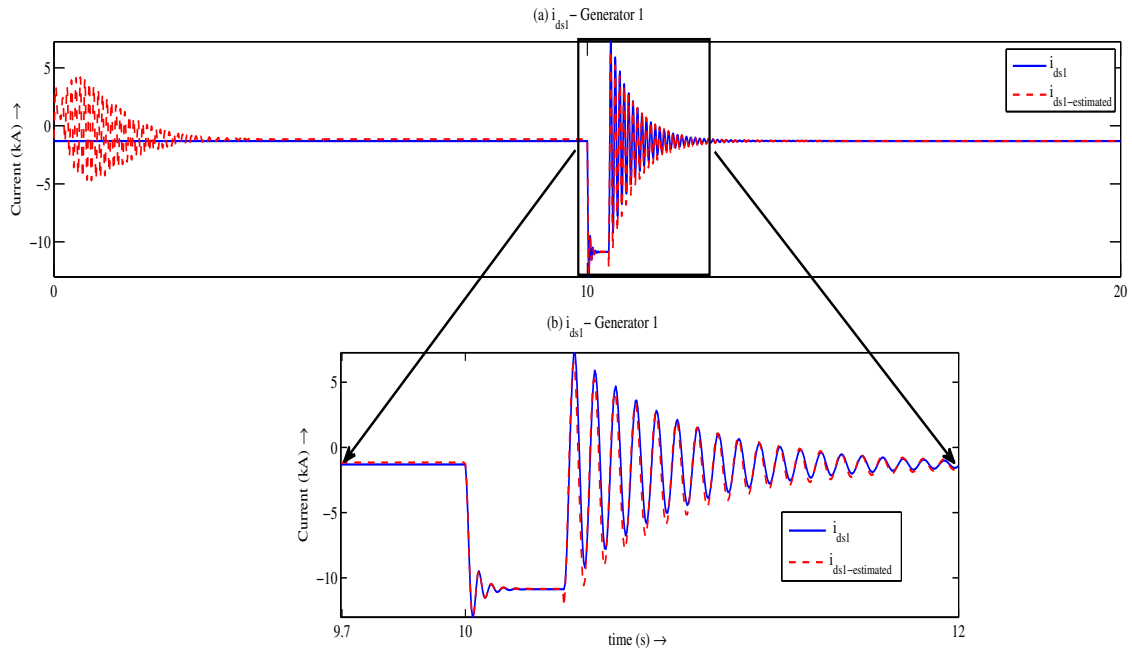


Figure 3.7: Actual and estimated i_{ds1} under steady-state and transient condition for synchronous generator #1 showing initial convergence of estimation algorithm

Further, using the PMU measurements, an accurate estimation is observed for current states of DFIG *viz.* $i_{ds2}, i_{qs2}, i_{dr2}, i_{qr2}$ and synchronous generator #3 *viz.* $i_{ds3}, i_{qs3}, i_{fd3}, i_{D3}$ as depicted in Fig. 3.9 and Fig. 3.10 respectively. From the estimation results, it is evident that with the proposed integrated model, EKF based estimator described here, estimates dynamic states of generators concurrently with accuracy in the event of bus fault.

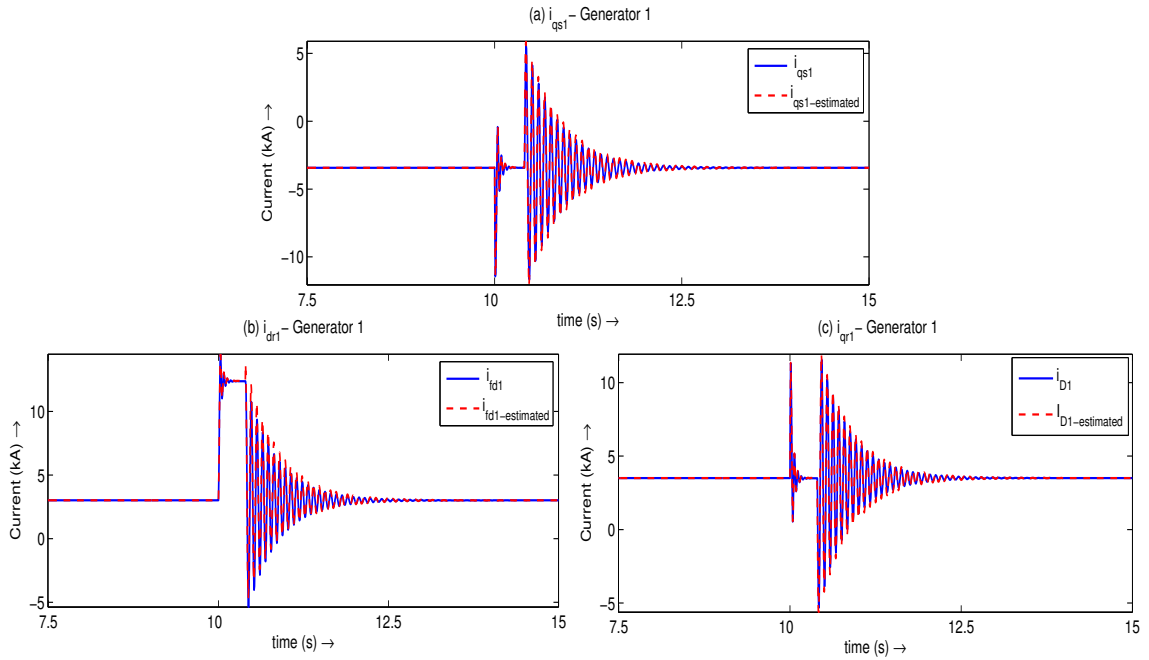


Figure 3.8: Actual and estimated i_{qs1}, i_{fd1}, i_{D1} under steady-state and transient condition for synchronous generator # 1

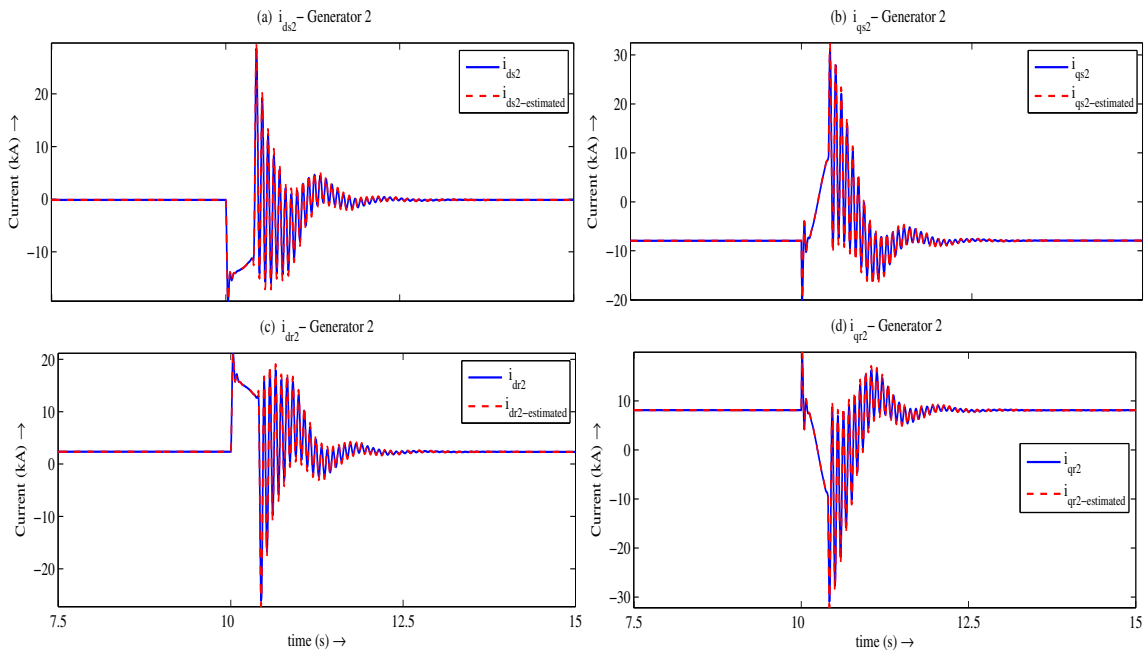


Figure 3.9: Actual and estimated $i_{ds2}, i_{qs2}, i_{dr2}, i_{qr2}$ under steady-state and fault condition for DFIG

Case II: Sudden reduction in output active power from wind generator

Stochastic nature of wind governs the output power from individual wind generator and in turn from wind farm. A dynamic condition is simulated and analyzed where

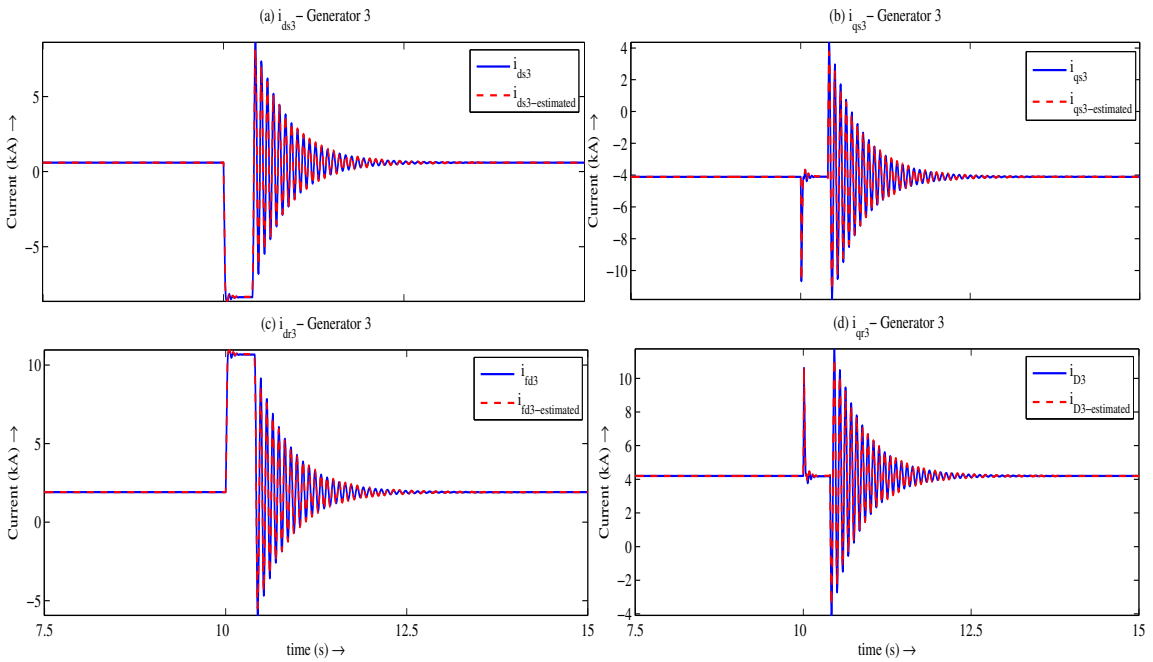


Figure 3.10: Actual and estimated i_{ds3} , i_{qs3} , i_{fd3} , i_{D3} under steady-state and fault condition for synchronous generator #3

due to sudden reduction in wind speed and hence, the input mechanical power to wind turbines of wind farm, the output active power from wind generator suddenly reduces by 50% at simulation time instant $t = 10$ s. The wind farm continues to feed the grid in this condition for the remaining simulation period. It is apparent that sudden reduction in the wind power generation, with load maintained as before, the synchronous generators in the system are required to meet the prevailing load. The states of all the generators are affected due to the change and is to be estimated by the discussed multi-machine model.

For the case under discussion, DFIG now delivers 81.5 MW of active power, in the reduced wind speed condition. It is important to notice that majority of active power deficit is supplied by the swing bus (as shown in Fig.3.11) due to large load at bus #5 and overall less line impedance. An insignificant change is observed in delivery of active power from generator #3 and reactive power from all three generators.

The effect of generation change from each generator is apparent in reduction in wind power on all the state variables. Change in output active power causes substantial variation in d and q axis currents of stator and rotor belong to Gen. #1 and Gen. #2 and a modest change is observed for Gen. #3. Changed active and

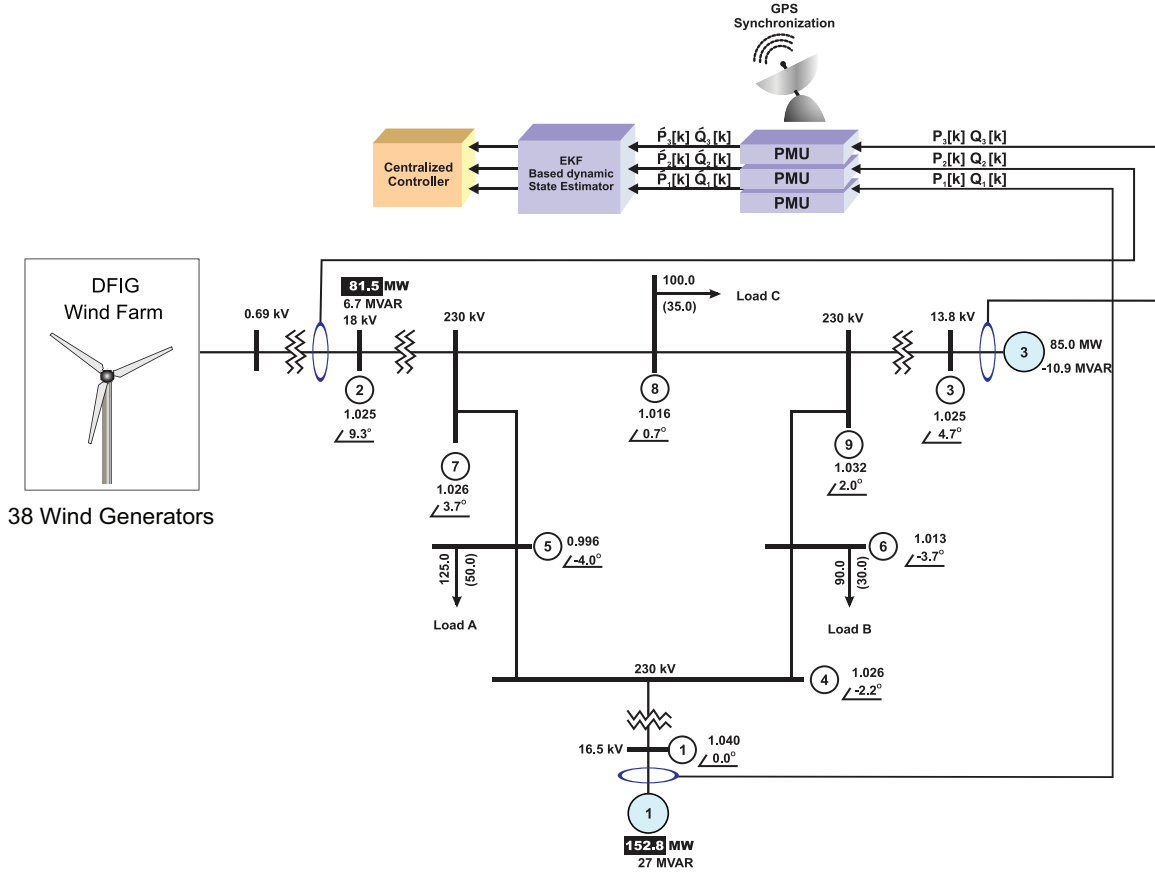


Figure 3.11: WSCC 3-generator 9-bus system in steady state with sudden 50% reduction in output active power of DFIG wind farm

reactive power injected to generator bus #1, #2 and #3 are measured using PMUs and are given as input, with an added noise, to EKF based estimation algorithm. From Fig. 3.12, it is observed that, for all four current quantities of Gen. #1, satisfactory estimation is achieved with the help of proposed model and EKF.

The centralized dynamic state estimator simultaneously estimates dynamic states of DFIG (Gen. #2) as Fig. 3.13. The state estimator removes the measurement and process noise and faithfully estimates the DFIG states. The active power compensation offered by swing and other synchronous generator is clearly traced by the estimator and the quantities with appropriate changes are shown in Fig. 3.12 and 3.14.

Important to note that having achieved accurate dynamic current states of all generators using (3.10) active and reactive power output can be derived easily for all generators. This consequently offers an added advantage to achieve other important dynamic states of synchronous generator *viz.* load angle- δ , rotor speed - ω , tran-

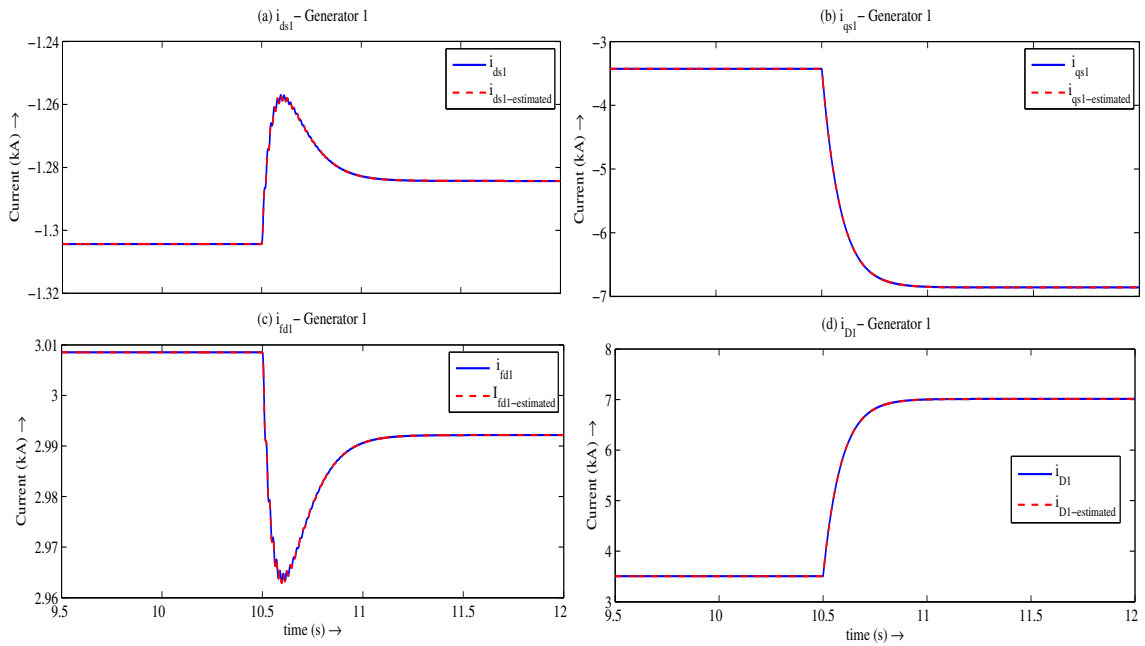


Figure 3.12: Swing generator #1 current states - actual and estimated, due to output active power reduction in DFIG

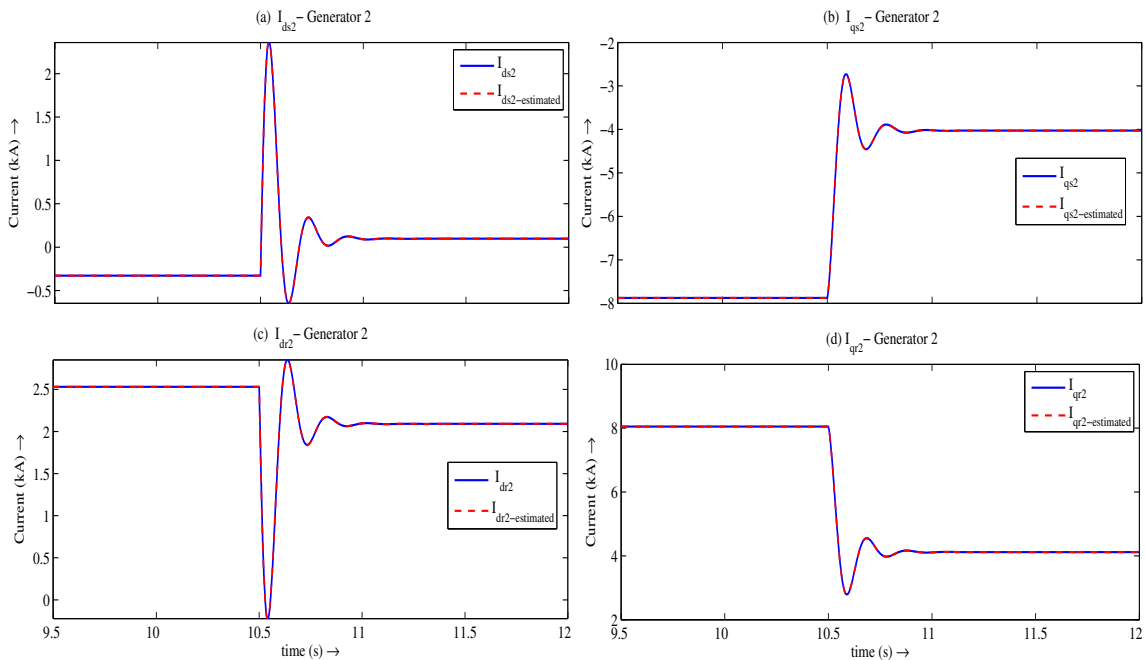


Figure 3.13: DFIG current states - actual and estimated, due to output active power reduction in DFIG

sient voltage behind d axis - E'_d and transient voltage behind q axis- E'_q in real time using standardized equations (Kundur, Balu, and Lauby). Similarly, knowledge of dynamic states of DFIG can help to obtain its other dynamic states *viz.* rotor speed-

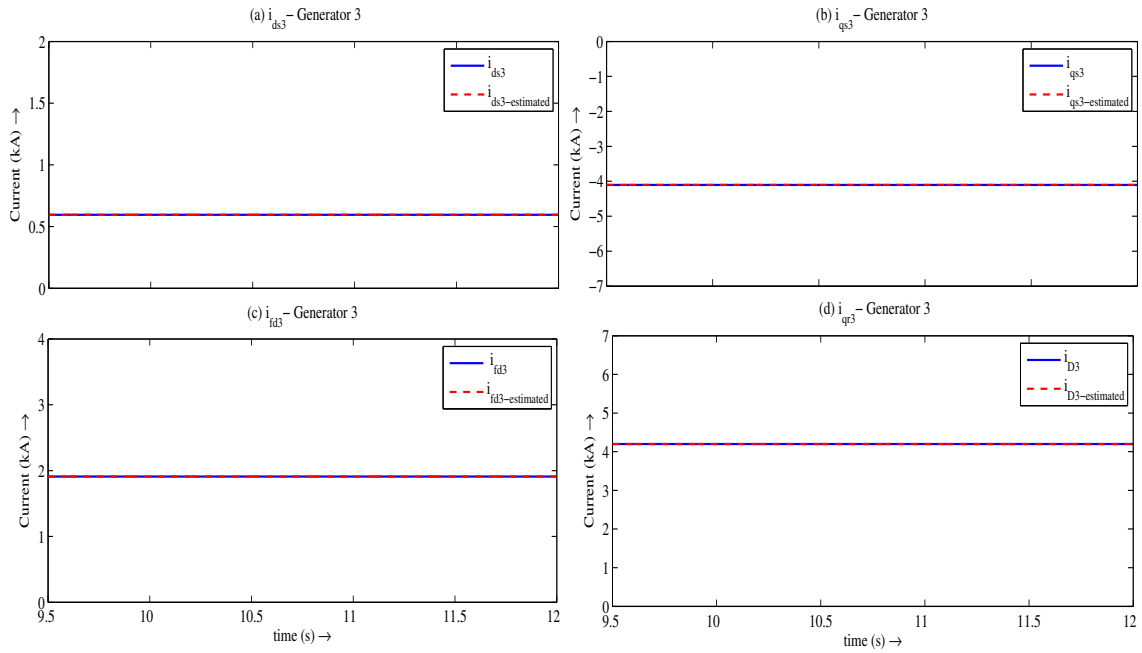


Figure 3.14: Synchronous generator #3 current states - actual and estimated, due to output active power reduction in DFIG

ω_r and capacitor voltage - v_{dc} (Ekanayake, Holdsworth, and Jenkins EL-Hagry and Eskander).

In summary, the simulation results in Fig. 3.7 to Fig. 3.14 show quite convincingly that the estimated states can track the actual responses, relatively well, under nonlinear simulations with proposed state-space model. This satisfactory estimation results endorses the use of proposed state-space model to build centralized coordinated dynamic state estimator using EKF which can estimate dynamic states of synchronous generators and DFIG concurrently. With the help of PMUs, this approach can give boost to idea of global centralized approach for control and stability of wide power system having significant penetration of wind energy.

3.2 UKF based centralized concurrent DSE of multi-machine system

3.2.1 UKF as a DSE tool

Though EKF has been accepted widely as DSE tool, it suffers from few limitations. Generally encountered limitation in implementing EKF are,

- **Linearization error**

With highly nonlinear and complex mathematical model, especially in large power system, inherent Jacobian implementation while prediction of dynamic states there exist a potential for linearization error. Once it exist, due to imbibed nature of EKF, it will result in cascading effect. This results in divergence of EKF and provides erroneous results of DSE.

- **Computation time**

EKF employs Jacobian matrices calculation for prediction of state from one instance to the next one. In case of large power system, calculation of Jacobian matrices take much time. High computation time leads to a paradox to requirement of DSE which itself offers information and trends of fast changing dynamics in real time. This aspect constraints application of EKF as DSE tool, especially for large power system.

To overcome limitation of EKF, approach of UKF is proposed for DSE which works on principle of unscented transform (UT) to achieve estimation of dynamic states (Julier, Uhlmann, and Durrant-Whyte). DSE for multi-machine power system (WSCC 3-generator 9-bus system) incorporating synchronous generators is detailed by (Valverde and Terzija Wang, Gao, and Meliopoulos). Implementation of UKF in multi-machine power system to estimate dynamic states of only DFIG which is integrated with conventional synchronous generators is presented in (S. Yu, “Realization of State-Estimation-Based DFIG Wind Turbine Control Design in Hybrid Power Systems Using Stochastic Filtering Approaches” S. Yu, “State Estimation of Doubly Fed Induction Generator Wind Turbine in Complex Power Systems”). This section of work presents the centralized DSE of synchronous generators and DFIG simultaneously using UKF. Detailed algorithmic steps have been presented in many literatures, hence only important steps of UKF algorithm for DSE is narrated in **Appendix D**.

3.2.2 Simulation preliminaries

In this section, to present a case, standard WSCC 3-generator 9-bus system is selected. Alike first section, enhanced wind energy penetration is simulated by replacing generator # 2 with equal rating of consolidated wind farm as shown in Fig. 3.15.

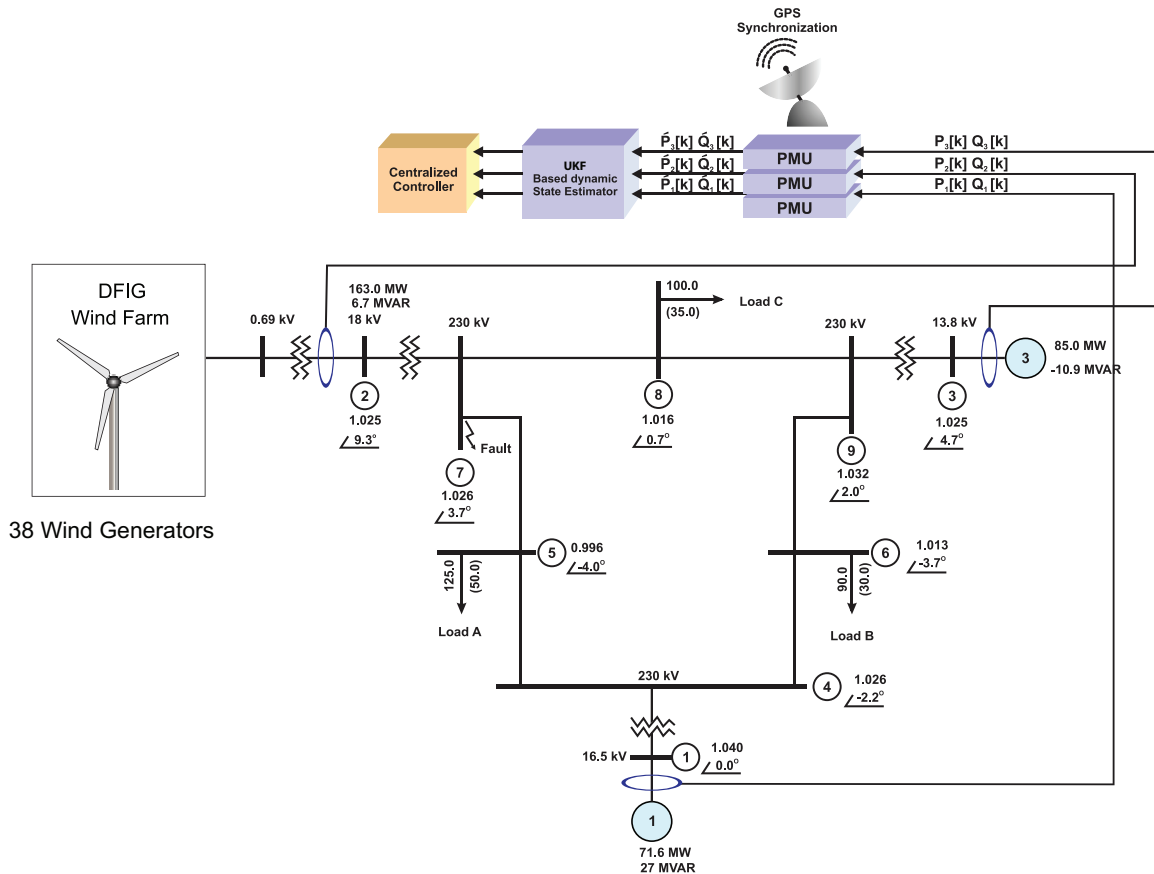


Figure 3.15: WSCC three-generator nine-bus test system, where synchronous gen. #2 is replaced with equally rated DFIG based wind farm

All simulation aspects of MATLAB/Simulink model of WSCC system are similar to the presented in first section of this chapter. Dynamic condition adopted as well as mathematical modelling for implementation of WSCC system for UKF is identical to first section. The focus of this section is the UKF implementation in state estimation and related discussion.

3.2.3 Simulation results and discussion

After 3-phase-to-ground metallic short circuit fault near bus #7 on transmission line # 5-7 (Fig.3.15) at $t=10$ s, fault is cleared by reclosure of circuit breakers on both sides of transmission line. During pre-fault, during fault and post-fault conditions, active and reactive power measurements are collected by PMUs installed at all generator buses as shown in Fig. 3.15. Similar to first case, all measurements are corrupted with Gaussian noise having 1% of standard deviation. All measurements are given to UKF based centralized dynamic state estimator to achieve DSE of all dynamic states

of all generators. The i_{ds} , i_{qs} , i_{dr} and i_{qr} are the dynamic states to be estimated for DFIG and i_{ds} , i_{qs} , i_{fd} and i_D are the dynamic states to be estimated for remaining two synchronous generators using UKF. The estimation results obtained using UKF are presented in Fig. 3.16, Fig. 3.17 and Fig. 3.18.

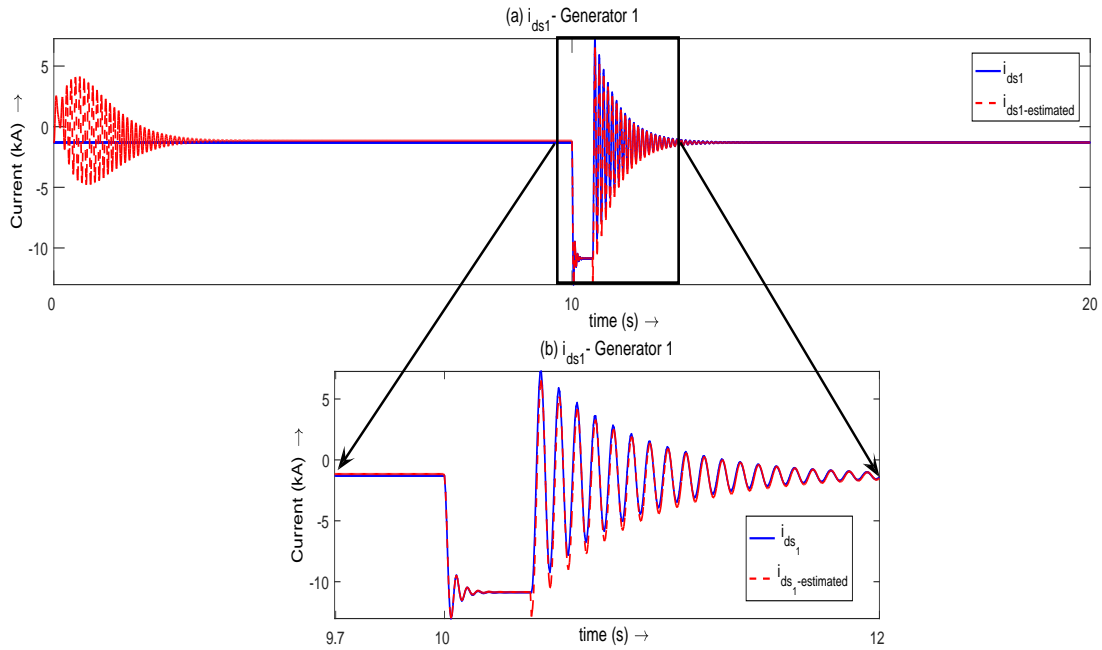


Figure 3.16: Actual and estimated i_{ds1} under steady-state and transient condition for synchronous generator #1 showing initial convergence of estimation algorithm

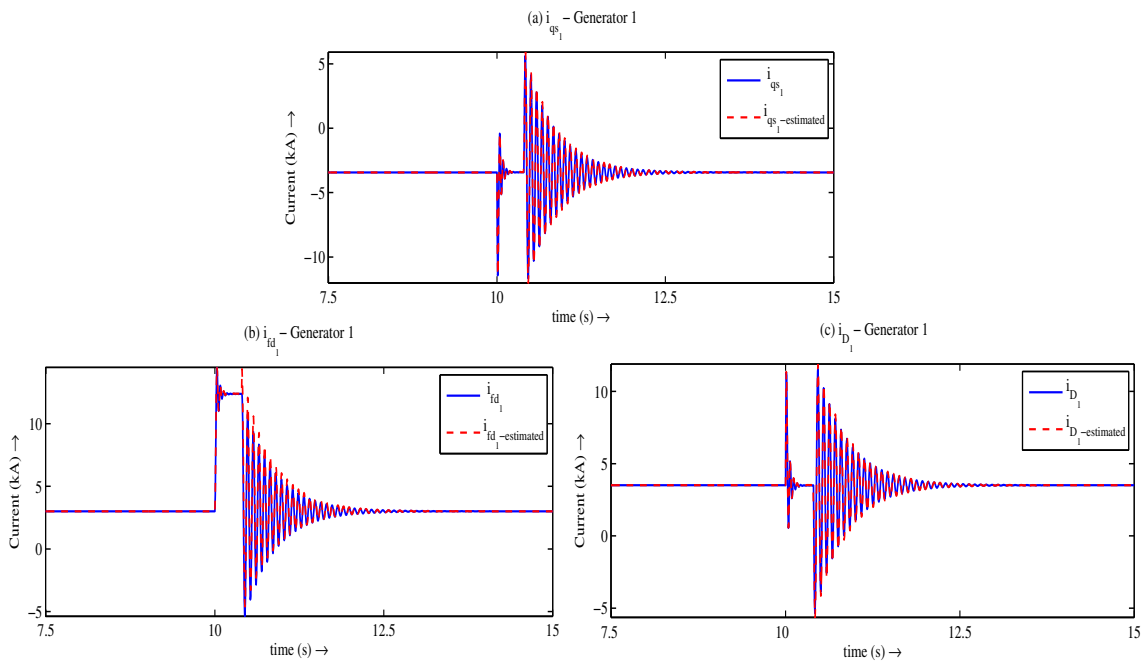


Figure 3.17: Actual and estimated i_{qs1} , i_{fd1} , i_{D1} under steady-state and transient condition for synchronous generator #1

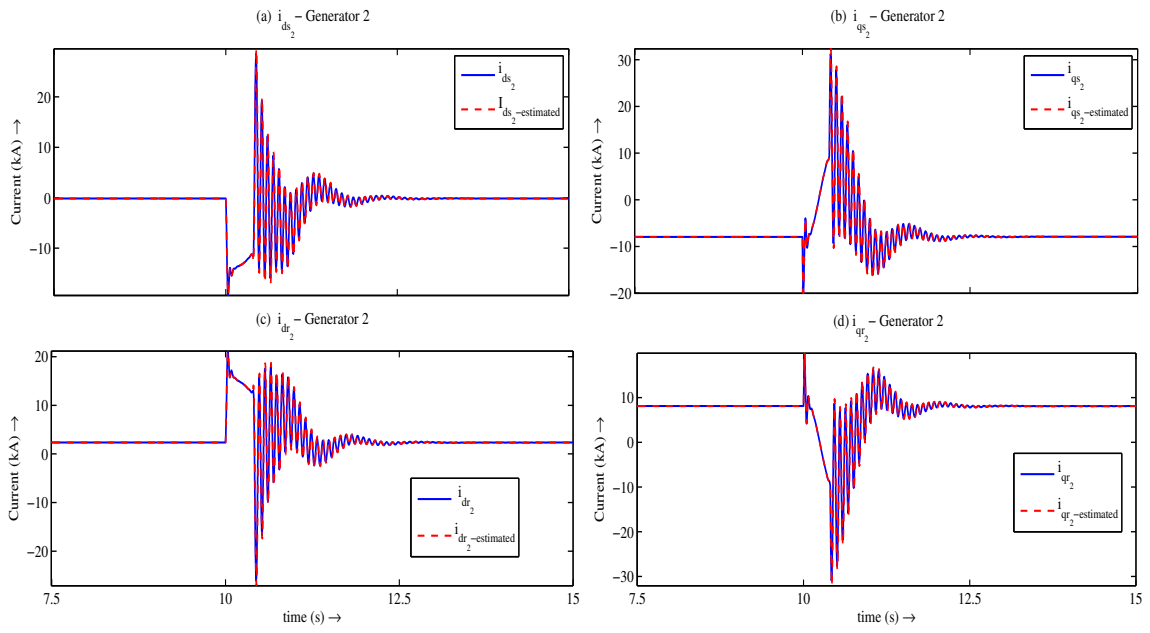


Figure 3.18: Actual and estimated $i_{ds_2}, i_{qs_2}, i_{dr_2}, i_{qr_2}$ under steady-state and fault condition for DFIG

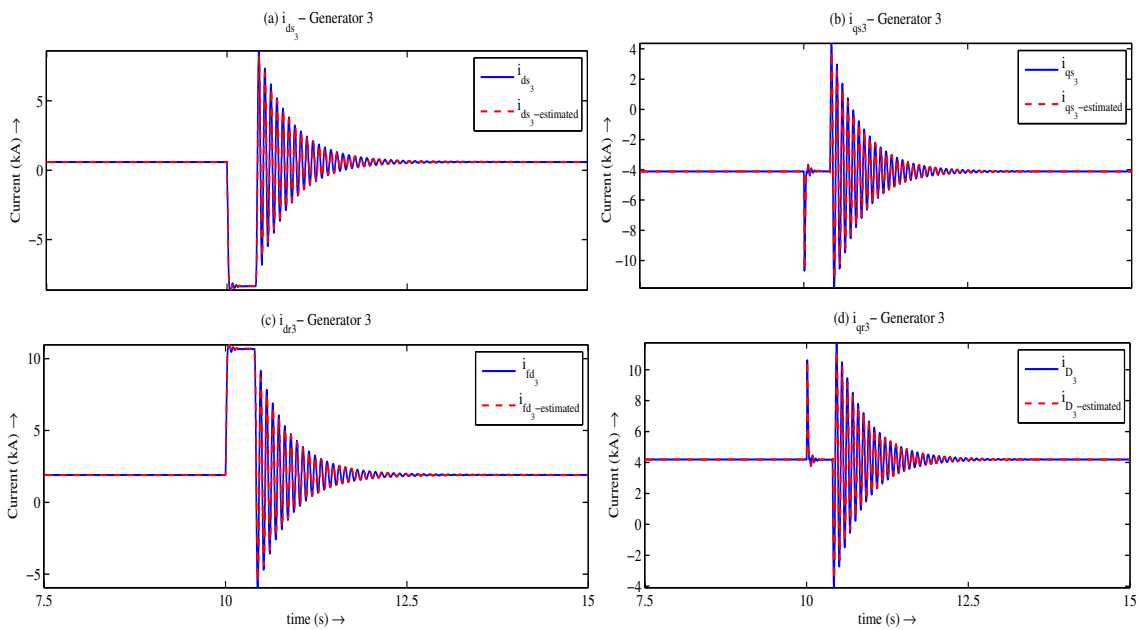


Figure 3.19: Actual and estimated $i_{ds_3}, i_{qs_3}, i_{fd_3}, i_{D_3}$ under steady-state and fault condition for synchronous generator #3

Prior knowledge of accurate initial values of estimated states (12 states in this case) is the phenomenon does not exist always. As shown in Fig.3.16(a), assumption of initial value of state is different (taken 5 % of initial deviation), and hence, UKF based

estimation depict initial oscillations and converges within very short time duration as can be observed for one case of i_{ds1} for generator #1. Accurate estimation of i_{ds1} displaying the capability of UKF based DSE tool, under dynamic condition, can be seen in Fig. 3.16(b) for pre-fault, during fault and post-fault conditions. Authentic estimation is observed for other states of generator #1 *viz.* i_{qs1} , i_{fd1} and i_{D1} as shown in Fig.3.17.

Employment of proposed current source model is for centralized concurrent DSE using UKF is further enforced by observing estimation results of generator # 2 (DFIG) and generator # 3 (SG) as shown in Fig.3.18 and Fig. 3.19 respectively. Result prove that with proposed current source model, dynamic states of both kind of generators i.e. synchronous generators and DFIGs can be estimated, concurrently, using both Kalman filter based estimation tools *viz.* EKF and UKF.

3.3 Observations on comparative performance of EKF and UKF

Successful concurrent DSE for synchronous generators and DFIG is achieved employing EKF and UKF. EKF and UKF both are equipped with their own *pros* and *cons*. It is important to investigate and analyze performance aspects of both DSE tools which are significant for concurrent dynamic state estimation, which subsequently helps to decide their applicability to most suitable condition for optimum results.

1) Root mean square error (RMSE) comparison

To evaluate the performance of EKF and UKF, standard RMSE approach is adopted. RMSE method commonly used to avail the information regarding error between values predicted by estimation algorithm and actual values obtained from the actual model. RMSE approach is presented by,

$$RMSE = \sqrt{\frac{\sum_{i=1}^n (x_{actual_i} - x_{estimated_i})^2}{n}} \quad (3.13)$$

where i represents particular instance, n is total number of samples. Individual difference at instance i , $(x_{actual_i} - x_{estimated_i})$ is the residual. However, RMSE aggregates individual residuals to represent single entity which symbolizes accuracy of predictions.

To represent a case, 12 states of 3 generators *viz.* SG #1 , DFIG and SG #3 is presented here in its entirety. Initial oscillatory nature of DSE is due to normally arbitrary initial values of states. This condition can be avoided in case of knowledge of initial states. Hence, sample size of $n = 4000$ is taken excluding condition dependent initial oscillatory span to precisely check RMSE of EKF and UKF. In accordance to (3.13), \mathbf{x}_{actual} is a vector comprised of original values of all 12 states at instant i . Similarly $\mathbf{x}_{estimated_i}$ represents vector of estimated output of all 12 states using EKF and UKF respectively. The RMSE obtained for all 12 states are shown in Table 3.1. It is important to note that, all RMSE are presented as normalized percentage value

Table 3.1: Comparison of RMSE for EKF and UKF

State	% RMS Error for EKF	% RMS Error for UKF
i_{ds_1}	13.36795	16.32879
i_{qs_1}	2.98479	5.11601
i_{fd_1}	5.40765	6.69298
i_{D_1}	2.85792	4.89716
i_{ds_2}	15.67944	33.42504
i_{qs_2}	2.73335	5.71519
i_{dr_2}	8.19939	17.47713
i_{qr_2}	2.61697	5.47068
i_{ds_3}	10.43923	38.38857
i_{qs_3}	1.18061	4.56137
i_{fd_3}	2.44148	8.98722
i_{D_3}	1.13025	4.36593

with reference to their steady state value. For standard two area system (Kundur,

Balu, and Lauby) comprised of synchronous generators, accuracy of EKF over UKF is endorsed by (Zhou et al.).

Results presented in Table 3.1 emanates the fact that in case of limited bus power network (9-bus system) incorporating DFIGs, EKF based centralized concurrent DSE also reflects better accuracy as compared to UKF. For almost all states observed error differences of both EKF and UKF are insignificant. However, Large RMS errors in a few states is mentioned in Table 3.1. This is due to algorithmic limitations of UKF approach as highlighted in (Zhou et al.). Considering detailed (or higher order) modelling (at the cost of time involved in estimation) with insignificant measurement noise would help to reduce these RMS errors.

2) *Estimation time during fault*

DSE results are obtained using measurements from PMU with 0.001 s of measurement update rate. It may be noted that as the no. of states to be estimated increases, the time required for estimation too shall increase and *vice versa*. It becomes difficult to provide sample-wise time calculations per state due to algorithm initializations, time required for adding noise and loading of samples etc., and hence average estimation time is presented.

Once measurement data are available to dynamic state estimator, DSE algorithm must be able to produce accurate estimates in shortest possible span. This feature results in information about critical states ahead of its measuring counterpart. Use of information of dynamic states achieved in advance, can be a boon for better monitoring and control. This section evaluates estimation time taken by EKF and UKF algorithms for centralized concurrent estimation.

Estimation time is calculated only during dynamic condition of fault. The dynamic condition of fault is same as mentioned in Section 3.1.3 (Case I). To present a case, from $t= 10$ s to $t=10.083$ s (for 84 measurements at the measurement update rate of 0.001 s) time to estimate all 12 states employing EKF and UKF is determined. The average time of estimation is derived from total estimation time required for 84 samples. Result are tabulated in Table 3.2. It is important to note that, all results

Table 3.2: Comparison of estimation time

	Total estimation time for 84 measurements (t = 10.0 s to 10.083 s)	Average estimation time
EKF	13.0499 s	0.1554 s
UKF	21.0371 s	0.2504 s

are obtained using MATLAB 8 R2014b platform with Intel Core i7-4500 CPU 1.80 GHz processor supported by 8 GB of RAM. Results highlight the fact that in case of centralized concurrent DSE for 12 dynamic states of synchronous generators and DFIG, EKF takes lesser time as compared to UKF. These results are in affinity to the case of synchronous generators presented in (Zhou et al.). However for large power systems, having large number of buses and associated dynamic states, due to need of linearization through Jacobian calculation may incur more estimation time for EKF than UKF.

3) *Convergence time with initialization errors*

For DSE process in power network, initialization of dynamic states is done using steady state results achieved by load flow. However, accurate information regarding initial values of non-measurable states of power network is not the condition which frequently prevail. In such cases, approximate values of initial states are assumed employing postulations and knowledge of network synthesis. Hence, it becomes significant to investigate the performance of DSE tools, based on aspect of convergence time, with different initialization error as a consequence to assumption of initial values of dynamic states. Important to note that convergence time is derived using same processing hardware capability mentioned in previous case.

The investigation on convergence time is carried out for EKF and UKF with three cases *viz.* 10%, 20 % and 30% of initialization error in dynamic states respectively. DSE is carried out afterwards. In methodology adopted, maximum tolerance considered in settling is $\epsilon_t = 5\%$. With initial state value error of 10 %, 20 % and 30

%, time up to convergence of differential state vector ($\hat{\mathbf{x}} - \mathbf{x}_{actual}$) for 12 states lesser than ϵ_t is noted and results are presented as shown in Table 3.3.

Table 3.3: Comparison of convergence time with different % of initialization error

Initialization error	Convergence time for $(\hat{\mathbf{x}} - \mathbf{x}_{actual}) < \epsilon_t$	
	EKF	UKF
10 %	3.293 s	6.322 s
20 %	3.641 s	6.439 s
30 %	3.927 s	6.729 s

Results indicate, unscented transform based UKF takes more time to converge for all 12 states to tolerance level ϵ_t . Result endorses, use of EKF is preferable, over UKF, for small system involving reasonable non-linearity of state-space model.

3.4 Conclusions

The research in the domain of simultaneous DSE of multiple generators in a multi-machine test system is presented in this work. A synchronous generator current source model is presented using the asynchronous generator (DFIG) current source model as base model. The work depicts the integration of synchronous and asynchronous generators' integration with the power system network. The mathematical approach for the integration is validated against results from PSCAD platform. Assuming power measurement data availability using PMUs, installed at generator buses, this work proposes to estimate the current states of all the generators. The presented mathematical approach, combined with EKF based dynamic state estimator offers noise removal as well as the predictability. The performance of estimation algorithm for the state-space model is tested under dynamic conditions *viz.* network fault and sudden change in DFIG output. Results embedded in the section prove that EKF based estimator, with proposed mathematical model, track dynamic states precisely and concurrently for all generators. Expansion in this approach for wide power system having larger integration of renewable can be helpful to EMS operator, to acquire

information of internal dynamic states and future trends of generators for better monitoring and control of power system i.e. a real time wide area monitoring. Results of centralized concurrent DSE of synchronous and asynchronous generators' using UKF approach endorses use of presented model for DSE employing multiple Kalman filter based DSE tool. Comparative investigation for EKF and UKF for root mean square error (RMSE), estimation time during dynamic condition of fault and convergence time to different errors in initialization of state is presented. Results defend use of EKF over UKF for comparatively smaller and unremarkable non-linear system.

Postscript : DFIG based wind generator is installed, on-shore or off-shore, operates in adverse environmental conditions. Moreover, the operation of DFIG is emphatically dependent on various voltage and current sensors used inside the DFIG. Significant dependence of DFIG operation on internal sensors opens up new debate of possibility of its faithful operation under sensor mal-operation, either current sensors or voltage sensors. Can dynamic state obtained in real time provide solution this problem ? Next chapter deals with application of DSE to overcome mal-operation of DFIG under the condition of erroneous sensor function.

Chapter 4

Application of EKF based DSE for DFIG under Faulty Current Sensor Measurements

4.1 Introduction

Increasing presence of wind power has made it essential for EMS operator to have knowledge of dynamic states of conventional as well as induction generators. Reason for increasing avenues of research in dynamic state estimation (DSE) for DFIG states is its highly nonlinear model, involving complex equivalent circuit, existence of converters as well as controllers (Khedher, Khemiri, and Mimouni). El-hagry and Eskander presented estimation of i_{ds} , i_{qs} , i_{qr} and ω_r (rotor speed) using EKF over sub-synchronous to super-synchronous speed range of DFIG while employing i_{ds} , ω_r and capacitor charging current - i_{dc} as measurement variables (EL-Hagry and Eskander). Further, estimated i_{ds} , i_{qs} , i_{qr} and ω_r of DFIG are used to derive v_{ds} , v_{qs} , v_{dr} and v_{qr} . These derived variables are consequently used in the control loop to obtain control parameters to regulate rotor voltage and rotor position of DFIG (EL-Hagry and Eskander). Estimation of five states of DFIG *viz.* i_{dr} , i_{qr} , i_{ds} , i_{qs} , ω_r and a parameter J (moment of inertia) using EnKF is documented (Fan et al.). Here, Fan *et. al.* gives insight to parameter calibration along with estimation of parameter. Sensitivity of EnKF algorithm to different measurement noise levels, initial state and parametric errors are discussed in (Fan et al.). With the help of state space model

of DFIG with reference to stationary axis *viz.* α and β , DSE of stator and rotor current I_α and I_β , rotor speed ω_r and its position, θ with augmented integrals of I_α and I_β is conceptualized using EKF for SMIB system in (Malakar, Tripathy, and Krishnaswamy). In IEEE-39 bus system, dynamic states of DFIG (which is connected to an additional bus # 40) is estimated using UKF in (S. Yu, “State Estimation of Doubly Fed Induction Generator Wind Turbine in Complex Power Systems”). It uses measurement data of voltage phasor and current phasor obtained by PMU installed at bus # 40. Along with comparative performance of EKF and UKF for DSE of DFIG dynamic states, solution is proposed to overcome condition of bad measurement. In work suggested by Yu *et. al.*, algorithm is proposed using normal innovation ratio to detect outliers (bad data) in measurement data as well as in the pseudo-input variables derived using PMU data. After detection of bad data, that bad data and/or pseudo-input variables are discarded and replaced with corresponding data available at previous instant (“State Estimation of Doubly Fed Induction Generator Wind Turbine in Complex Power Systems”).

With the sudden variations in active and reactive powers supplied to point of common coupling (PCC), control circuit of DFIG undergoes rapid variations of different control variables. Quick and frequent changes in control variables is also supported by fast operation of sensors. This may cause mal-operation or failure of sensors. For better stability and control of DFIG, knowledge of accurately estimated dynamic states offers an opportunity to explore in case of a mal-functioned current sensor conditions. The noisy measurement case, measurements with outliers and condition of measurement data unavailability are simulated for faulty current sensor operations. Output of EKF based estimation algorithm is proposed as substitute of mal-functioned current sensor measurements for controlling of DFIG rotor circuit behaviour. In brief, application of estimated output using EKF algorithm for better control of DFIG based wind power forms core of presented work in this chapter.

4.2 Mathematical Approach for DSE of DFIG

The DFIG in an SMIB system, described in Fig. 2.1, is considered here for the discussion.

Generally, DFIG operating speed is restricted to $\pm 30\%$ of synchronous speed.

During wide variations in speed, two main components *viz.* rotor side converter (RSC) and grid side converter (GSC) play significant role in injecting power at grid frequency. In the present research, rotor side control circuit is presented for analysis. Operation of RSC control circuit is explained through block diagram representation in Fig. 4.1. The $P^*, Q^*, i_{qr}^*, i_{dr}^*, v_{qr}^*$ and v_{dr}^* represent pre-determined and/or derived reference signals.

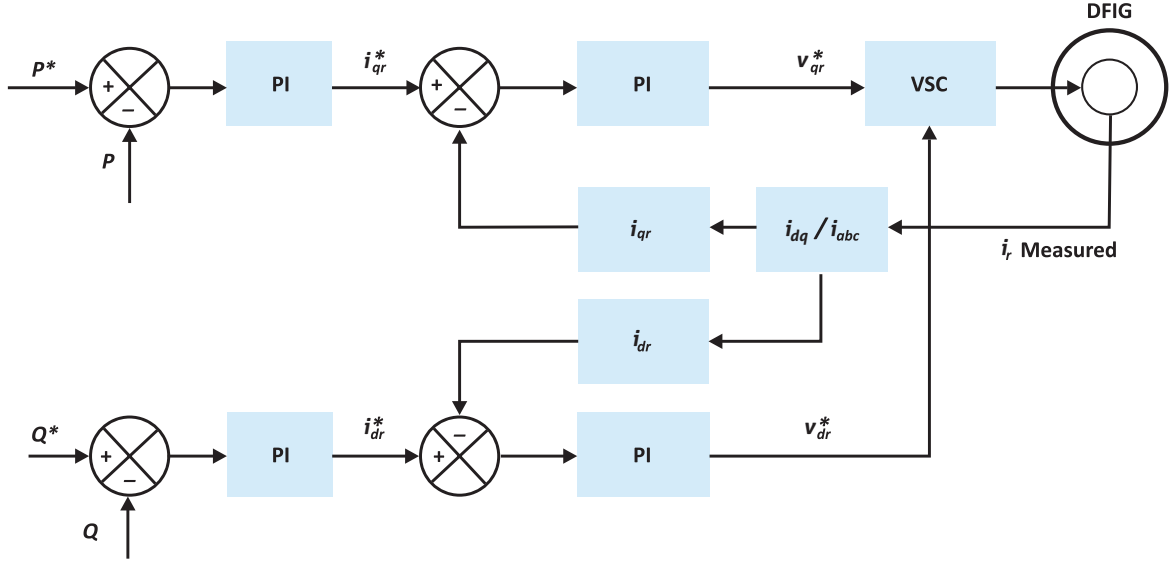


Figure 4.1: Rotor side converter (RSC) control circuit for DPC

Considering stator field oriented (SFO) DFIG operation, the stator direct axis voltage is assumed to be $v_{ds} = 0$. SFO allows decoupled control of P and Q by employing measurement signals i_{qr} and i_{dr} respectively as shown in Fig. 4.1.

Total simulation duration considered is 6 s for all the cases. Relatively small simulation period supports consideration of wind speed to be constant during simulation. The dynamics and mathematical modelling of mechanical components of system are not been focused. However, it is possible to perform the estimation of desired variables provided, a state-space model adaptable to EKF algorithm is employed. Currents entering in to machine are positive i.e. motoring conventions are adopted for the DFIG operation as denoted in Fig. 2.1. As shown in control circuit (Fig. 4.1), outer measurement loop continuously monitors P and Q , whereas for RSC operation rotor current i_r is observed continuously by inner measurement loop using current sensor. The rotor current measurements i_{dr} and i_{qr} are fed to the RSC circuit to control active and reactive power output. Primary focus of presented work is application of resulting (estimated) states (as EKF output) for controlling of rotor power. EKF

algorithm runs concurrently with DFIG operation and provides estimated dynamic states using measurement data collected using PMU i.e. in this case active and reactive power output of DFIG. The linearized operation of converters, controllers and control circuit is considered as the parameter variations are slower as compared to controller actions.

The voltage and flux linkage equations for the DFIG as an induction machine are available in (Ekanayake, Holdsworth, and Jenkins Bourdoulis and Alexandridis), and presented in Chapter #2 are used for simulation objective (2.1-2.3).

Rotor current components *viz.* direct and quadrature axis components, are the vital variables to control active and reactive power output of DFIG (Wu et al., “Decentralized Nonlinear Control of Wind Turbine With Doubly Fed Induction Generator”). These currents are considered here as state variables along with direct and quadrature axis components of stator current. Differential equations presented in Chapter #2 (2.4) are utilized here, hence not presented again. Active and reactive power output of DFIG, acquired from PMU, are used as measurement variables for EKF based DSE. Stator active and reactive power of DFIG is presented as,

$$\begin{aligned} P_s &= \frac{3}{2}(v_{ds}i_{ds} + v_{qs}i_{qs}) \\ Q_s &= \frac{3}{2}(v_{qs}i_{ds} - v_{ds}i_{qs}) \end{aligned} \quad (4.1)$$

Rotor active and reactive power is given by,

$$\begin{aligned} P_r &= \frac{3}{2}(v_{dr}i_{dr} + v_{qr}i_{qr}) \\ Q_r &= \frac{3}{2}(v_{qr}i_{dr} - v_{dr}i_{qr}) \end{aligned} \quad (4.2)$$

Total active and reactive power output from DFIG is formed by following equations,

$$\begin{aligned} P &= \frac{3}{2} \underbrace{(v_{ds}i_{ds} + v_{qs}i_{qs})}_{P_s} + \underbrace{(v_{dr}i_{dr} + v_{qr}i_{qr})}_{P_r} \\ Q &= \frac{3}{2} \underbrace{(v_{qs}i_{ds} - v_{ds}i_{qs})}_{Q_s} + \underbrace{(v_{qr}i_{dr} - v_{dr}i_{qr})}_{Q_r} \end{aligned} \quad (4.3)$$

Measurement matrix \mathbf{y} for EKF algorithm is,

$$[\mathbf{y}] = [P \ Q]^T \quad (4.4)$$

Stator and rotor voltages referred to d and q axis are input to EKF based DSE algorithm. Hence, input vector \mathbf{u} is given by,

$$[\mathbf{u}] = [v_{ds} \ v_{qs} \ v_{dr} \ v_{qr}]^T \quad (4.5)$$

4.3 EKF implementation for DFIG

In present work, EKF a variant of Kalman filter approach is used for dynamic state estimation of DFIG based wind generating system connected to infinite bus (an SMIB). DFIG based power system modelling and necessary mathematical steps for EKF implementation are covered in literature (Huang, Schneider, and Nieplocha Simon). A detailed description of mathematical steps involved in EKF implementation is presented in **Appendix C**.

4.3.1 Discrete model of DFIG for EKF implementation

To perform EKF based state estimation, discretized model of DFIG is employed. Stator currents i_{ds} , i_{qs} and rotor currents i_{dr} , i_{qr} are the states to be estimated using DSE algorithm. DFIG's output active power - P and reactive power - Q, the measurement variables, are considered to be available from PMU. Differential algebraic equations (DAEs) presented in previous section are discretized to achieve DSE. State equations shown in Chapter # 2 - (2.4) and measurement equations in (4.4) are represented in discretized form as (4.6) and (4.7) respectively ,

$$\begin{bmatrix} i_{ds_k} \\ i_{qs_k} \\ i_{dr_k} \\ i_{qr_k} \end{bmatrix} = \begin{bmatrix} i_{ds_{k-1}} \\ i_{qs_{k-1}} \\ i_{dr_{k-1}} \\ i_{qr_{k-1}} \end{bmatrix} + f(i_{ds_{k-1}}, i_{qs_{k-1}}, i_{dr_{k-1}}, i_{qr_{k-1}}, u_{k-1}) \nabla t \quad (4.6)$$

Here, k indicates the number of instance and ∇t is time step.

$$\begin{aligned} P_k &= \frac{3}{2}(v_{ds_k} i_{ds_k} + v_{qs_k} i_{qs_k} + v_{dr_k} i_{dr_k} + v_{qr_k} i_{qr_k}) \\ Q_k &= \frac{3}{2}(v_{qs_k} i_{ds_k} - v_{ds_k} i_{qs_k} + v_{qr_k} i_{dr_k} - v_{dr_k} i_{qr_k}) \end{aligned} \quad (4.7)$$

Apart from the state and measurement equation, the input vector \mathbf{u} is presented in discrete form as 4.8,

$$[\mathbf{u}_k] = [v_{ds_k} \quad v_{qs_k} \quad v_{dr_k} \quad v_{qr_k}]^T \quad (4.8)$$

4.3.2 Simulation preliminaries and DSE of DFIG using EKF

- **Simulation aspects**

SMIB system (Fig.2.1) is mathematically simulated using MATLAB / Simulink platform. Details of machine specifications is provided in **Appendix 4.1** (at the end of chapter). Total simulation time is 6 s and system frequency is 50 Hz. Dynamic condition is simulated by considering sudden demand reduction in active power by grid. The demand is reduced by 40 % at an instance $t = 2$ s. Sudden drop in required active power output warrants for change in reference active power of DFIG. Direct power control (DPC) scheme is employed to adapt to new power requirements. RSC control circuit adapts to change its output in accordance to new power requirement. In this work, synchronized operation of GSC and RSC control circuit is considered to adjust to dynamic conditions. Output active power from DFIG to grid is changed from 5.69 MW to 3.4 MW and output reactive power is changed from 0.3293 to 0.3986 MVAR as shown in Fig. 4.2. It is important to note that the reduction in power delivery is met by the reduction observed in the stator and rotor output both, as limited power control is offered by the rotor circuit.

With reduced power output condition, RSC control loop causes proportionate change in other current parameters *viz.* i_{ds} , i_{qs} , i_{dr} and i_{qr} and voltage parameters *viz.* v_{ds} , v_{qs} , v_{dr} and v_{qr} .

- **EKF implementation for DFIG**

EKF algorithm provides dynamic estimation of the states using measurements collected at faster rate. Normally active power and reactive power are measured with the help of current transformer (CT) and potential transformer (PT) on AC side and with the help of sensors on converter side. Due to unforeseen hostile conditions of operation for wind generator, the possibilities exist where measurement data obtained from these instrument transformers are corrupted with noise. To simulate such

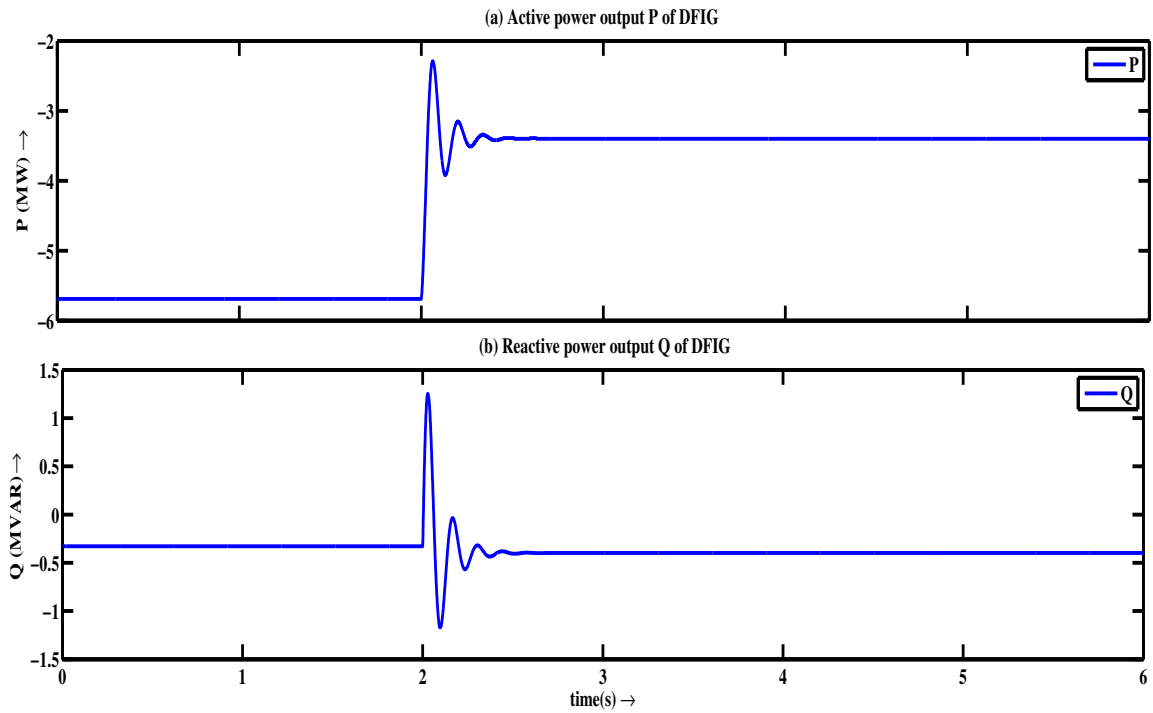


Figure 4.2: (a) Change in output active and (b) change in output reactive power, under dynamic condition

a noisy measurement environment, measured P and Q are corrupted with Gaussian noise (standard deviation of 1%) as shown in Fig. 4.3. Process noise is considered having SD of 0.01%.

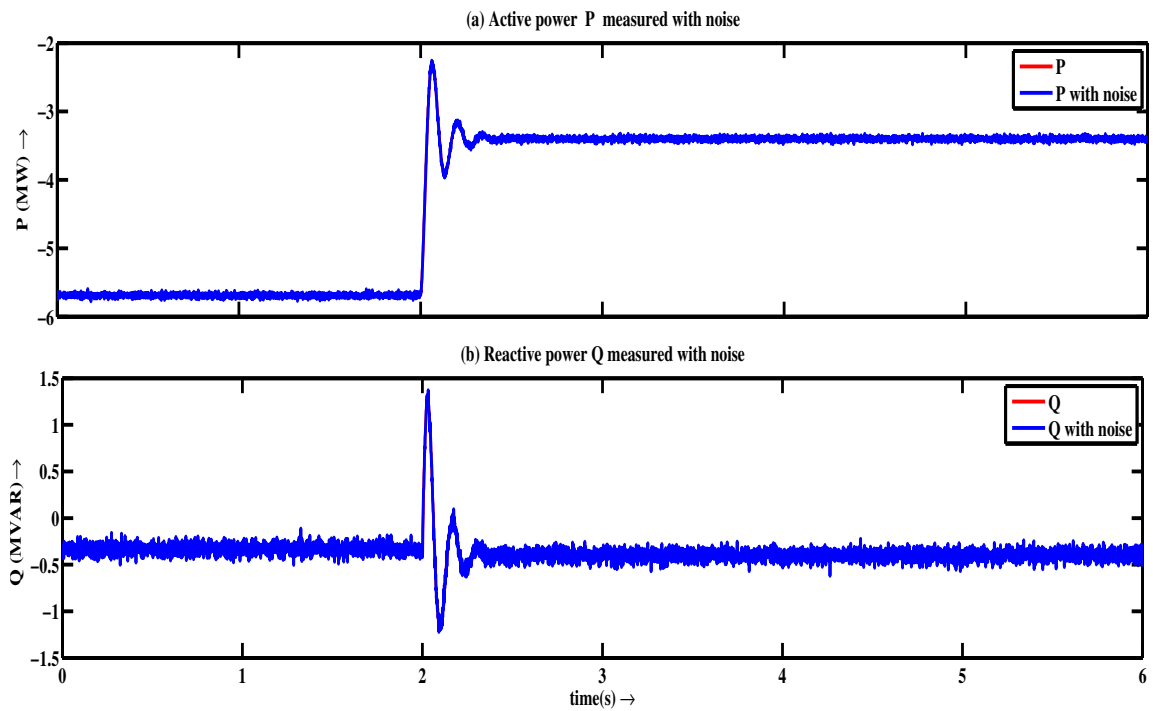


Figure 4.3: (a) Active power and (b) reactive power, with and without noise

EKF algorithm is employed to estimate quantities for rotor control circuit *viz.* i_{dr} and i_{qr} as well as stator currents i_{ds} and i_{qs} . For EKF based DSE, P and Q forms measurement matrix \mathbf{y} . EKF works perfectly as DSE tool and it estimates all four dynamic state *viz.* i_{dr}, i_{qr}, i_{ds} and i_{qs} of DFIG accurately as shown in Fig. 4.4 and Fig. 4.5 and hence, validating accuracy of EKF algorithm.

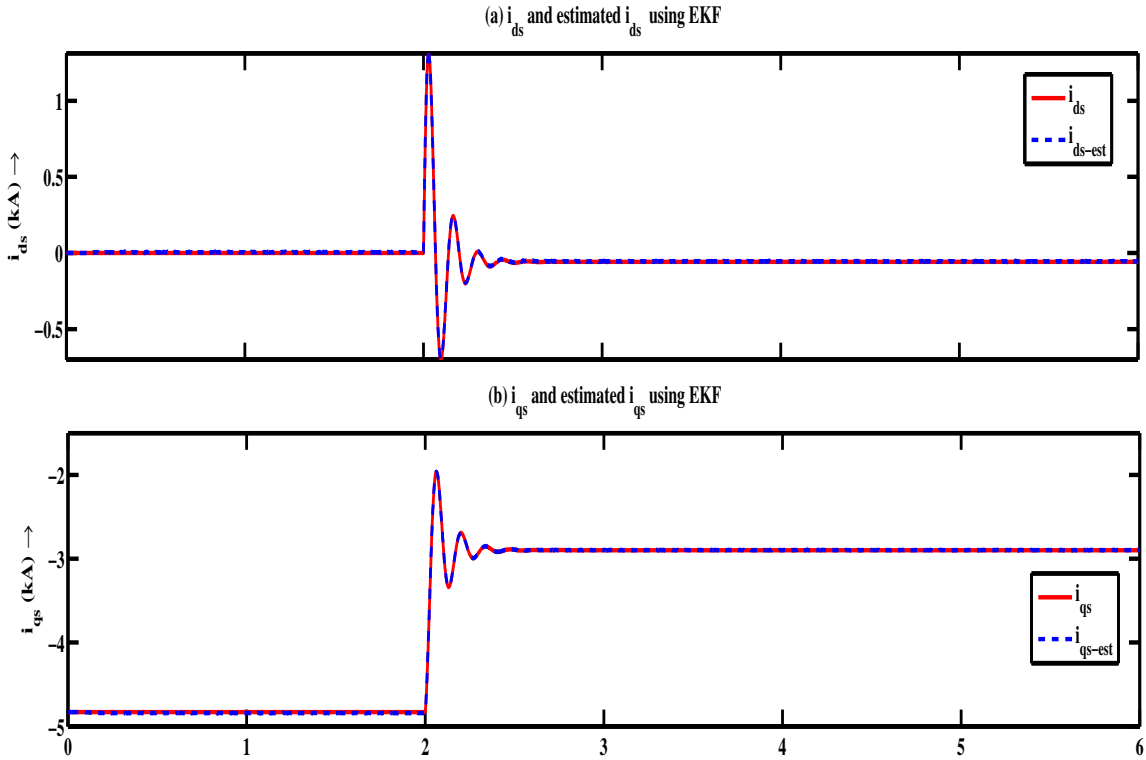


Figure 4.4: (a) i_{ds} actual and i_{ds-est} estimated using EKF algorithm (b) i_{qs} actual and i_{qs-est} estimated using EKF algorithm

4.4 Case studies and discussions

4.4.1 Case I: Current sensor measurement with noise

In DFIG, i_{dr} and i_{qr} , rotor currents are sensed using internal current sensors and then used for control of active and reactive power output. Post sudden output active power changes at $t = 2$ s, the output of current sensor is assumed to be corrupted by noise at $t = 2.3$ s. This simulates faulty current output from sensor. The decoupled measurements i_{dr} and i_{qr} contains Gaussian noise having standard deviation of 5 %. Effect of noise on measurements of i_{dr} and i_{qr} are depicted in Fig.4.6(a) and Fig.

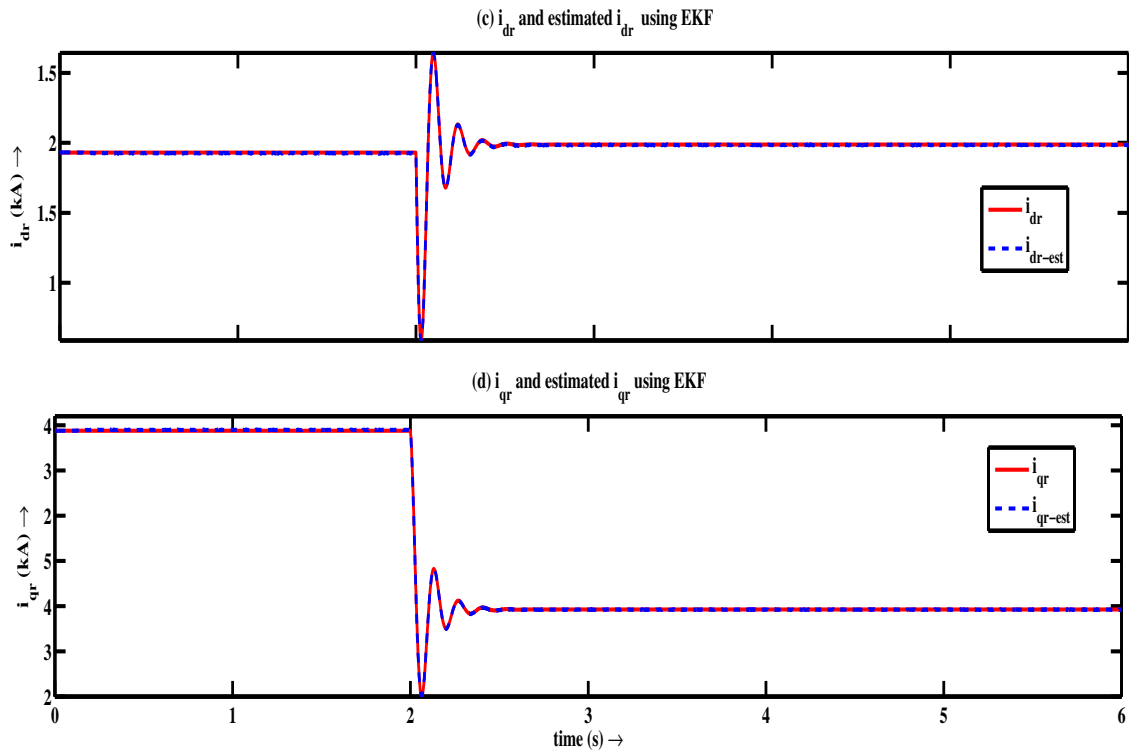


Figure 4.5: (a) i_{dr} actual and i_{dr-est} estimated using EKF algorithm (b) i_{qr} actual and i_{qr-est} estimated using EKF algorithm

4.7(a) respectively.

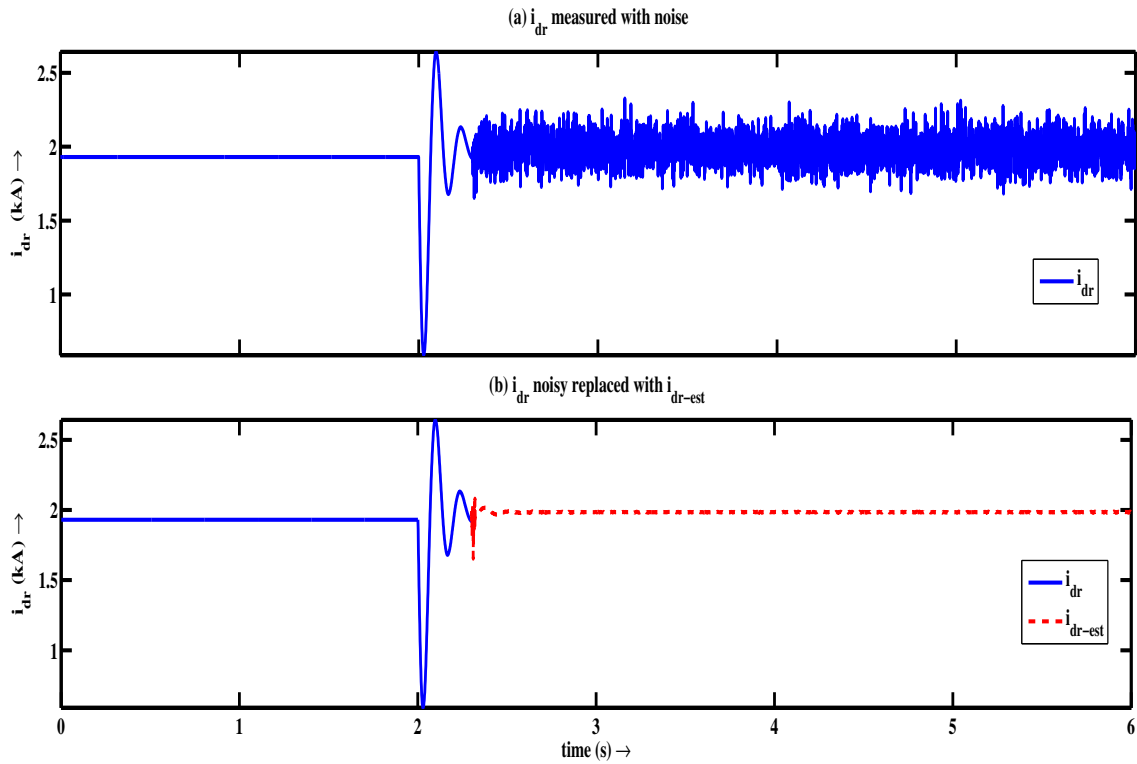


Figure 4.6: (a) Effect of noise on i_{dr} (b) noisy i_{dr} is replaced with i_{dr-est}

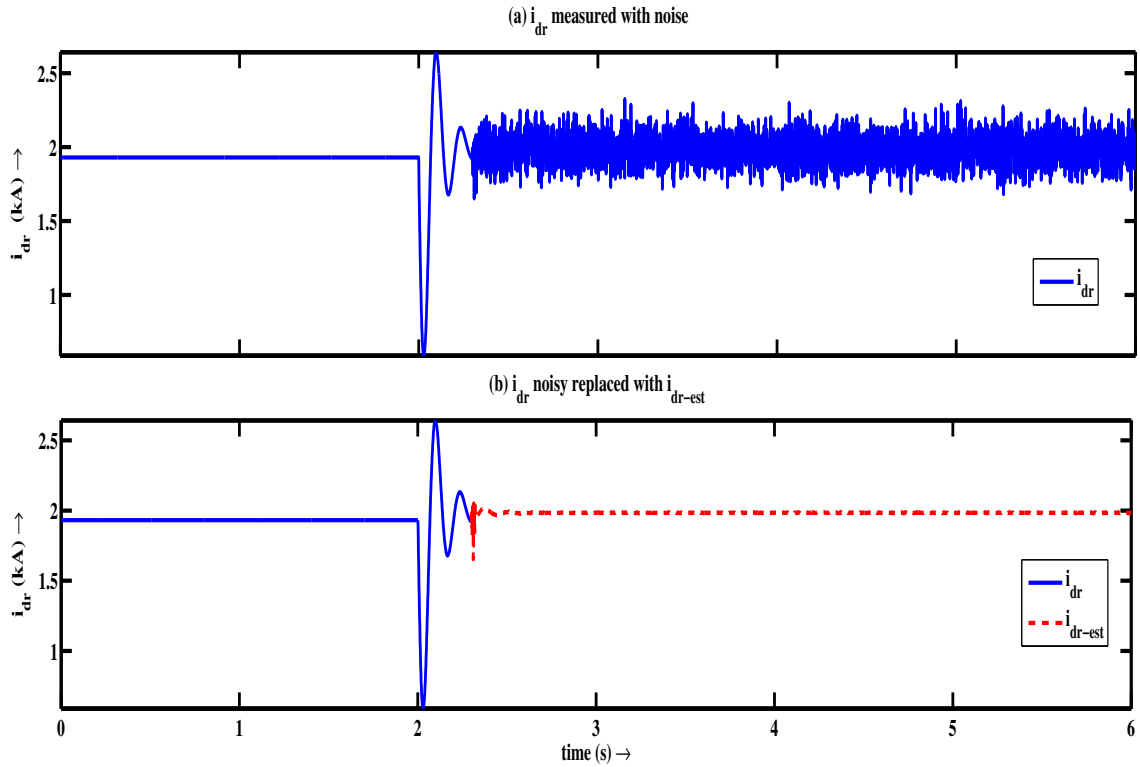


Figure 4.7: (a) Effect of noise on i_{qr} (b) noisy i_{qr} is replaced with i_{dr-est}

Effect of noise in i_{dr} and i_{qr} deteriorate the performance of control loop and hence, its effect on rotor active power P_r and reactive power Q_r are seen in Fig.4.8(a) and Fig.4.9(a) respectively. Noisy power output from rotor also tend to affect total power output of DFIG (4.7). Main focus is to observe impact of noise on various quantities due to noisy i_r (i_{dr}, i_{qr}), hence linearized propagation of noise to P_r and Q_r , to P and Q is assumed.

The moment at which effect of consistent noise is observed in output of current loop and consequently on active and reactive power at $t = 2.3$ s, in a short while ($t = 2.32$ s) output of current sensors i_{dr} and i_{qr} are replaced with output of EKF based estimation algorithm \hat{i}_{dr}^+ and \hat{i}_{qr}^+ as shown in Fig. 4.6(b) and Fig. 4.7(b). From $t = 2.32$ s onwards estimated currents \hat{i}_{dr}^+ and \hat{i}_{qr}^+ compared with i_{dr}^* and i_{qr}^* (Fig. 4.1) to produce controlled rotor output P_r and Q_r to desired level in RSC control circuit. With estimated current inputs of \hat{i}_{dr}^+ and \hat{i}_{qr}^+ , nature of output rotor active and reactive power is observed as shown in Figs. 4.8(b)-4.9(b) respectively. This consequently causes noise free active power P and reactive power Q (4.7). Results endorses successful application of EKF based dynamic states to overcome effect of

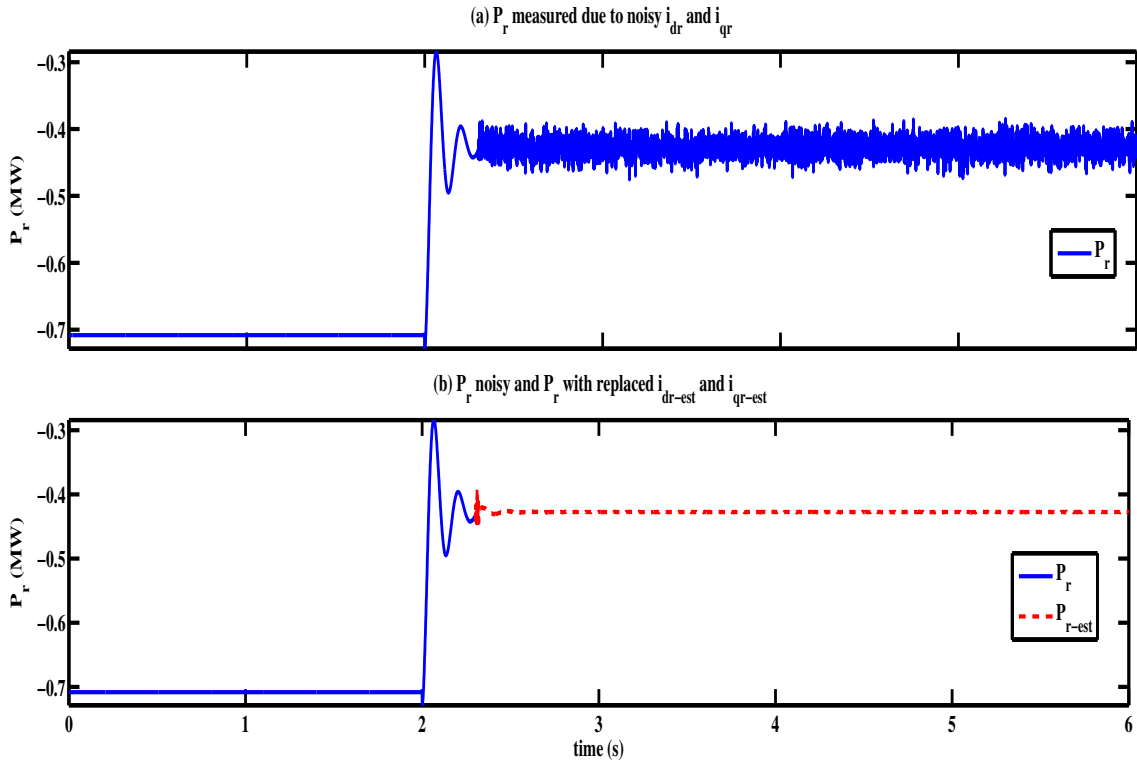


Figure 4.8: a) Effect of noisy i_{dr} and i_{qr} on P_r (b) P_r after noisy currents replaced with i_{dr-est} and i_{qr-est}

high magnitude noise on active and reactive rotor power output.

4.4.2 Case II: Current sensor measurement with outliers

Apart from noise, internal current sensors may also have gross errors that deflect significantly from the real data due to hostile environment. DFIG being low in inertia and supported with fast controlling actions of RSC and GSC, outputs may tend to diverge from delivering pre-defined active and reactive powers. Power network with large penetration of DFIG may see an imbalanced power delivery and consequent change in frequency of power network when connected in multi-machine power system. Therefore, it becomes imperative that bad data must be detected and eliminated from measurement pool. Simulating another possibility, the realistic condition is tested where random outliers show up in measurements by current sensors (in i_r and hence in i_{dr} and i_{qr}) as shown in Fig. 4.10(a) and Fig. 4.11(a) respectively.

Due to outliers in measurement signals, rotor active and reactive power change abruptly. The abrupt change in P_r and Q_r due to change in i_{dr} and i_{qr} are shown in Fig. 4.12-(a) and Fig. 4.12-(b) respectively.

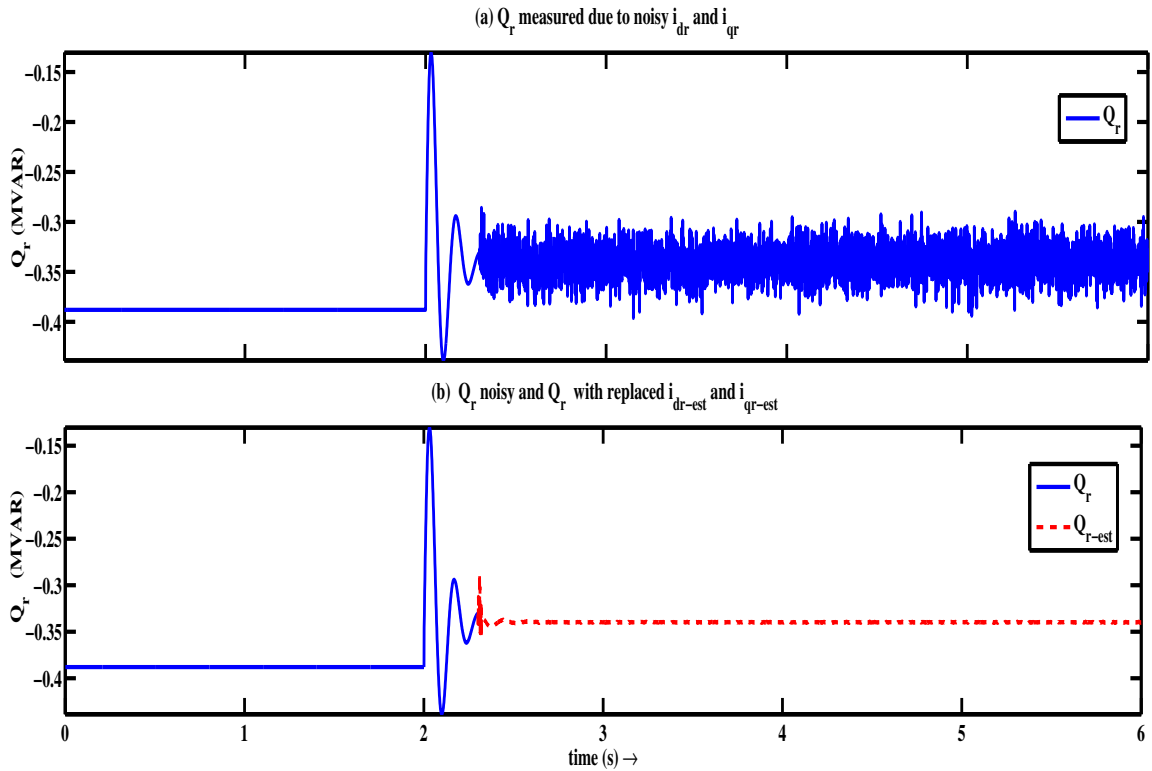


Figure 4.9: (a) Effect of noisy i_{dr} and i_{qr} on Q_r (b) Q_r after noisy currents replaced with i_{dr-est} and i_{qr-est}

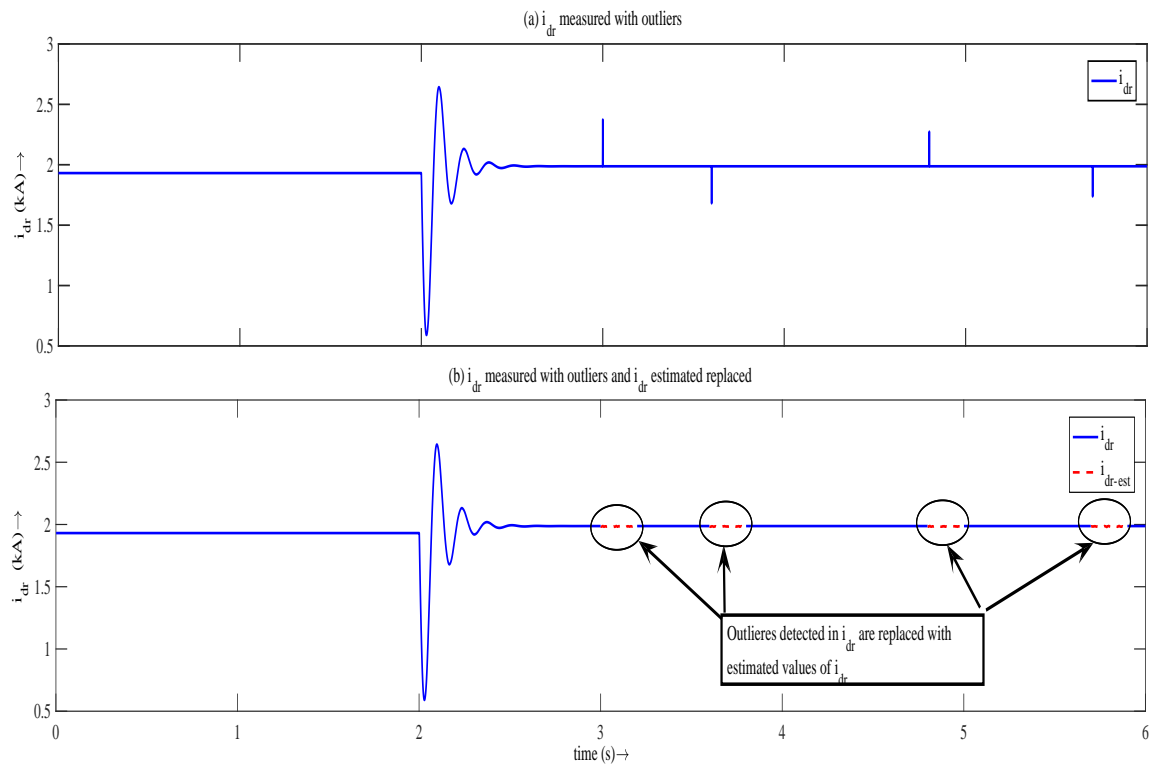


Figure 4.10: (a) Effect of outliers on i_{dr} (b) i_{dr} with outliers replaced with i_{dr-est}

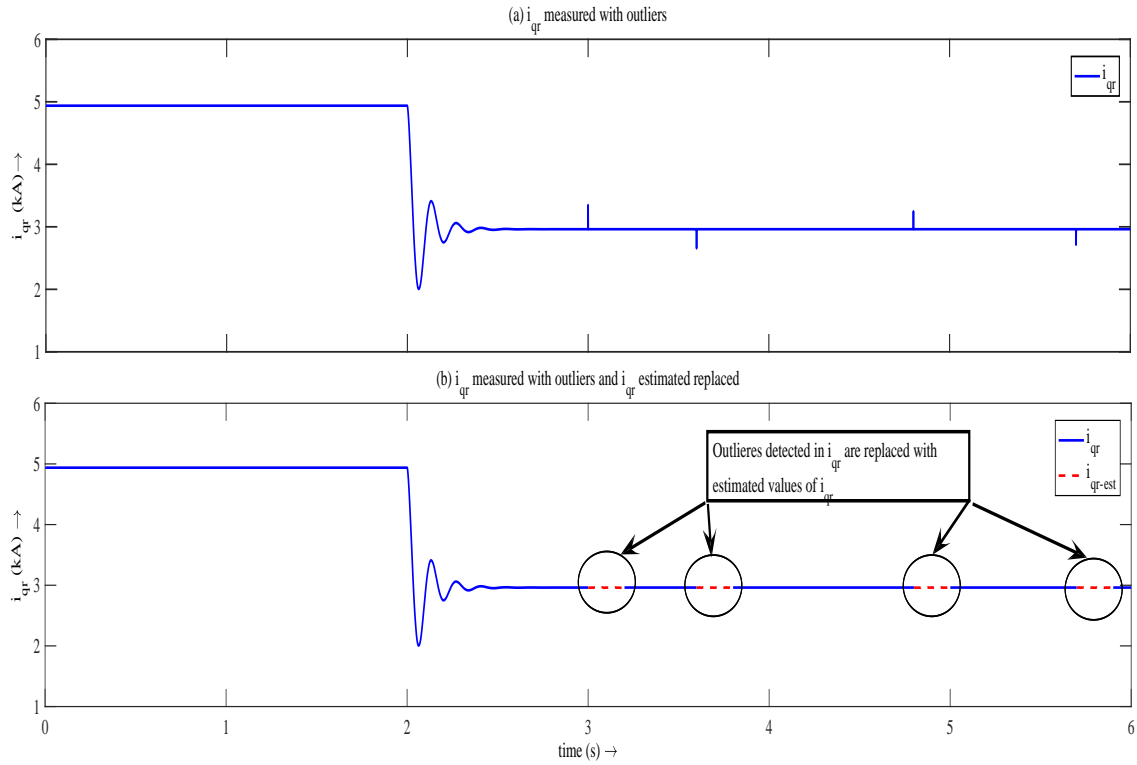


Figure 4.11: (a) Effect of outliers on i_{qr} (b) i_{qr} with outliers replaced with i_{qr-est}

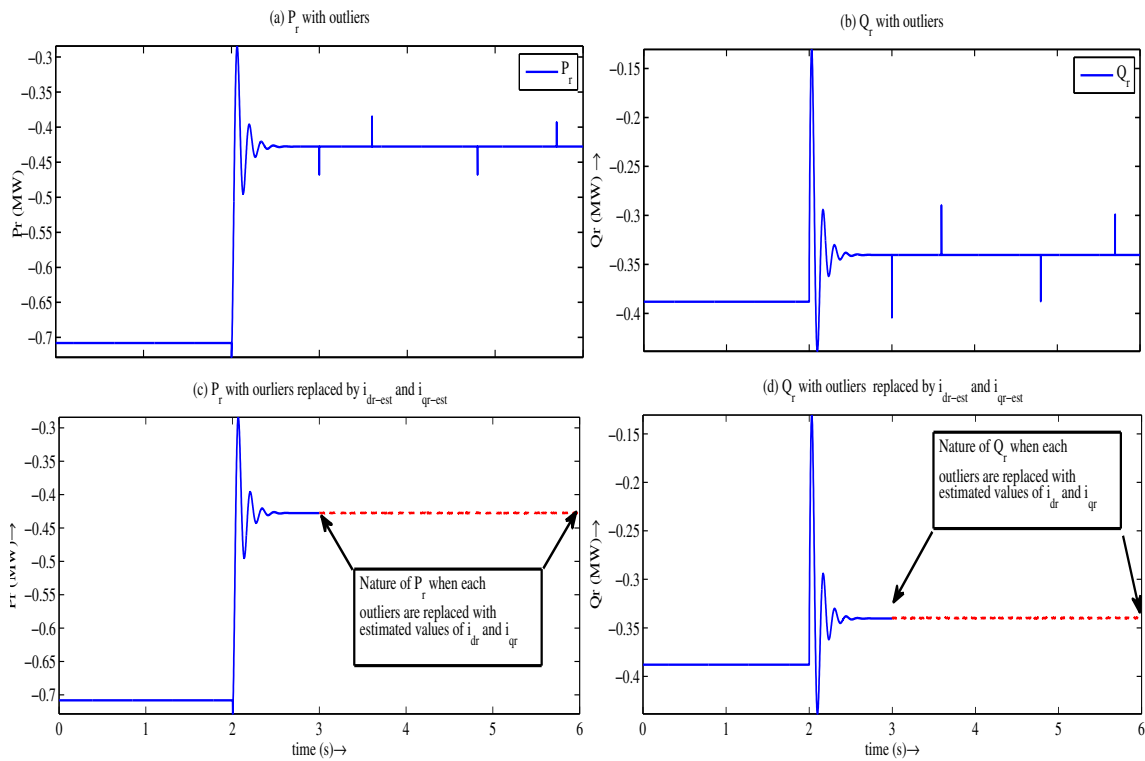


Figure 4.12: (a)-(b) Effect of i_{dr} and i_{qr} having outliers on P_r and Q_r , (c)-(d) P_r and Q_r after measurement with outliers replaced with i_{dr-est} and i_{qr-est}

To detect the unwanted outliers, method of normalized innovation ratio is proposed by (S. Yu, “State Estimation of Doubly Fed Induction Generator Wind Turbine in Complex Power Systems”). **Appendix 4.2** (at the end of chapter) provides an overview of this method of normalized innovation ratio to detect outliers.

To overcome effect of outliers in measurement, suggested algorithm (**Appendix 4.2**) detects for existence of outliers at any instant k in output of i_{dr} current sensor. In presented case, once outlier is detected by the algorithm at $t = 3$ s, immediately current measurement from sensor (which are input to rotor control circuit) is replaced with \hat{i}_{dr}^+ and \hat{i}_{qr}^+ instead of i_{dr} and i_{qr} , as shown in Fig. 4.10(b) and Fig.4.11(b) respectively. Generally, outliers or bad data are momentary in nature. Hence, to ensure smooth and uninterrupted power output, estimated values of i_{dr} and i_{qr} i.e. \hat{i}_{dr}^+ and \hat{i}_{qr}^+ are continued to provide input for duration of $t = 0.2$ s. Subsequently, normal measurement from i_{dr} current sensor resumes as an input to RSC. If bad data is detected again in output of current sensor, then same procedure is repeated for every such incidence. In the present case, 4 random occurrence of outliers are considered. Replacement with estimated variables \hat{i}_{dr}^+ and \hat{i}_{qr}^+ gives smooth and error free control of DFIG. Once erroneous values are replaced with accurate output of EKF algorithm, it provides outlier free rotor active power P_r as indicated in Fig.4.12(b). Results endorse that EKF based estimator values can be used as back-up for better control of DFIG when current sensor used in RSC control circuit is infected with outliers. Similar abrupt effect of measurement outliers and removal of unstable output using \hat{i}_{dr}^+ and \hat{i}_{qr}^+ has been observed for other variables *viz.* P and Q as shown in Fig.4.13.

Second possibility is considered, when the outliers exist in measurement of current sensor during dynamic condition. Generally change in current due to dynamic condition is slower as compared to bad data generated due internal current sensor mal-function. Algorithm for outlier detection differentiate between sudden change in measurement from current sensor considering the abrupt differential change in measured quantity in respective time duration. The condition of outliers in currents i_{dr} and i_{qr} during dynamic condition are shown in Fig. 4.14(a) and Fig. 4.15(a) respectively.

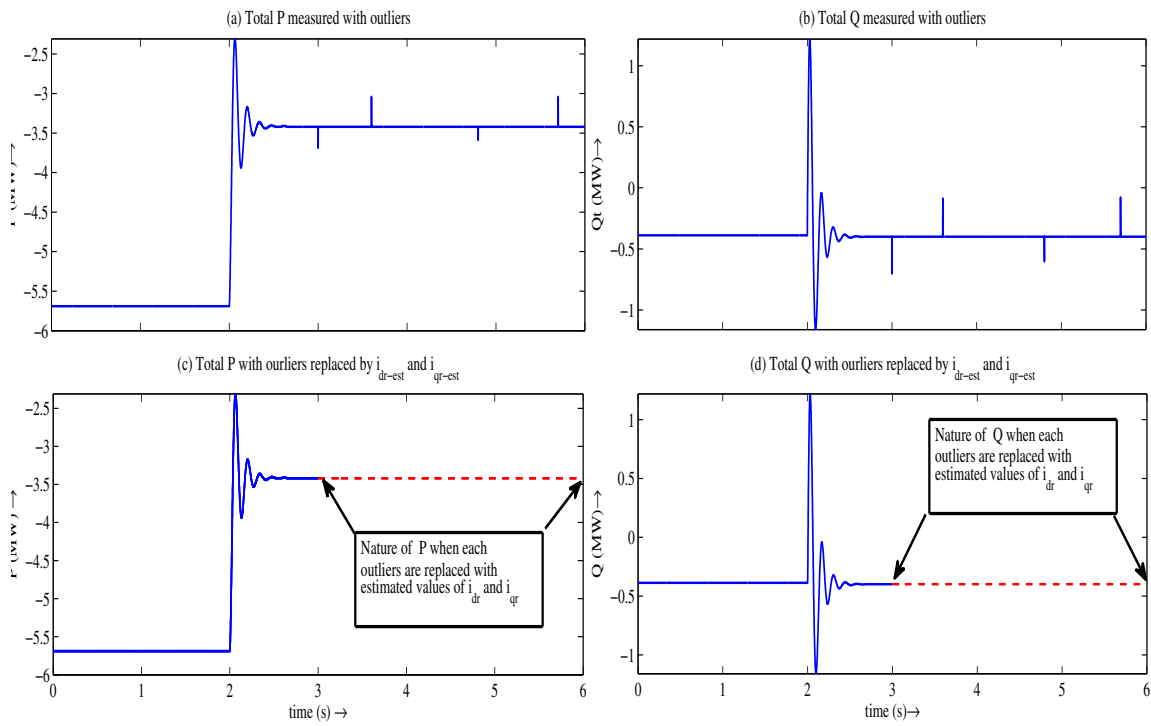


Figure 4.13: (a)-(b) Effect of i_{dr} and i_{qr} having outliers on P and Q , (c)-(d) P and Q after measurement with outliers replaced with i_{dr-est} and i_{qr-est}

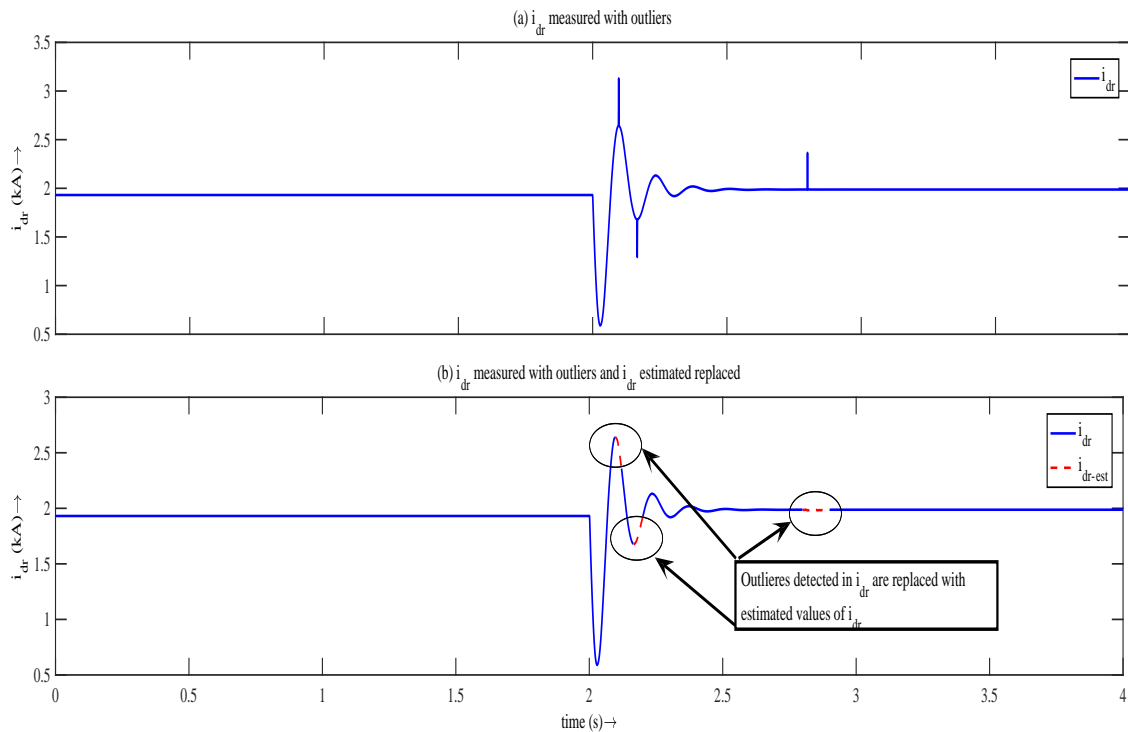


Figure 4.14: (a) Effect of outliers during dynamic condition on i_{dr} (b) i_{dr} with outliers replaced with i_{dr-est}

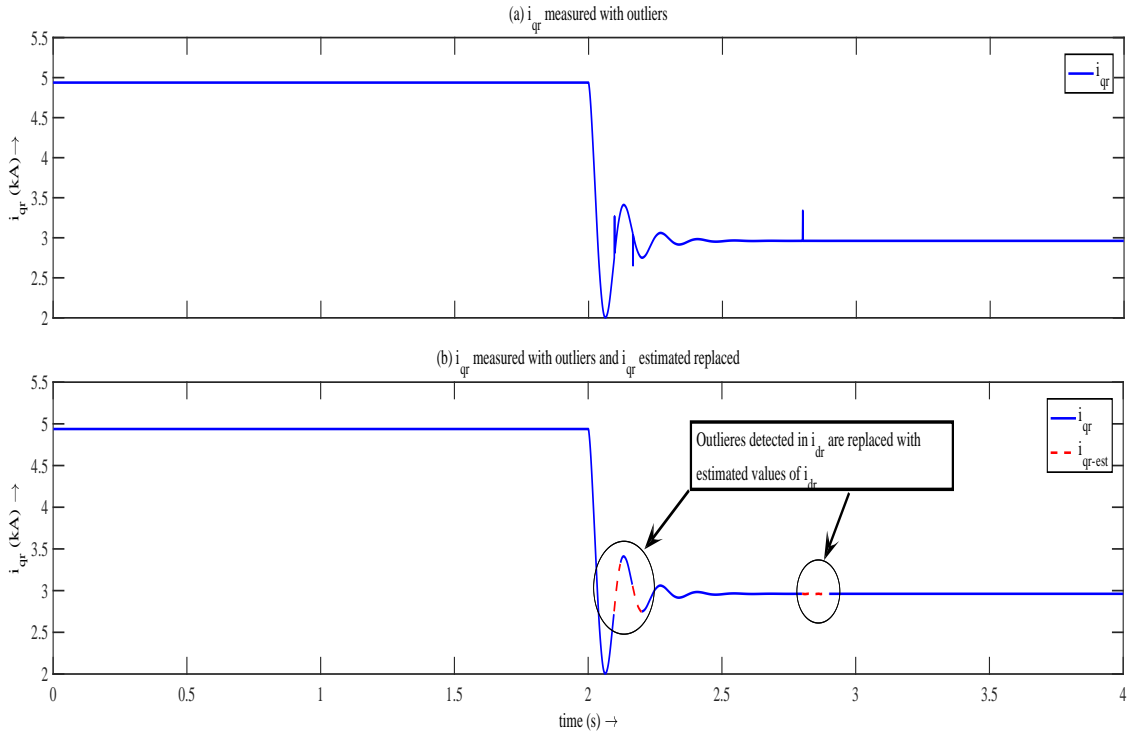


Figure 4.15: (a) Effect of outliers during dynamic condition on i_{qr} (b) i_{qr} with outliers replaced with i_{dr-est}

EKF algorithm estimates dynamic states *viz.* i_{dr} , i_{qr} alongwith i_{ds} , i_{qs} using the active power and reactive power output of DFIG as an measurement. As suggested in **Appendix 4.2**, once outliers are detected during dynamic conditions, immediately i_{dr} , i_{qr} are replaced with i_{dr-est} , i_{qr-est} respectively. Then onwards, i_{dr-est} and i_{qr-est} are input to rotor power control circuit. Hence, i_{dr-est} and i_{qr-est} are fed for small duration alike to first condition, thereafter normal measurement data available from current sensor are given as control signal to RSC. At every detection of outliers similar method is adopted. The effect of i_{dr-est} and i_{qr-est} are observed in Fig. 4.14(b) and Fig. 4.15(b) respectively. The effect of outliers on P_r and Q_r are depicted in Fig. 4.16(a) and Fig. 4.16(b) respectively. Employing dynamically estimated states i_{dr-est} and i_{qr-est} , achieved using EKF, smooth and accurate active and reactive power delivery is observed under dynamic condition as shown in Fig. 4.16(c) and Fig. 4.16(d) respectively.

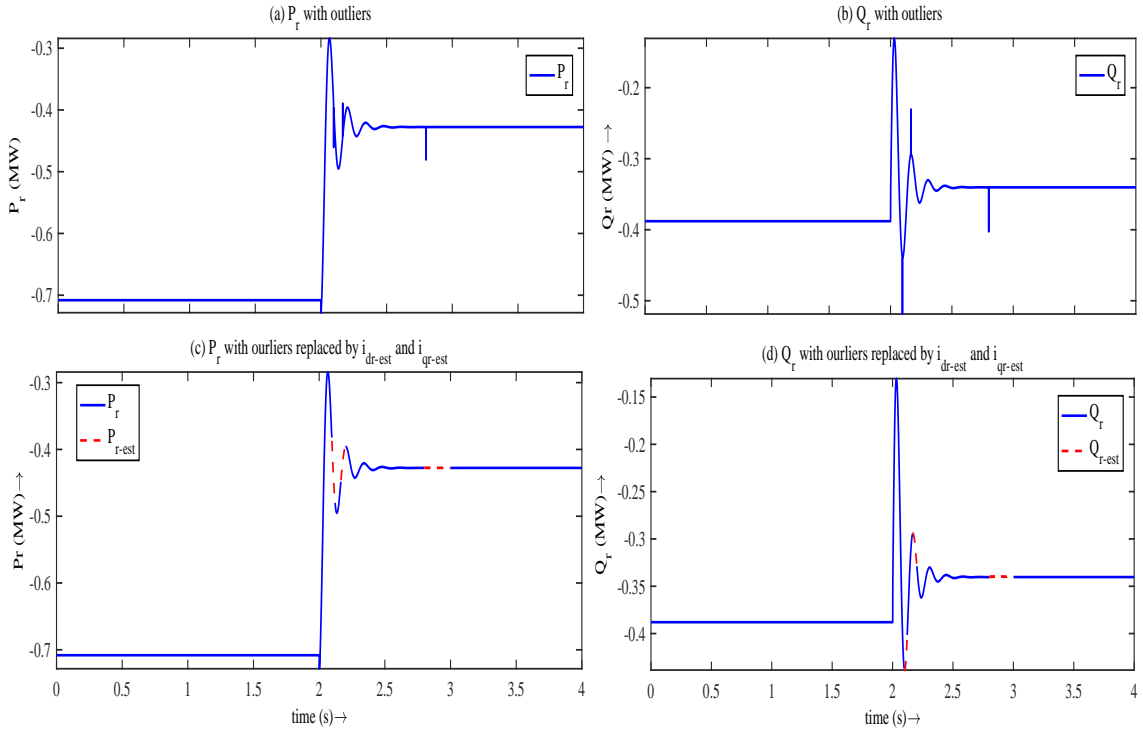


Figure 4.16: (a)-(b) Effect of i_{dr} and i_{qr} having outliers on P_r and Q_r , (c)-(d) P_r and Q_r after measurement with outliers replaced with i_{dr-est} and i_{qr-est}

4.4.3 Case III: Measurement unavailability due to current sensor failure

Another possibility, taking a worst case scenario following transient load change, a current sensor fails and hence measurement data to RSC control circuit are not available continuously. This results in random intermittent measurement packet drop. This condition is simulated by taking random periods of measurement unavailability. The measurement current i_r i.e. i_{dr} and i_{qr} to RSC control circuit is considered to be erratically unavailable due to faulty current sensor. Faulty current sensor conditions cause measurement unavailability in i_{dr} and i_{qr} for a period of 0.5 s from $t = 2.3$ s to $t = 2.8$ s and subsequently for a period of 1.4 s i.e. from $t = 3.8$ s till $t = 5.2$ s as shown in Fig. 4.17(a)-(b).

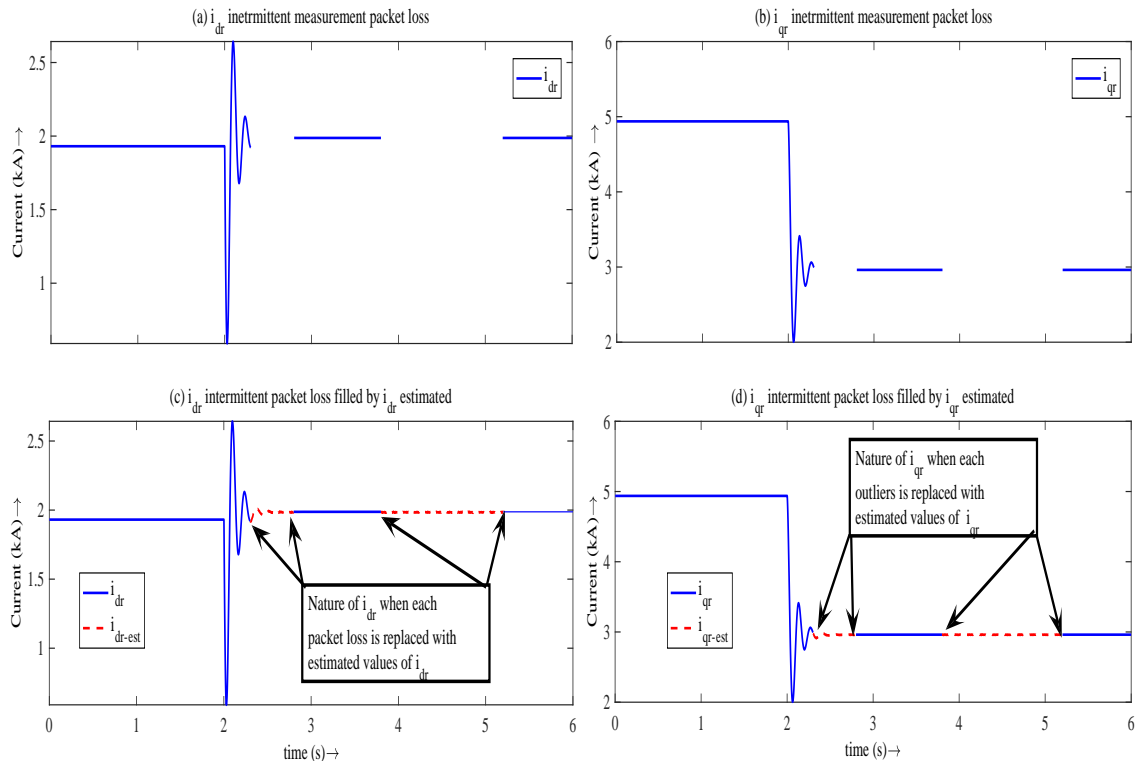


Figure 4.17: (a)-(b) i_{dr} and i_{qr} measurement unavailability for 0.5 s and 1.4 s duration, (c)-(d) i_{dr} and i_{qr} when unavailable measurements are replaced with i_{dr-est} and i_{qr-est}

To overcome this condition, following algorithm is used:

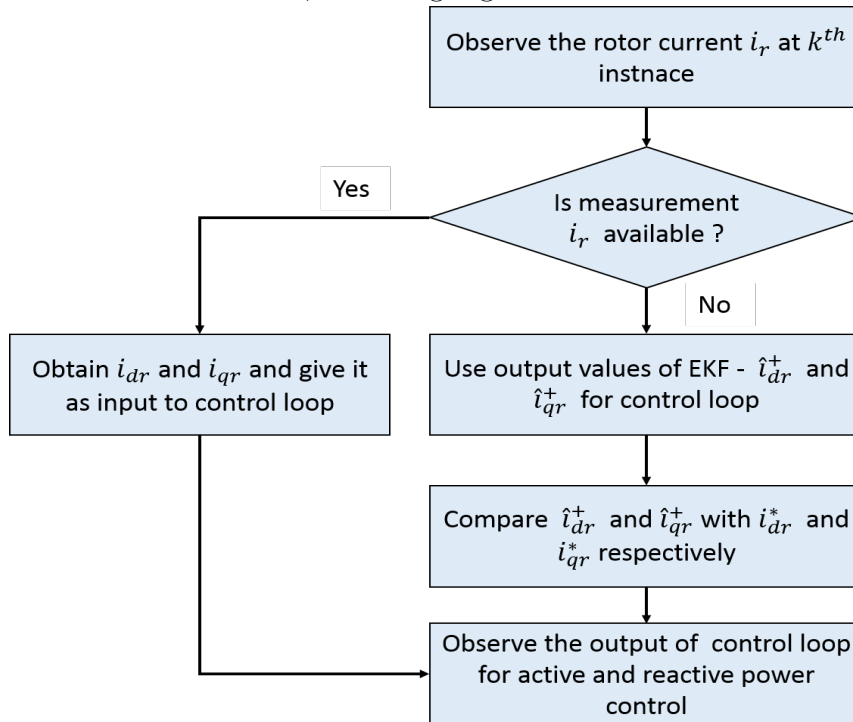


Figure 4.18: Flowchart showing application of DSE under measurement data unavailability

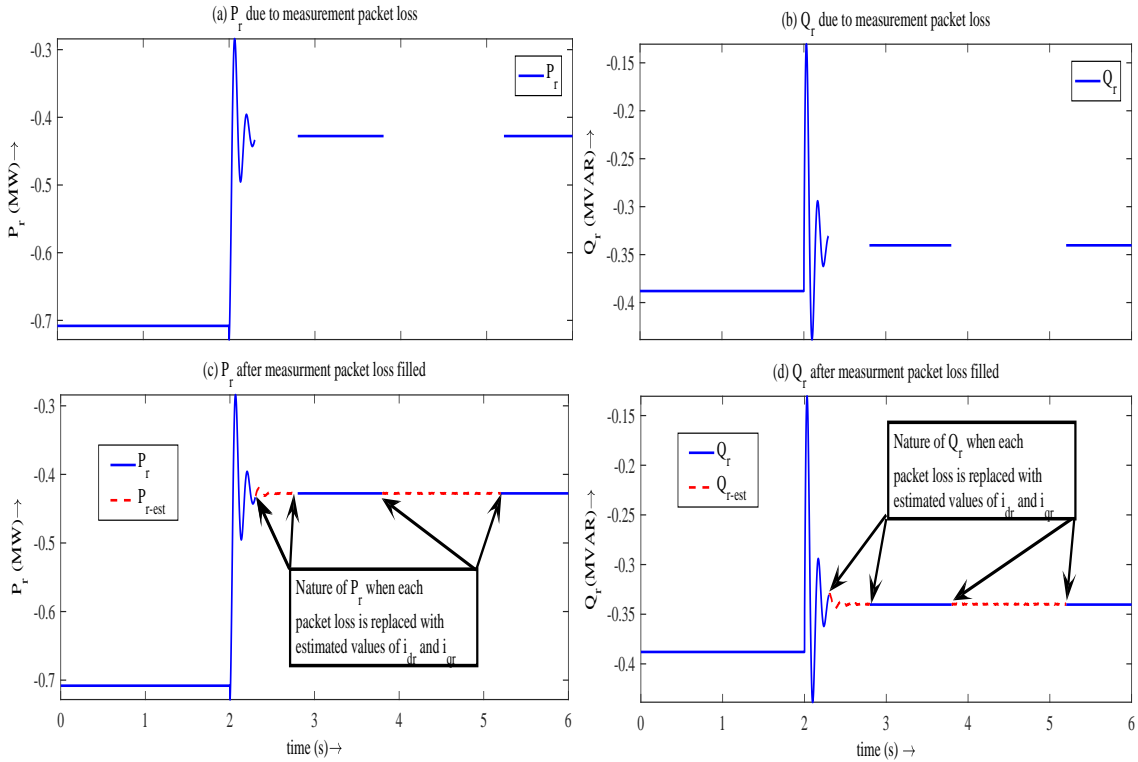


Figure 4.19: (a)-(b) P_r and Q_r measurement unavailability for 0.5 s and 1.4 s duration, (c)-(d) P_r and Q_r when unavailable measurements are replaced with i_{dr-est} and i_{qr-est}

Proposed algorithm first checks availability of measurement and if it recognizes the unavailability of measurement (in this case at time $t=2.3$ s), input to RSC control circuit is provided with the output of EKF algorithm *viz.* \hat{i}_{dr}^+ instead of i_{dr} and \hat{i}_{qr}^+ instead of i_{qr} until input from current measurement resumes (in this case at time $t = 2.8$ s) as shown in Fig. 4.17 (c)-(d). Results indicate that estimated values obtained using EKF based DSE faithfully fills the measurement void existed due to faulty current sensor operation. Hence, EKF based DSE works as a substitute to actual measurement from current sensor during measurement data unavailability. As seen in Fig. 4.19(a)-(b), absence of measurements i_{dr} and i_{qr} also affects active and reactive power output of rotor. This discontinuity in rotor power is also overcome when current sensor measurement are replaced with \hat{i}_{dr}^+ and \hat{i}_{qr}^+ as shown in Fig.4.19(c)-(d). It assures that during unavailable measurement condition, continuity in active and reactive power from rotor and consequently total active and reactive power can be maintained utilizing estimated values obtained using EKF. Similar effect of i_{dr} and i_{qr} unavailability and their replacement with \hat{i}_{dr}^+ and \hat{i}_{qr}^+ is also observed on other output

quantities *viz.* P and Q (4.3). Results prove ability of EKF based DSE algorithm, operating concurrently with DFIG, to achieve dynamically estimated state variables. Outcome also endorses that states achieved through DSE can be used to overcome different internal current sensor issues.

4.5 Conclusions

DFIG based wind power has made it imminent for an EMS operator to have knowledge of its dynamic states for better power control. After obtaining accurate DSE of DFIG, it can be used further to provide better control of DFIG, mainly for controlling its rotor active and reactive power. Inherent nature of continuous dynamic operation of DFIG, sometimes causes mal-operation and / or faulty operation of current sensor. The work presented demonstrates successful application of estimated dynamic states achieved using EKF to provide robust control under different faulty conditions of current sensor. Faulty conditions of current sensor which measures i_r (i_{dr} and i_{qr}) for RSC control circuit is simulated by considering three conditions *viz.* noisy measurement output, measurements with outliers and measurement unavailability. In all three conditions, the moment abnormality is detected in current sensor measurements, actual measurements are replaced by faithfully estimated quantities \hat{i}_{dr}^+ and \hat{i}_{qr}^+ resulted from EKF algorithm. Results indicate use of proposed novel scheme which employs dynamically estimated states instead of faulty measurements and successfully overcomes disadvantage of undesired output from DFIG due to ambiguous input to control circuit under current sensor malfunctions.

Appendix 4.1

DFIG parameters

Rated MVA: 6 MVA, rated line voltage 0.69 kV, rotor resistance (R_r)= 0.5779 m Ω , rotor inductance (L_r) = 1.1657 mH, mutual inductance (L_m) = 1.1138 mH, stator resistance (R_s)= 0.514 m Ω , stator inductance(L_s) = 1.1632 mH, frequency(f) = 50 Hz, synchronous speed (ω_s) = 314 rad/s, rotor speed (ω_r)=360 rad/s, slip (s) = - 0.1469.

Appendix 4.2

Normalized innovation ratio for particular measurement is the ratio of difference of predicted measurement and actual measurement to square root of covariance of that measurement i.e.

$$\epsilon_k = (y_{i_k} - \hat{y}_{i_k}^+) / \sqrt{P_{yy_k}} \quad (4.12)$$

where $i=1,2,\dots,m$, m = number of measurement. k is number of instance, ϵ_k is normalized innovation ratio for measurement i at k^{th} instance. y_{i_k} is i^{th} measurement collected from sensor and $\hat{y}_{i_k}^+$ is estimated i^{th} measurement acquired using EKF algorithm at the k^{th} instance. Here, P_{yy_k} represents error covariance and hence, standard deviation is $\sqrt{P_{yy_k}}$. Result of normalized innovation ratio is compared with maximum tolerance level ϵ_{max} to detect the outliers. Procedural steps to detect and remove bad measurements or outliers at k^{th} instance and thereafter use of estimated states instead of removed bad measurements are:

- a. Acquire i^{th} measurements y_{i_k} and obtain predicted i^{th} measurements $\hat{y}_{i_k}^+$ at k^{th} instance (i_r i.e. i_{dr} and i_{qr})
- b. With the help of P_{yy_k} and using (4.12) find normalized innovation ratio ϵ_{y_k} .
- c. If $\epsilon_{y_k} < \epsilon_{max}$ then outlier does not exist at k^{th} instance.
- d. If $\epsilon_{y_k} > \epsilon_{max}$ then outlier exist in measurement at k^{th} instance.
- e. Replace the measured value i_{dr_k} and i_{qr_k} with the predicted value $\hat{i}_{dr_k}^+$ and $\hat{i}_{qr_k}^+$ respectively.
- f. Observe the output of the control loop. Keep on feeding output estimated values \hat{i}_{dr}^+ and \hat{i}_{qr}^+ till condition in step no. d does exist.

Chapter 5

Conclusions

DSE in power system has been implemented using wide variety of approaches / tools i.e. from earlier WLSE approach to recent different variants of Kalman filters and others. With the implementation of PMUs, capable of providing faster and accurate measurement than conventional remote terminal units (RTUs), DSE in power system has attained a great leverage. DSE of conventional synchronous generators under transient conditions, using EKF and UKF, is widely adopted. With the detailed modelling of induction generators, requirement of DSE of DFIG is also met. With increasing penetration of DFIGs, the need of concurrent DSE of conventional synchronous generators and DFIG based wind generators emerges.

This thesis contributes a novel approach for concurrent DSE of multi-type generators in a large power systems. A mathematical model of the generators integrated in the power system is provided so as to realize centralized DSE. Extended Kalman filter (EKF) and unscented Kalman filter (UKF) are the two tools employed to estimate accurate dynamic states of synchronous generators (SG) and doubly fed induction generator (DFIG) simultaneously. Applicability of both the DSE tools is checked for standard WSCC 3-generator 9-bus test system considering measurement availability from PMUs. Encouraging results of dynamic state predictions supports the model proposed and the approach adopted. The comparison of results obtained using EKF and UKF indicate selection of the appropriate tool for the state estimation. For continuous and desired operation of DFIG (or its circuitry) under mal-functioned sensor conditions, real time application of estimated dynamic states is well discussed in thesis.

Chapter #1 is a brief introduction, focusing on the need of centralized concurrent DSE for a power network comprising of conventional and renewable energy sources. Erstwhile efforts for DSE in power network (consisting of synchronous generators) using EKF and UKF are analyzed and discussed. Literature referring performance of EKF and UKF subjected with anomalous measurement condition are also presented. Attempts for DSE of dynamic states of DFIG connected to power network dominated by synchronous generators are elaborated and scrutinized. Limited application of DSE for improvised operation of DFIG is deliberated. The usefulness of the DSE of DFIG, for its application for smooth and uninterrupted operation of DFIG is elucidated. As a direct repercussion of the analysis of published literature, research objectives are formulated. The chapter ended with scope of research work and outline of the thesis.

Chapter #2 comprises of a novel approach for modelling a SG and DFIG on a unified platform. DFIG, conventionally presented as current-source model is taken as base for representation of current-source model of synchronous generator. Critical observations led to an analogy between current-source state-space model of DFIG and state-space model for SG and it is deliberated. Minor modifications and inherent logical correspondence between DFIG and synchronous generator variables is presented. Mathematical representation of base DFIG model is prepared in MATLAB / Simulink and validated with standard software platform PSCAD / EMTDC. Incorporating minor modification and observations, current-source state-space model of synchronous generator is proposed. Performance of proposed synchronous generator MATLAB / Simulink model is established with synchronous generator model of standard PSCAD/EMTDC software under dynamic condition. Current envelops, of short circuit currents, observed at point-of-common-coupling (PCC) endorses the idea of current-source model of synchronous generator. Highlights of this chapter are:

- Except slip, inherent logical correspondence is observed for all four states of current-source state space models of DFIG and SG.
- Variation in rotor direct axis current of DFIG is analogous variation of field current of SG. Outcome suggest naturally imbibed effect of AVR in proposed current-source model of SG.
- Change in input voltage parameters and derived active and reactive power com-

ponents of state-space current-source model of SG is similar to standard PSCAD / EMTDC model.

Chapter #3 encompasses a novel approach of centralized concurrent DSE of power network comprised of synchronous generators with significant penetration of wind energy sources (DFIGs). WSCC 3 - generator 9 - bus multi-machine system is taken as reference in which Gen. #2 is replaced with similar rating of coherently operative DFIG wind generator farm (comprised of 38 generators). Model of multi-machine power system (WSCC 3-generator 9-bus system) is presented using MATLAB / Simulink platform where both synchronous generators and DFIGs are represented as current-sources. Proposed multi-machine current-source model is validated with identical PSCAD/EMTDC model. EKF and UKF are tools used to form centralized concurrent dynamic state estimator, supported with PMU measurements, to estimate dynamic states of SGs and DFIG. Results of simultaneously estimated dynamic states of SGs and DFIG endorses ability of proposed novel approach for DSE under dynamic condition, as well. The dynamic conditions arising due to stochastic nature of DFIG as well as due to network fault, suggested approach of centralized concurrent DSE delivers accurate results. Chapter ends with aspects on comparative analysis of EKF and UKF performance. Noteworthy outcomes of this chapter are:

- Suggested novel approach using current source models can be expanded for larger power network comprised of more synchronous generators and DFIGs after due consideration of intricacies.
- Dynamic states achieved based on current source models of both kind of generators, can further used to achieve real time information of other critical states of both types of generators.

Chapter #4 focuses on application of estimated dynamic states achieved, in real time, for uninterrupted and robust control of DFIG during conditions of sensor mal-operation. Emphatic dependence of DFIG on internal rotor current sensor is discussed in direct power control (DPC) scheme. Normally encountered erroneous conditions of current sensor includes high noise, content of outliers and intermittent communication link failure post transient conditions are discussed. Subsequent effect of current sensor faulty operation on output rotor power and total power of DFIG is inevitable.

Supported with algorithms to detect faulty operation of current sensor, scheme to replace these current sensor measurement with dynamically estimated states is discussed at length. Results portray that replacement of dynamic state with current sensor measurement as an input to rotor side power control circuitry is successful in overcoming after effects caused by current sensor faulty operation.

5.1 Future Scope

In above discussion, centralized concurrent DSE is proposed for multi-machine power network consists of synchronous generators and DFIG. As far as wind energy is concerned, wide spread installation of fixed speed induction generator (FSIG) is already in existence and permanent magnet synchronous generator (PMSG) has started acquiring its space. Alike to DFIG and SG, using current source model approach for FSIG and PMSG, centralized concurrent DSE of all kind of generator (SGs, DFIGs, FSIGs and PMSGs) using EKF and/or UKF offers new realm of research possibilities. The variations in the wind speed conditions, power train modelling, modelling with higher order terms and salient pole synchronous generator current source modelling is still an area to ponder upon. Considering geographical benefit, many nations like India have increased penetration of solar energy i.e. solar PV systems. These are typically an inverter system for the grid to view, acts inherently as current-source model. Thoughts may be put to integrate the inverters along with the modelling approaches of the machines can offer a new domain for research.

PMU aided measurement allows DSE estimator to avail knowledge of critical states in real time and in lesser time as compared to measurement devices measuring similar quantities. In fast changing and highly dynamic power network, knowing critical information regarding dynamic states e.g. δ , ω_r , frequency for synchronous generators and ω_r , capacitor voltage v_{dc} in real time offers a new domain to activate controlling action like AVR, TG much quicker than activation initiated by conventional measurement devices. This shall help to achieve quicker stabilization of vast power networks.

More penetration of renewable energy sources in power network can alter criterion for relay based protection- designed in accordance to ubiquitous synchronous generators. Increased complexity and renewable integration can cause occasional

zonal mis-coordination of relays. New realm of opportunities can be explored to overcome shortcomings of present protection system and to adapt to new coordination requirement arises due to renewable integration by using DSE-based protection (EBP) (Meliopoulos et al.).

Postscript: DSE tools *viz.* EKF and UKF are emphatically rely on measurement data provided by fast sensors, PMUs and SCADA. Though PMU is fast and accurate in providing measurement data, the communication link error and measurement packet drop hamper the desired performance (Gu and Jirutitijaroen). Hence, it becomes interesting to know performance of EKF and UKF under the condition of measurement packet drop along with different measurement update rates. **Appendix A**, as an offshoot of preceding work, gives performance comparison of EKF and UKF for intermittent measurement condition with different measurement update rates.

The weighted least square estimation (WLSE) method, normally used for static state estimation (Grainger, Grainger, and Stevenson), in coordination with load flow, to provide steady state picture of power system considering power network's quasi-static nature. Conventionally load flow is done by collecting various measurement from RTU. What effect would be on load flow, if RTU measurements provide bad data in any of measurements? And can WLSE be the solution of the that? **Appendix B**, briefly, conveys an effort to answer these questions.

Appendix A

Comparative Analysis of EKF and UKF with Multiple Measurement Update Rate during Intermittent Measurement

A.1 Introduction

EKF based DSE algorithm application to power system has been widely deliberated in literature. This algorithm has capability to incorporate non-linearity in power system functions. EKF has limitation due to propagating linearization error and high computation time for Jacobian calculation. (Julier, Uhlmann, and Durrant-Whyte Valverde and Terzija Wang, Gao, and Meliopoulos) Unscented Transform based UKF offers better estimation performance as compared to EKF, especially for large system. The reason is linearization and Jacobian calculation are not required in UKF (Valverde and Terzija Wang, Gao, and Meliopoulos).

Both DSE algorithms' (*viz.* EKF and UKF) performances significantly depend on measurement data update interval and noise content in measurement (Huang, Schneider, and Nieplocha Valverde and Terzija Wang, Gao, and Meliopoulos Zhou et al.). Measurement data update rate is crucial factor to judge estimation aspects of DSE tools. Normally PMU provides measurements at the rate of 120 sa/s (Zhou et al.). However, in recent times PMUs have observed significant technological de-

velopment. PMUs are capable to provide and transmit data at sampling rate of 48 samples/cycle i.e. 2880 sa/s for 60 Hz system (CERTS). Wide range of measurement update rate of PMU warrants for evaluation of EKF and UKF algorithms provided with different measurement update rates. It is noticed that UKF performs better than EKF in measurement conditions wherein exist high measurement update time interval and high measurement noise content (Wang, Gao, and Meliopoulos). State tracking ability of EKF and UKF, and other filters *viz.* particle filter (PF) and ensemble Kalman filter (EnKF), is presented using 100 Monte Carlo simulations for two-area four-machine system (Zhou et al.). The performance of EKF and UKF in case of missing measurement data is addressed in Zhou *et.al.*. Issue of measurement unavailability for a duration of 1 sec is addressed by (Zhou et al.). Here estimation algorithm is provided measurement through linear interpolation, which consequently increases effective measurement update rate (Zhou et al.). With this linearly interpolated measurement data, computation time of all filters are compared and EKF offers least computation time of 4.9 s with interpolated effective measurement update time interval of 0.005 s (i.e. measurement update rate of 200 sa/s)(Zhou et al.). However, the performance of both the EKF and UKF based DSE algorithms under unavailability of partial and complete measurement data with different measurement update rate needs attention. It is to be clarified here that partial data unavailability to the algorithm means that a few data set are not available for certain duration (and no algorithmic data manipulation is performed), whereas complete unavailability of data means all the data sets are failed to update the algorithm with required sets of input information.

Though PMU technology has made measurement data reliable and accurate with insignificant transmission delay, a worst case condition of complete measurement data loss to SE algorithm may arise. It could be due to malfunction or failure of communication link (Zhou et al.). The rare possibility seeks attention to observe the DSE algorithm's performances, if all measurement data is lost for a few cycles. Addressing this, the work presented here compares and analyzes capability of EKF and UKF algorithms to estimate dynamic states *viz.* synchronous generator rotor speed, rotor angle, under partial and complete measurement data unavailability (loss) condition for a few cycles with different measurement data update rates. Results

suggest desirable trade-off in selection of suitable measurement update time interval for certain duration of data unavailability for observing convergence of both filters. The possibility is explored on two multi-machine standard test systems *viz.* WSCC 3-generator, 9-bus system and IEEE 14 bus system (Anderson and Fouad Sauer, Pai, and Chow Pai and Chatterjee Christie).

A.2 Test systems and simulations preliminaries

A.2.1 State representation and measurement aspects

All synchronous generators' rotor speed ω_i , rotor angle δ_i are the dynamic states to be estimated. Initialization of the states is done using load flow data. For mathematical modelling, the classical model of synchronous generator is preferred, and related differential equations are reproduced in (A.1)-(A.2) with usual notations (Anderson and Fouad Sauer, Pai, and Chow). Automatic voltage regulator and turbine governor have not been considered as a part of the model. Frequency is taken 50 Hz for both the systems.

$$M_i \frac{d\omega_i}{dt} = P_{m_i} - P_{g_i} - P_{d_i} \quad (\text{A.1})$$

where $P_{d_i} = D_i(\omega_i - \omega_s)/\omega_s$ and $i = 1$ to n , n = number of generators.

$$\frac{d\delta_i}{dt} = \omega_i - \omega_s \quad (\text{A.2})$$

Unless specified, the p.u. representation is used. δ_i rotor angle is in (elec.rad). M_i is inertia constant and D_i is damping constant of synchronous generators. Input mechanical power P_{m_i} is assumed constant. P_{g_i} is electrical power generated, ω_i is actual rotor speed and ω_s is synchronous speed.

The state vector \mathbf{x} is presented as,

$$\mathbf{x} = [\omega_i \ \delta_i]^T$$

The measurements for both test systems are : 1) active and reactive power at generator buses; 2) bus voltage magnitudes and angles.

Hence measurement equation are,

$$[\mathbf{h}] = \begin{bmatrix} \mathbf{P}_{g_i} \\ \mathbf{Q}_{g_i} \\ \mathbf{V}_m \\ \boldsymbol{\theta}_m \end{bmatrix} + \begin{bmatrix} \mathbf{v} \end{bmatrix} \quad (\text{A.3})$$

$m = 1, 2, \dots, b$, b is total number of buses. \mathbf{P}_{g_i} and \mathbf{Q}_{g_i} are injected active and reactive power at generator bus respectively. \mathbf{V}_m and $\boldsymbol{\theta}_m$ represent bus voltage magnitude and bus voltage angle respectively. \mathbf{v} is a random white Gaussian measurement noise.

To obtain measurement data for active and reactive powers at every generator bus, current is derived using \mathbf{Y}_{exp} expanded nodal bus matrix (which includes internal transient reactances of generators X'_d), is given as below (Huang, Schneider, and Nieplocha Anderson and Fouad)

$$\underbrace{\begin{bmatrix} \mathbf{Y}_{nn} & \mathbf{Y}_{nb} \\ \mathbf{Y}_{bn} & \mathbf{Y}_{bb} \end{bmatrix}}_{\mathbf{Y}_{exp}} \begin{bmatrix} \mathbf{E}_g \\ \mathbf{V} \end{bmatrix} = \begin{bmatrix} \mathbf{I} \\ 0 \end{bmatrix}$$

\mathbf{I} is vector of current injected to bus, \mathbf{E}_g is vector of internal complex voltages behind transient reactance for every generator. \mathbf{V} shows complex bus voltage vector i.e.

$$\mathbf{V} = \mathbf{R}_V \mathbf{E}_g = -\mathbf{Y}_{bb}^{-1} \cdot \mathbf{Y}_{bn} \mathbf{E}_g \quad (\text{A.4})$$

\mathbf{R}_V is bus reconstruction matrix. Using \mathbf{I} , active and reactive powers injected to generator buses are derived.

Intentional corruption of white Gaussian noise having zero mean and standard deviation of 0.01 p.u is introduced in all measurements. Uniform process noise covariance of 0.0001 p.u. is used and initial state error covariance is 0.0001 p.u.. Initial state error covariance matrix \mathbf{P}_0 , \mathbf{R}_k as measurement noise covariance matrix and \mathbf{Q}_k as process noise covariance matrix are presented as,

$$\left. \begin{aligned} \mathbf{P}_0 &= \text{diag}[0.0001]_{a \times a} \\ \mathbf{Q}_k &= \text{diag}[0.0001]_{a \times a} \end{aligned} \right\}, \quad a = \text{number of states}$$

$$\mathbf{R}_k = \text{diag}[0.0001]_{d \times d}, d = \text{number of measurements}$$

Procedural steps of EKF and UKF based DSE approaches are discussed optimally in **Appendix C** and **Appendix D** respectively. Hence, it is not presented here. Important to note that, in presented work, for estimation employing EKF and UKF techniques, fourth order Runge - Kutta method is used to achieve better accuracy (Kundur, Balu, and Lauby Bila).

A.2.2 Simulated anomalous measurement conditions

Three measurement data update rates are chosen i.e. 50 sa/s, 33 sa/s and 25 sa/s indicating measurement data update time intervals of 0.02 s, 0.03 s and 0.04 s respectively. Abnormal operations or failure of measurement communication devices can cause measurement data transmission interruption. Hence, data may become unavailable to DSE algorithm. Such condition is simulated at 4 s *i.e.* 2 s after three phase-to-ground metallic short circuit fault. The measurement data are lost, partially as well as completely, for a few cycle as mentioned in Table A.1.

Table A.1: Summary of anomalous measurement conditions for both test systems for all three measurement update rates (50 sa/s, 33 sa/s and 25 sa/s)

Measurement data unavailability	Measurement data unavailability for both EKF and UKF based estimator			
	Complete measurement unavailability			
duration	Active power	Reactive power	Bus voltage magnitude	Bus voltage angle
3 cycles	X	X	X	X
4 cycles	X	X	X	X
5 cycles	X	X	X	X
	Partial measurement unavailability			
3 cycles	√	√	X	X
4 cycles	√	√	X	X
5 cycles	√	√	X	X

√ - Measurement available

X - Measurement not available

Measurement data resumes after data lost duration. Test systems are analyzed for missing measurement data conditions having durations of 1 cycle to 5 cycles using EKF and UKF approaches. Only a few results are presented here for brevity.

A.3 Case studies

A.3.1 Complete loss of measurement data

Case 1 – WSCC three generator nine bus system : Performance of both algorithms *viz.* EKF and UKF is checked for complete unavailability of measurement using WSCC 3-generator 9-bus system (Anderson and Fouad Sauer, Pai, and Chow). Total duration for simulation is 10 s.

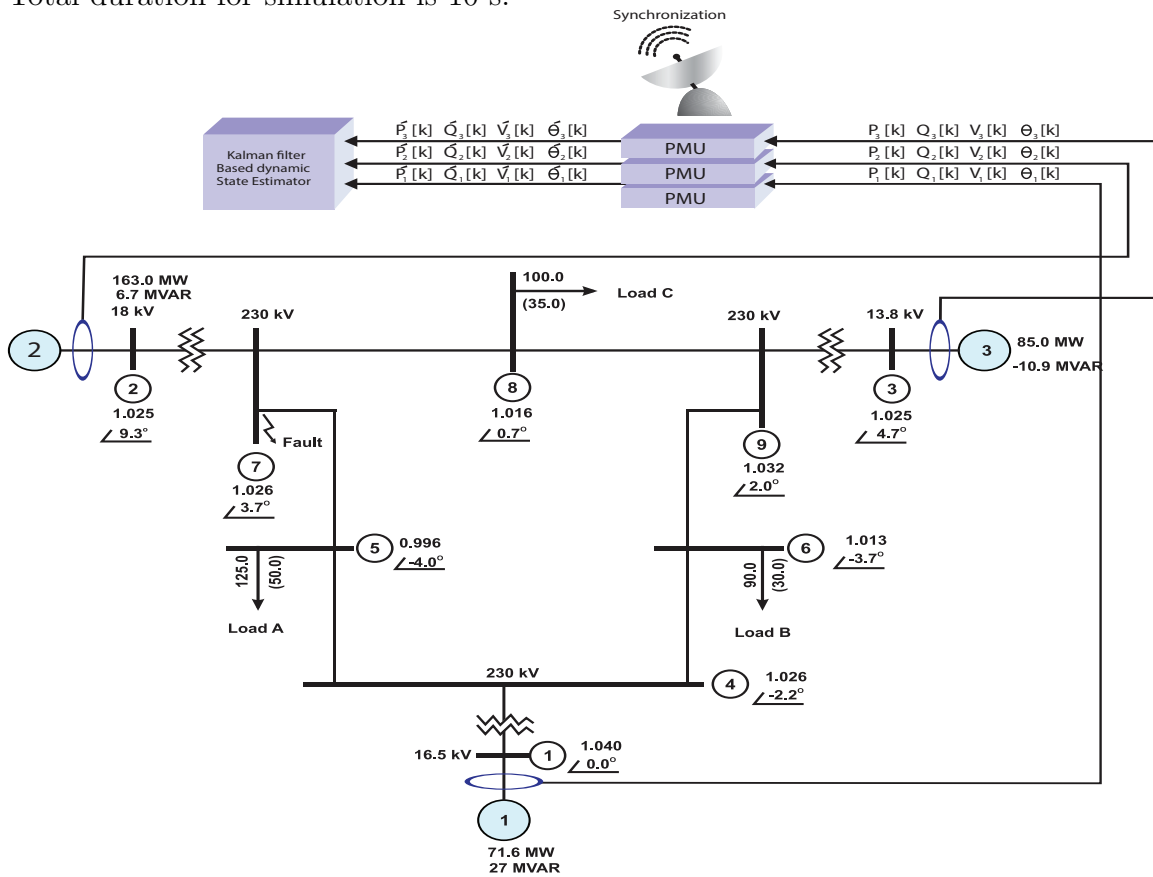


Figure A.1: WSCC- three generator nine bus test system (Anderson and Fouad).

Three phase-to-ground, metallic short, fault is simulated at $t= 2$ s between bus #5 and #7. Fault is cleared after 100 ms by removing the line between bus #5 and bus #7 leading to topological change (change in network configuration) of

system. This leads to changes in \mathbf{Y}_{bus} matrix. After clearing the fault, at time $t=4$ s all measurement data got interrupted for time duration of 3 cycles. In the similar manner, measurement data lost durations of 4 cycles and 5 cycles are also presented.

In Fig.A.2, Fig.A.3 and Fig.A.4, it is depicted to show EKF and UKF algorithms' performance for measurement update time intervals of 0.02 s (50 sa/s) , 0.03 s (33 sa/s) and 0.04 s (25 sa/s) respectively.

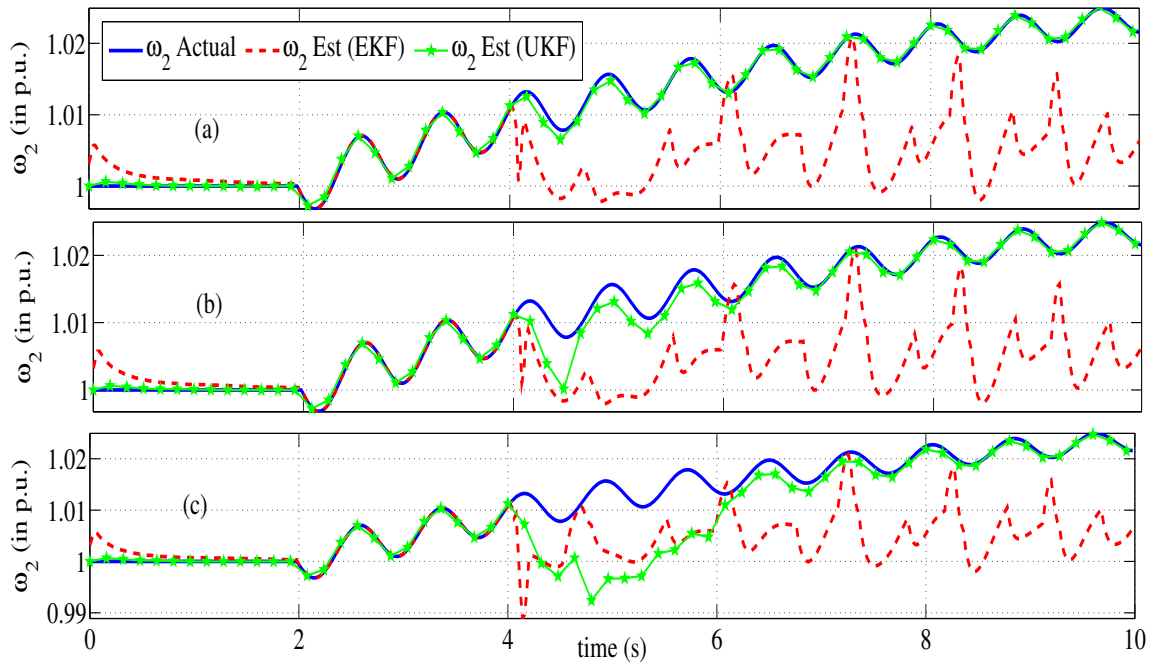


Figure A.2: Performance of EKF and UKF in estimation of variations in speed of generator 2 (ω_2) (WSSC system), measurement update interval of 0.02 s and all measurements missing for (a) 3 cycles, (b) 4 cycles and (c) 5 cycles duration

Keeping in view the location of fault, results are presented only for estimation of speed of generator 2 (ω_2) for EKF and UKF algorithms. Results of similar analysis of other dynamic states are not presented for the brevity.

Case 2 – IEEE 14-bus system : The IEEE 14 bus test system (Pai and Chatterjee Christie) is employed for proposed observation. Similar to previous case, three phase-to-ground metallic short circuit fault is simulated at $t = 2$ s on the line between bus #4 and #5 and faulty line between bus #4 and #5 is removed by opening relevant circuit breakers after 100 ms. Necessary topological changes are used while formation of pre-fault and post-fault \mathbf{Y}_{bus} . Classical model of generator is considered and hence in absence of AVR and TG, system takes longer to settle to a

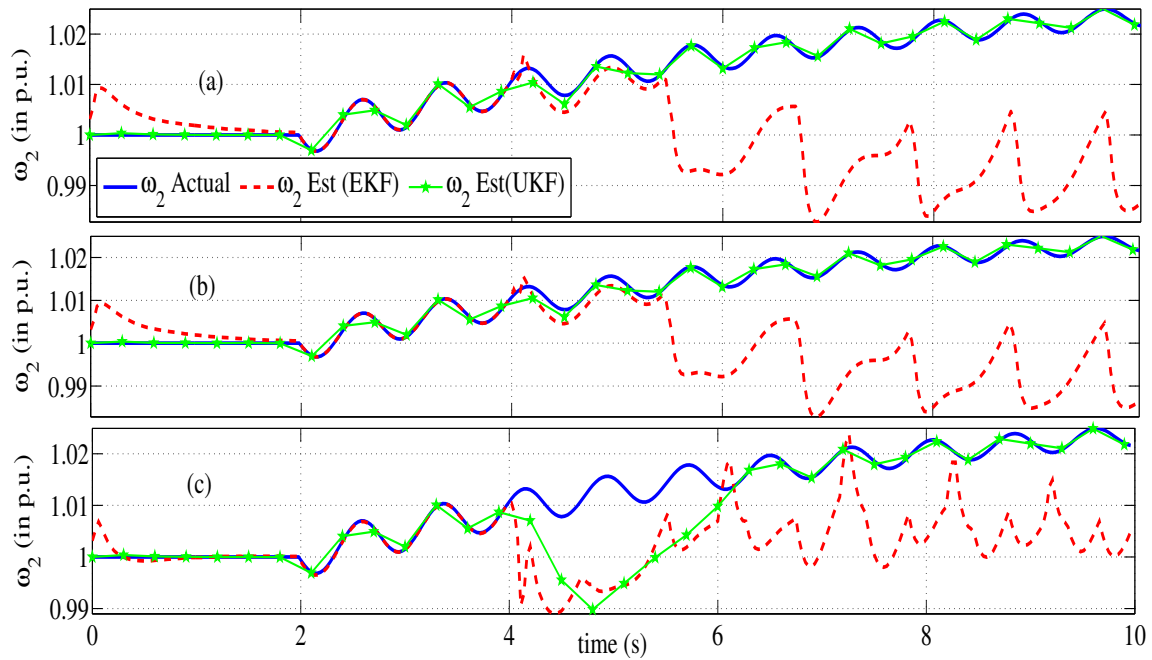


Figure A.3: Performance of EKF and UKF in estimation of variations in speed of generator 2 (ω_2) (WSCC system), measurement update interval of 0.03 s and all measurements missing for (a) 3 cycles, (b) 4 cycles and (c) 5 cycles duration

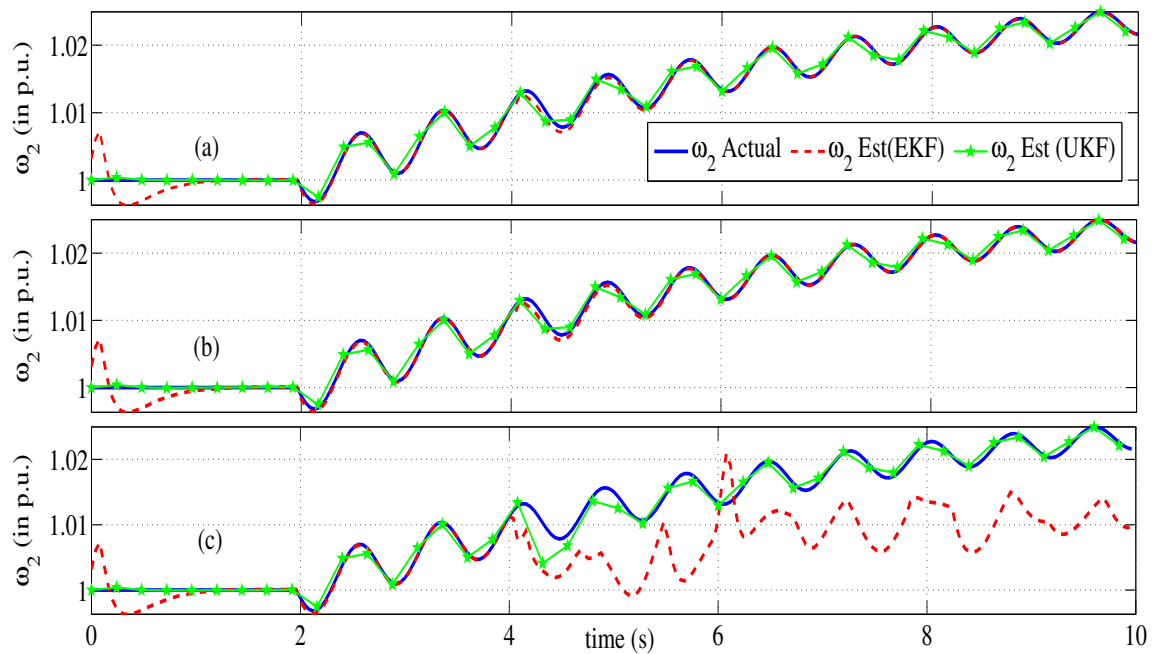


Figure A.4: Performance of EKF and UKF in estimation of variations in speed of generator 2 (ω_2) (WSCC system), measurement update interval of 0.04 s and all measurements missing for (a) 3 cycles, (b) 4 cycles and (c) 5 cycles duration

new equilibrium condition after clearing of fault as shown in Figs. A.2 - A.8.

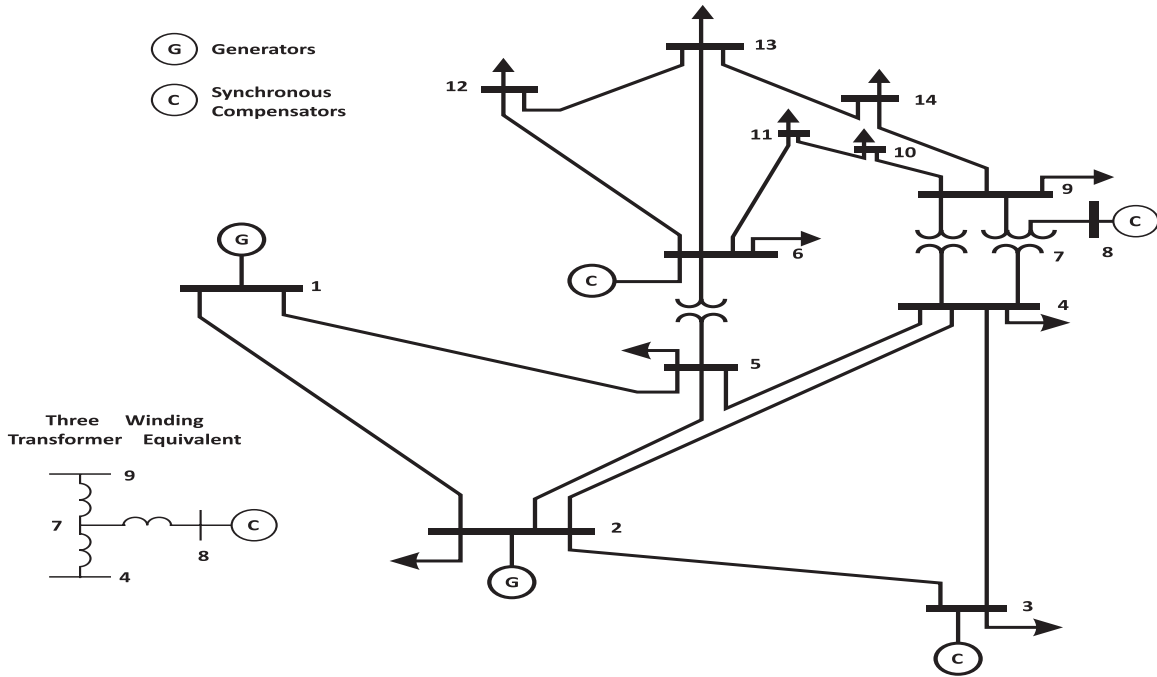


Figure A.5: IEEE 14 bus test system (courtesy: internet source).

At $t = 4$ s, measurement data update is terminated to algorithm input for different three time periods (as shown in Table A.1) and then resumes. For these missing data time durations, the tracking ability of both- EKF and UKF algorithms is observed with three measurement update rates. Total duration for observation is 20 seconds in this test case so as to check convergence possibility of both algorithms.

Considering location of fault, only representative results of estimation of speed of generator 2 (ω_2) for both EKF and UKF algorithms are presented here.

A.3.2 Partial loss of measurement data

In a second case, performance of EKF and UKF is analyzed for both the test systems under the condition of partial loss of measurement data i.e. out of four measurements only two measurements are unavailable. At $t = 4$ s, only two measurements i.e. active and reactive power are available for state estimation to both DSE algorithms as indicated in Table A.1. Remaining two measurements i.e. voltage magnitude and voltage angle of buses are not provided to both estimation algorithms for the period of 3, 4 and 5 cycles. Ability of estimation is analyzed for measurement update interval of 0.02 s (update rate 50 sa/s) which displayed divergence for all three missing measurement durations in previous case. Under these conditions, with the availability of two

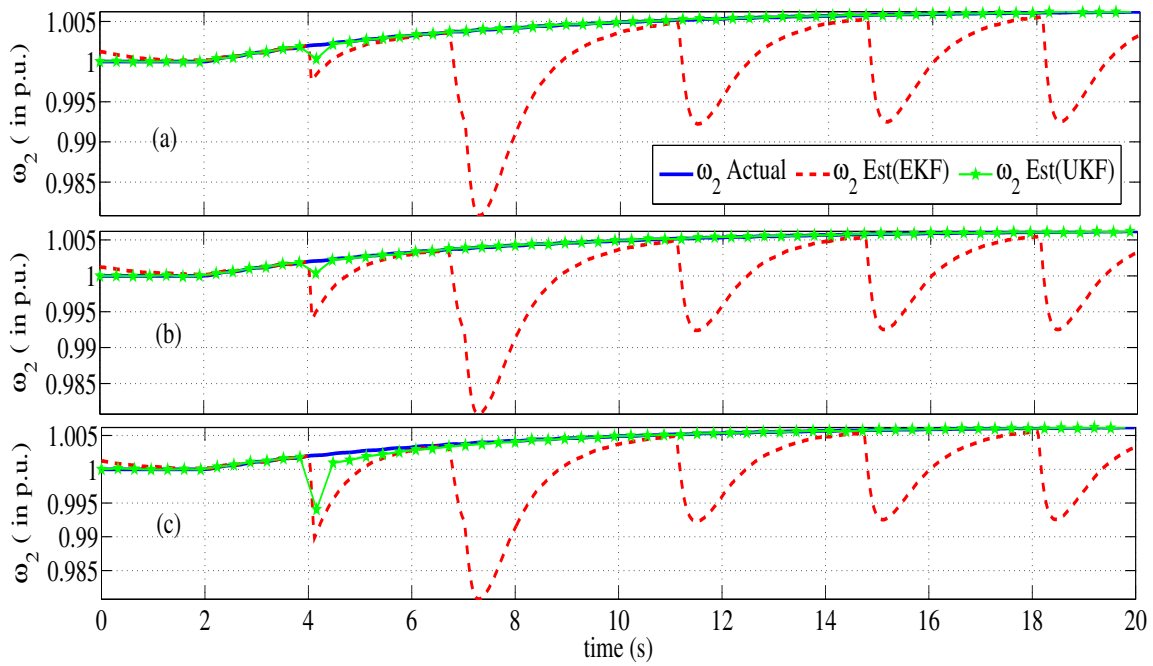


Figure A.6: Performance of EKF and UKF in estimation of variations in speed of generator 2 (ω_2) (IEEE 14 bus system), measurement update interval of 0.02 s and all measurements missing for (a) 3 cycles, (b) 4 cycles and (c) 5 cycles duration

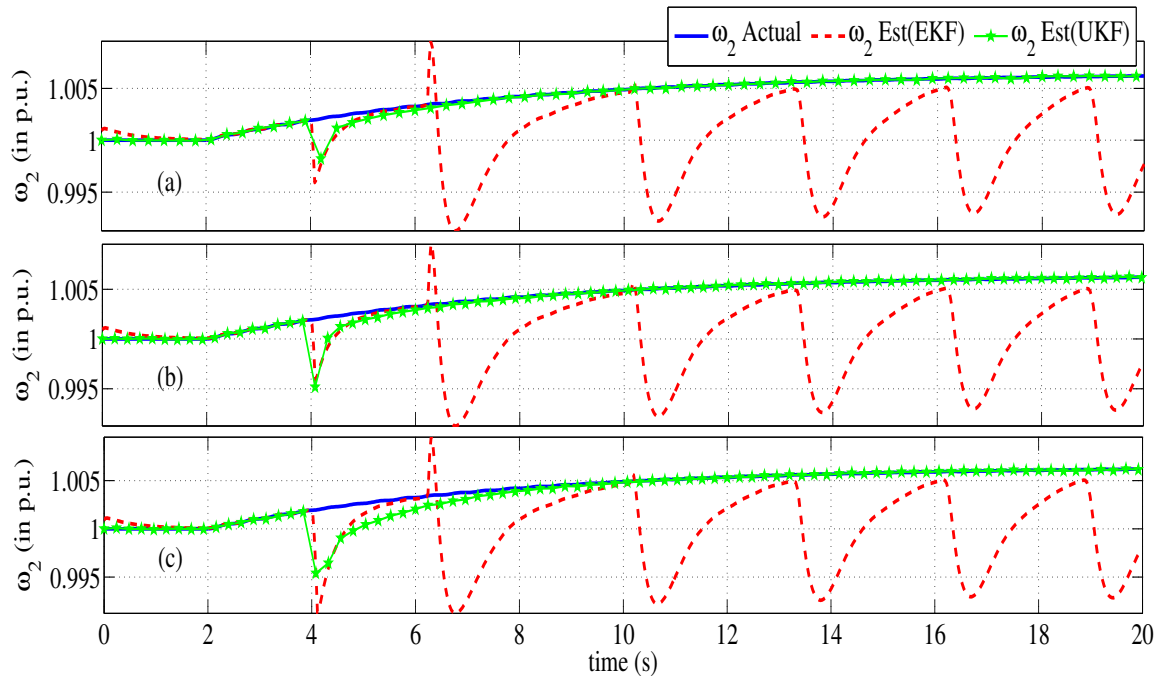


Figure A.7: Performance of EKF and UKF in estimation of variations in speed of generator 2 (ω_2) (IEEE 14 bus system), measurement update interval of 0.03 s and all measurements missing for (a) 3 cycles, (b) 4 cycles and (c) 5 cycles duration

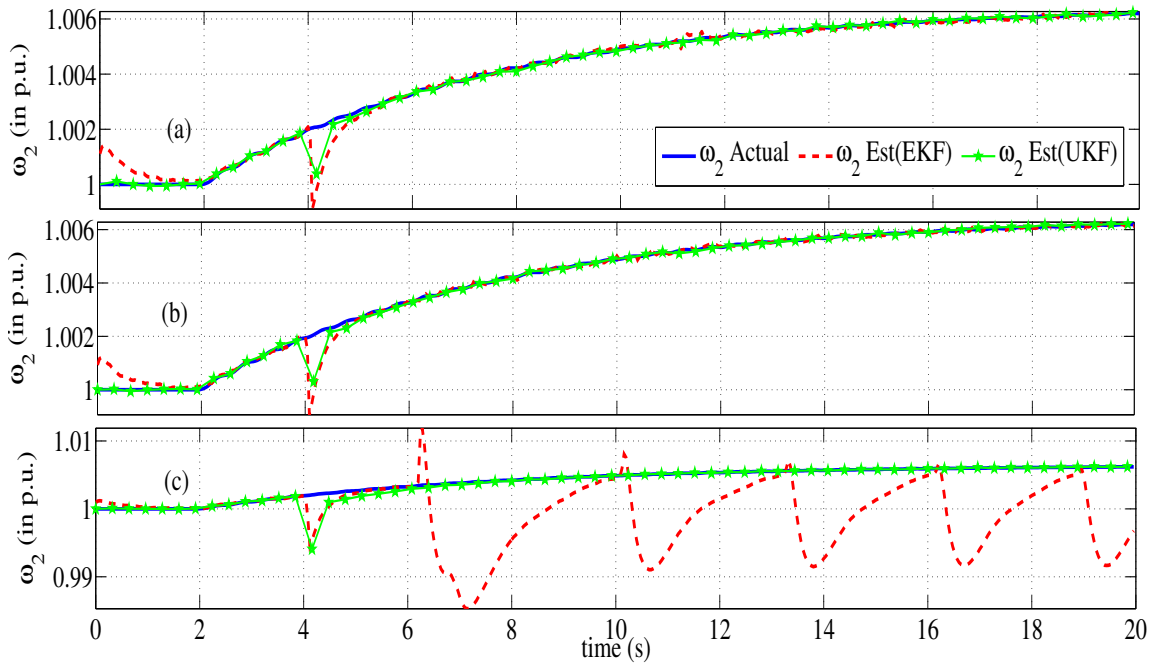


Figure A.8: Performance of EKF and UKF in estimation of variations in speed of generator 2 (ω_2) (IEEE 14 bus system), measurement update interval of 0.04 s and all measurements missing for (a) 3 cycles, (b) 4 cycles and (c) 5 cycles duration

measurements of active and reactive powers, both EKF and UKF algorithm estimates variation in speed of generator 2 (ω_2) accurately for WSCC system and IEEE 14 bus system as shown in Fig. A.9 and Fig. A.10 respectively. With successful estimation of one dynamic state under the condition of partial availability of measurement data, similar result of other dynamics states are not presented here.

A.4 Discussion

A.4.1 Case I – WSCC test system

Ability of EKF and UKF algorithms to estimate dynamic states, post transient condition is observed under the condition of measurement data unavailability. Estimation performance is tested for data unavailability durations of 3, 4 and 5 cycles with measurement data update rates of 50 sa/s, 33 sa/s and 25 sa/s each.

For measurement update rate of 50 sa/s (measurement time interval=0.02 s) as well as for 33 sa/s (measurement time interval 0.03 s), EKF estimator fails to track variation in speed of generator 2 (ω_2) for all three measurement data unavailability

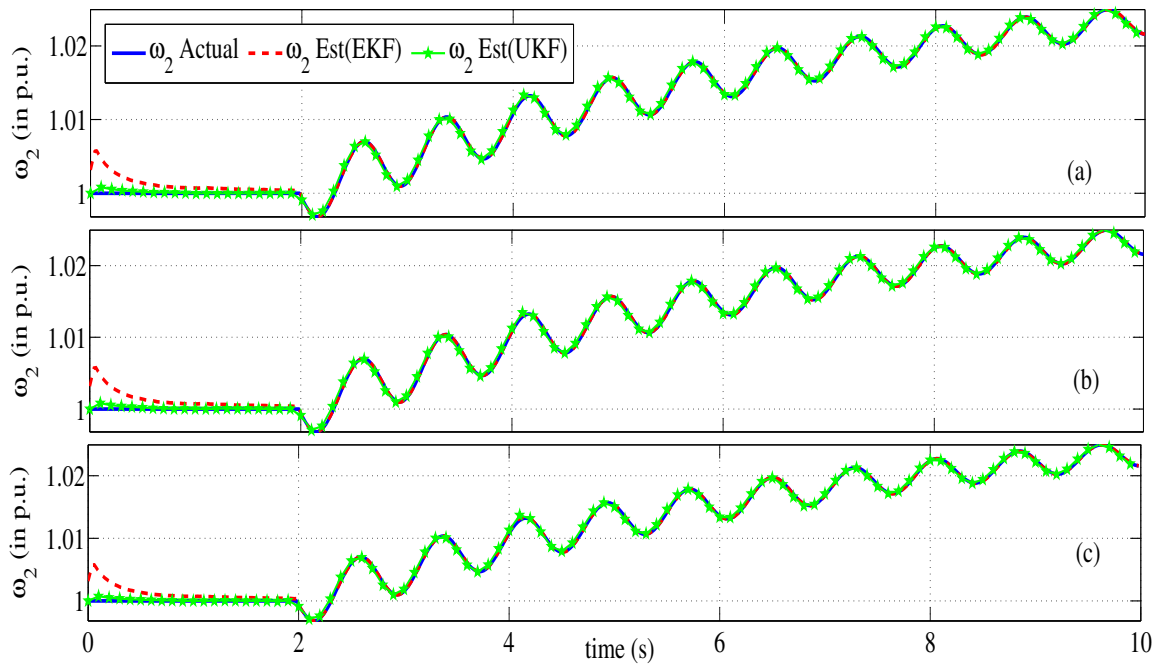


Figure A.9: Performance of EKF and UKF in estimation of variations in speed of generator 2 (ω_2) (WSCC system), measurement update interval of 0.02 s and two measurements missing for (a) 3 cycles, (b) 4 cycles and (c) 5 cycles duration

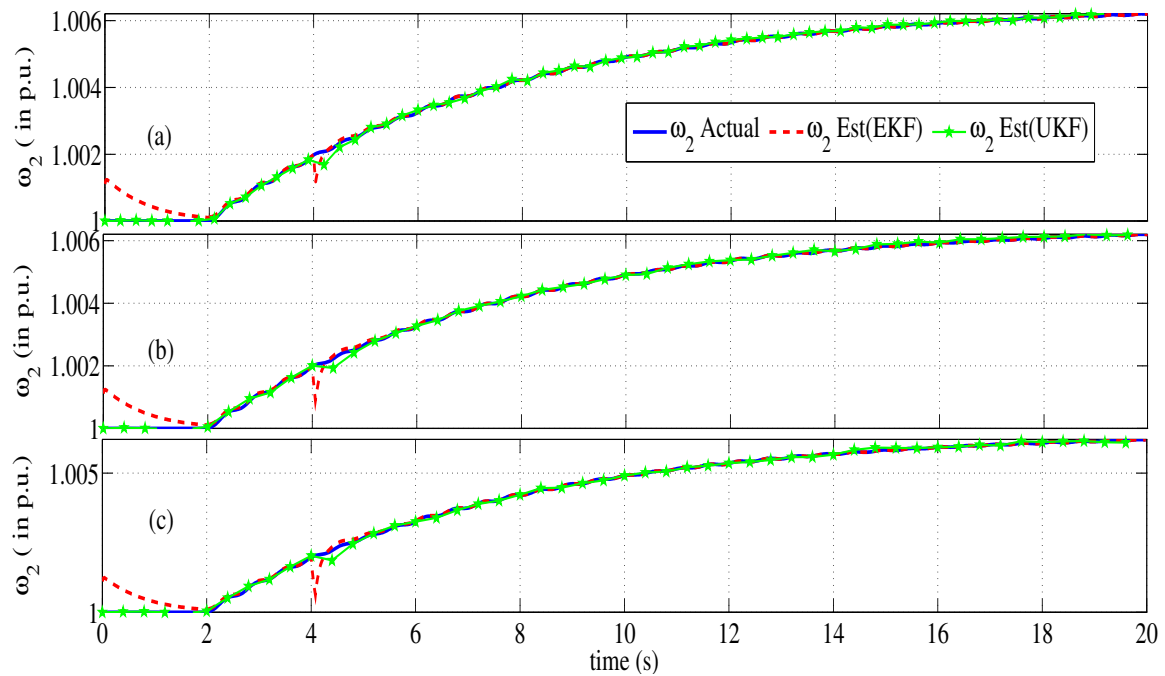


Figure A.10: Performance of EKF and UKF in estimation of variations in speed of generator 2 (ω_2) (IEEE 14 bus system), measurement update interval of 0.02 s and two measurements missing for (a) 3 cycles, (b) 4 cycles and (c) 5 cycles duration

durations i.e. 3 , 4 and 5 cycles as shown in Fig.A.2 and Fig.A.3 respectively. Divergence continues though availability of measurement data resumes. On the contrary, UKF based estimator displays efficient estimation of variations in speed of generator 2 (ω_2) for measurement update rates of 50 sa/s and 33 sa/s under all three measurement data unavailability durations as Figs. A.2-A.3 depict.

Further, in case of measurement update rate of 25 sa/s (measurement update interval 0.04 s), EKF estimation diverges the moment data is lost (for durations of 3 and 4 cycles), but converges as measurement data resumes. The estimation diverges in case of data lost duration of 5 cycles and divergence continues even after measurement data resumption as shown in Fig.A.4. For measurement update interval of 0.04 s, UKF estimates speed of generator 2 (ω_2) with accuracy except a momentary divergence.

Inherent nature of limited linearization and Jacobian matrix calculation in EKF cause sustained divergence once measurement data become unavailable at specific update rate. Derivation of mean and covariance of non-linear measurement functions of power system state using UT contributes to convergence after measurement data unavailability.

A.4.2 Case II – IEEE 14 bus test system

Considering location of fault, results for estimation of variation in speed of generator 2(ω_2) is discussed here in detail. Fig. A.6 and Fig. A.7 show UKF's edge over EKF. For higher measurement update interval (0.04 s), efficient estimation noticed for EKF in case of 3 and 4 cycles data lost duration but divergence observed when data are missing for 5 cycles duration as shown in Fig. A.8. For measurement update rate of 25 sa/s, UKF based estimator accurately estimates variation in speed of generator 2(ω_2) in all three cases as displayed in Fig. A.8.

It has been observed that if measurement data become unavailable for prolonged duration, however such severe condition may arise very rarely, the UKF based estimator shows divergence in case of both the multi-machine systems. Also important to note that, computational time (for 5 cycles measurement data unavailable with measurement update interval of 0.04 s) of EKF based estimator are 0.348217 s and 0.493501 s for WSCC system (total simulation time - 10 s) and IEEE 14 bus system

(total simulation time - 20 s) respectively. With similar simulation conditions, the computation time of UKF based estimator are 0.47624 s and 0.653194 s for WSCC system and IEEE 14 bus system respectively. Computation time is calculated using MATLAB version *2009a* for a computer having 3.1 GHz processor, 32-bit operating system and 4 GB of RAM.

Summary of results, for both systems, is presented in Table A.2.

Table A.2: Comparison of EKF and UKF based estimators' performance for three measurement data unavailable conditions and measurement update time intervals

Measurement data unavailability duration	Measurement data update time interval (s)					
	EKF			UKF		
	0.02 s	0.03 s	0.04 s	0.02 s	0.03 s	0.04 s
3 cycles	<i>X</i>	<i>X</i>	✓	✓	✓	✓
4 cycles	<i>X</i>	<i>X</i>	✓	✓	✓	✓
5 cycles	<i>X</i>	<i>X</i>	<i>X</i>	✓	✓	✓

✓ - Estimation feasible *X* - Estimation diverges

A.5 Conclusions

Abnormal operation or failure of measurement communication devices may cause unavailability of measurement data, either partially or completely. This work has focused on behaviour of Kalman filter based DSE algorithms *viz.* EKF and UKF under the rare condition in which, post to transient condition, all measurement data become unavailable for a few cycles. For EKF based estimator, normally preferred high measurement update rate, can cause divergence in case of measurement data unavailability. Application of EKF as dynamic state estimator in power system demands for trade-off between measurement data missing durations and specific measurement update rate to achieve sustained convergence. On the contrary, results shows UKF

based dynamic state estimator performs better than EKF for all three durations of missing measurement conditions in combination with all three measurement data update rates. Hence, employing UKF based dynamic state estimator is more suitable than EKF to achieve continued convergence in case of infrequent condition of all measurement data unavailability.

Appendix B

WLSE Assisted Load Flow under Bad Measurement Conditions

B.1 Introduction

The state estimation (SE) is very important for having a more secure and economic operation in today's complicated power system. F. C. Schweppe introduced the concept of power system state estimation in the 1970s and employed the weighted least square estimation (WLSE) method to solve the state estimation problem (Schweppe and Wildes). SE determines the best estimate of the real-time power system states *viz.* voltage magnitudes, their angles considering circuit breaker (CB) status, transformer tap positions etc. with the help of latest measurements provided by supervisory control and data acquisition (SCADA) system. The results of SE are then used in different power system operations like network contingency analysis, security enhancement, optimal power flow, transient security analysis and other applications (Schweppe and Rom).

Many contributions to SE have been made (Schweppe). Among many methods employed, the weighted least-squares estimation (WLSE) method was extensively employed (Debs and Larson Grainger, Grainger, and Stevenson). Considering the accuracy of different measuring instruments, relative weights are applied to the measurement quantities in WLSE. Other alternative estimators proposed are the weighted least absolute value (WLAV) estimator to deal with multiple gross errors. The least median of squares estimator (LMS) is another estimator alternative. Despite the

existing wide range of estimators, the WLSE is the most used estimator in power systems for static state estimation(SSE) , due to its simplicity.

Process of load flow in power system significantly depends on accuracy of measurements collected through remote terminal units (RTUs). Traditionally, after load flow, based on its result and subsequent analysis, controlling action is initiated by supervisory control and data acquisition (SCADA) system. There exist a possibility of occurrence of bad measurements in measurement system due to problems in a communication channel, measuring instruments, A/D converters etc. Gross errors or bad measurements, collected by load flow algorithm, can determine erroneous steady state condition of power network, which consequently leads to wrong decision making.

SSE process has the capability to estimate different states at specific instance using measurement data collected at that instance considering quasi-static nature of power network. Bad data detection algorithm can be used to identify gross errors in power systems and consequently SSE algorithm is used to estimate accurate states using remaining measurement. This makes the results of the SSE process reliable than the SCADA raw data (Falcao and Arias). To deal with unexpected violations caused by bad measurements, a number of methods have been proposed in the literature (Smith et al. Baldick et al.).

Presented work depict effect of one bad measurement data on load flow. Work envelopes WLSE method for state estimation after removing bad data using χ^2 algorithm. Further, use of estimated true states is suggested for monitoring and control in place of erroneous load flow results.

B.2 Brief on WLSE and bad data detection

SSE is essential for the observation and control of modern power system. The aim of SSE is to obtain the best possible values of the bus voltage magnitudes and angles by processing the available network measurement similar to load flow analysis. Before any security assessment undertaken or control actions performed, a reliable estimate of the existing state of the system is useful for the better decision making process. The inputs to the conventional power-flow program are confined to the P, Q injections at load buses and P, V values at voltage-controlled buses. If even one of these inputs is unavailable, the conventional power flow solution cannot be obtained. Moreover,

gross errors in one or more of the input quantities can diverge the expected power-flow results. In practice, other conveniently measured quantities such as P , Q line flows are available, but they cannot be used in conventional power-flow calculations. These limitations can be overcome by removal of bad data followed by state estimation based on WLSE calculations. The process involves removal of imperfect measurement data and then process of estimating the system states is based on a statistical criterion that estimates the true value of the state variables to minimize or maximize the selected criterion

B.2.1 Method of WLSE for static state estimation

Details of WLSE method and bad data detection is comprehensively covered in (Grainger, Grainger, and Stevenson). Hence, excerpts of both procedures are presented here. Let \mathbf{x} is a vector of n state variables ($x_1, x_2, x_3 \dots x_n$) and \mathbf{z} is another vector of m measurements ($z_1, z_2, z_3 \dots z_m$) and both are related as

$$\mathbf{z} = \mathbf{H}\mathbf{x} + \mathbf{e} \quad (\text{B.1})$$

where \mathbf{H} is a measurement Jacobian matrix of dimension ($m \times n$) and \mathbf{e} is a zero-mean random Gaussian error vector having the same dimension as \mathbf{z} which is ($m \times 1$). In (B.1), \mathbf{x} represents vector of true state variables, which is normally not known. Hence, estimation of state is required, which fulfills the criterion of

$$\hat{\mathbf{z}} = \mathbf{H}\hat{\mathbf{x}} \quad (\text{B.2})$$

where $\hat{\mathbf{x}}$ is accurate estimate of desired state. $\hat{\mathbf{z}}$ represents accurate estimated measurements derived using $\hat{\mathbf{x}}$. Based on error estimate $\hat{\mathbf{e}}$ is given by,

$$\hat{\mathbf{e}} = \mathbf{z} - \hat{\mathbf{z}} \quad (\text{B.3})$$

Finally, equation to obtain static state estimate of desired variables using WLSE is given by (B.4),

$$\hat{\mathbf{x}} = (\mathbf{H}^T \mathbf{W} \mathbf{H})^{-1} \mathbf{H}^T \mathbf{W} \mathbf{z} \quad (\text{B.4})$$

where, \mathbf{W} is a real symmetric diagonal weighting matrix of dimension ($m \times m$). Gain matrix \mathbf{G} is given by $\mathbf{H}^T \mathbf{W} \mathbf{H}$. It allows giving different weights to measurements depending on their accuracy and it is inversely proportional to error covariance matrix.

B.2.2 Bad data detection

When the system model is correct and the measurement data are accurate, there is a good reason to accept the state estimates calculated by the WLSE based estimator. But if a measurement is grossly erroneous or bad, it should be detected and then identified so that it can be removed from the estimator calculations. One or more of the measured data can be affected by malfunctioning of either the measuring instruments or the data transmission system or both. Even when care is taken to ensure accuracy, unavoidable random noise and/or outliers enters into the measurement process to distort more or less the physical results of states.

The weighted least-squares estimates $\hat{\mathbf{x}}_i$ at any i^{th} measurement vector $\hat{\mathbf{z}}_i$ is given using (B.4) as,

$$\hat{\mathbf{x}}_i = (\mathbf{H}_i^T \mathbf{W} \mathbf{H}_i)^{-1} \mathbf{H}_i^T \mathbf{W} \hat{\mathbf{z}}_i \quad (\text{B.5})$$

where i indicate all quantities at i^{th} measurements. Estimated value of the measurements $\hat{\mathbf{z}}_i$ can be calculated by using the obtained value of $\hat{\mathbf{x}}_i$ and then estimated error can be determined as in the (B.2). All the measurement errors are assumed to be Gaussian random variables. Objective function for bad data detection is evaluated as shown in (B.6).

$$\hat{f} = \sum_{i=1}^m W_i \hat{e}_i^2 = \sum_{i=1}^m \hat{e}_i^2 / \sigma_i^2 \quad (\text{B.6})$$

where σ represents standard deviation. Measurement errors and hence, measurements are considered Gaussian in nature. Method of χ^2 test is used to identify bad measurements.

According to the degrees of freedom $k = m - n$ (where $m =$ number of measurements and $n =$ number of states) and a confidence level α , critical value $\chi_{k,\alpha}^2$ is obtained which plays pivotal role in bad data identification. After obtaining value of objective function \hat{f} , the conditions to check bad data in measurement are given by,

- a. if $\hat{f} < \chi_{k,\alpha}^2$ i.e. no bad data exist in measurements.
- b. if $\hat{f} > \chi_{k,\alpha}^2$ i.e. bad data do exist in measurements.

If condition #2 exist, then it becomes imperative to find bad measurement among all measurement variables. After such detection, the measurement with largest standardized error e corresponding to each measurement is calculated using (B.7).

$$e_i = \frac{z_i - \hat{z}_i}{\sqrt{R'_{ii}}} \quad (\text{B.7})$$

where $\sqrt{(R'_{ii})}$ is standard gaussian random variable. The measurement with largest standardized error is omitted as bad measurement. Again the same procedure of omission is repeated till either new value of \hat{f} which satisfies $\hat{f} < \chi_{k,\alpha}^2$ - the *chi-square* test or the value of degree of freedom remains $k > 2$, whichever is earlier. In practical power system applications, the number of degrees of freedom is large (because number of measurements are higher than states to be estimated), which allows discarding a group of measurements corresponding to the largest standardized residuals.

B.3 Case study

To present a case, standard WSCC 3-generator 9-bus test system (Fig. A.1) is considered. Under steady state condition, load flow is carried out using conventional Newton-Raphson method. Result of the load flow is as displayed in (Fig. A.1) (Anderson and Fouad). Generally, load flow is aimed to deliver voltage magnitude and angle at all buses, especially at load buses. Adopting a conventional approach, voltage angles and voltage magnitudes of load bus #5, bus # 6 and bus # 8 *viz.* δ_5 , δ_6 , δ_8 , V_5 , V_6 and V_8 are taken as the state variables respectively, alike to load flow results. Known quantities of PV buses and PQ buses *viz.* real power injection at bus #2 , #3, #5, #6 and #8 *viz.* P_2, P_3, P_5, P_6, P_8 ; reactive power injection at bus #5, #6 and #8 *viz.* Q_5, Q_6, Q_8 are taken as measurements. This work proposes use of WLSE based estimation results for two purposes, one for verifying accuracy of load flow results and in case of bad measurements employing results of WLSE for control purpose instead of erroneous load flow results. Hence, having considered the knowledge of voltage magnitudes at bus #5, # 6 and #8 *viz.* V_5, V_6 and V_8 are taken as measurement inputs as well for the state estimation process. So, 11 measurements and 6 state variables have been taken into consideration. WSCC system simulation and data collection is performed using Power System Analysis toolbox (PSAT) environment.

Presented work focuses on effect of bad measurement i.e. measurement with gross error on load flow. Hence, to simulate the same, few measurements are intentionally corrupted with bad data at random time intervals. Considering the fact that

nature of error is random either in terms of magnitude as well as time of occurrence, real power measurement P_2 from bus # 2 is corrupted with random error of 0.37 p.u. at an instant of $t= 0.2$ s ; real power measurement P_5 from bus #5 is corrupted with gross error of 0.2 p.u. in at an instant of $t= 0.5$ s and corruption of bad data with magnitude of 0.2 p.u. is simulated to reactive power measurement Q_6 from bus #6 at an instant of $t= 0.8$ s . To observe the effect of this bad measurement on load flow, using Newton-Raphson method, load flow has been done for WSCC system. Then after results are presented of WLSE following bad data detection. Flowchart depicting methodology adopted is shown in Fig. B.1.

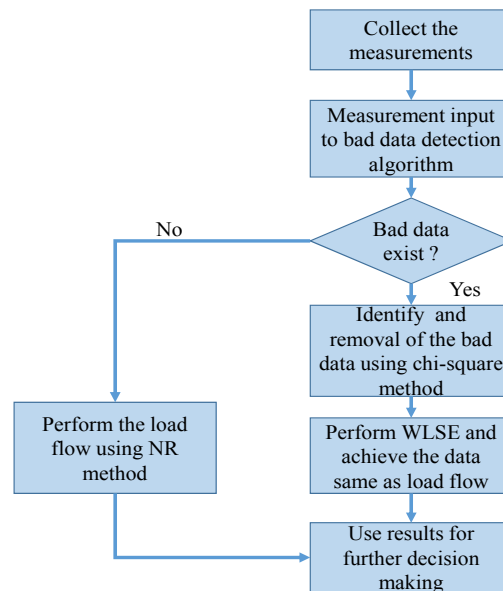


Figure B.1: Algorithm for WLSE backed load flow

B.4 Results and discussion

Without any bad data in measurement results of load flow and state estimation using WLSE is achieved. Result shown in Table B.1 validates use of both the approach to achieve voltage magnitude and angles in steady state.

To simulate the effect measurement with bad data, first case is presented where active power measurement from bus #2 is corrupted with gross error of 0.37 p.u. With the error of 0.37 p.u. in P_2 , the state variables output from load flow and SE

Table B.1: Results of WLSE and Load flow under without bad measurements

State variable	Load flow result	WLSE result
	(1)	(2)
δ_5	-0.0696	-0.0698
δ_6	-0.0644	-0.0645
δ_8	0.0127	0.124
V_5	0.9965	0.9954
V_6	1.0127	1.0124
V_8	1.0159	1.0159

are shown in Table B.2. As shown in column #1 of Table B.2, one bad measurement (in P_2) results in all erroneous output data of load flow. Effect of measurement error of 0.37 p.u. can be seen explicitly on load flow as shown in column #2 of Table B.2. Discussing about just one output variable of δ_5 is given by load flow with bad data is -0.0321 rad. against its original value of -0.0694 rad. .

To overcome effect of bad data in measurement, result are obtained using methodology shown in Fig. B.1. With proposed method, measurement with bad data - P_2 is detected using χ^2 test and using remaining measurement (i.e. 10 measurements out of 11) value of all load flow results are obtained. Results achieved are shown in Table B.3. As shown in column # 2, WLSE approach faithfully removes measurement with bad data and provide accurate result alike to load flow without any bad measurements. It is important to notice that even one bad measurement can affect the overall load flow results and hence, affecting the value of important decisive parameters of load flow i.e. bus voltage magnitude and angle. This can be overcome using standby results obtained using WLSE approach with bad data detection algorithm.

To validate the method, second case is considered when bad measurement or outlier exist in the measurement of reactive power delivery of bus # 6. Reactive power

Table B.2: Comparative results of WLSE and Load flow under static condition when P_2 is corrupted with 0.37 p.u. of error

State variable	Load flow result with bad data	WLSE result
	(1)	(2)
δ_5	-0.0321	-0.0698
δ_6	-0.0339	-0.0645
δ_8	0.0790	0.124
V_5	0.9989	0.9954
V_6	1.0083	1.0124
V_8	1.0133	1.0159

measurement - Q_6 is corrupted by error of 0.2 p.u. Effect of this bad measurement is shown in column # 1 of Table B.3.

Results displayed in column # 2 of Table B.3 endorses the capability of WLSE method to remove bad measurement using χ^2 test and it estimates accurate states analogous to load flow result without any bad measurement. Hence, results shown in Table B.2-B.3 proves that once bad measurement is detected, instead of load flow results, result obtained using WLSE can be used for monitoring of steady state condition of power network and further decision making process for control.

B.5 Conclusion

Two cases of load flow for WSSC 3-generator 9-bus test system are presented under the effect of bad measurement data of active and reactive power. One bad measurement results in a significant divergence of overall load flow with erroneous output results. Hence, output variables of load flow are taken as states to be estimated using WLSE method. WLSE method gives accurate results of voltage magnitude and angle after detection, identification and removal of bad measurements. In condition

Table B.3: Comparative results of WLSE and Load flow under static condition when Q_6 is corrupted with 0.2 p.u. of error

State variable	Load flow result with bad data	WLSE result
	(1)	(2)
δ_5	-0.0674	-0.0698
δ_6	-0.0691	-0.0645
δ_8	0.0133	0.124
V_5	1.0154	0.9954
V_6	1.0807	1.0124
V_8	1.0272	1.0159

of measurements corrupted with bad data, results obtained using load flow can be replaced with results obtained through SSE , after removal of bad measurement data for better monitoring and control in the power system. However, presented work considers one bad measurement at a time and keeping open the possibility to analyze the performance of WLSE under the condition of more than one bad measurements.

Appendix C

Extended Kalman Filter(EKF) Algorithm

Generic representation of non-linear system is as shown in (C.1) (Simon),

$$\dot{\mathbf{x}} = \frac{d\mathbf{x}}{dt} = f(\mathbf{x}, \mathbf{u}, \mathbf{w}) \quad (\text{C.1})$$

\mathbf{f} is vector of non-linear function, \mathbf{x} represents state vector, \mathbf{u} shows input vector and \mathbf{w} random white Gaussian process noise vector.

Measurement function having inherent non-linearity is represented as,

$$\mathbf{y} = \mathbf{h}(\mathbf{x}, \mathbf{u}, \mathbf{v}) \quad (\text{C.2})$$

where \mathbf{h} is vector of non-linear function and \mathbf{v} is random white Gaussian measurement noise vector. The error (\mathbf{e}) between actual measurement (\mathbf{y}) and estimated measurement ($\hat{\mathbf{y}}$) obtained using state \mathbf{x} is given in (C.3),

$$\mathbf{e} = \mathbf{y} - \hat{\mathbf{y}} \quad (\text{C.3})$$

Elaborative mathematical treatment for EKF is covered in literature (Ghahremani and Kamwa, “Dynamic State Estimation in Power System by Applying the Extended Kalman Filter With Unknown Inputs to Phasor Measurements” Wang, Gao, and Meliopoulos Huang, Schneider, and Nieplocha Simon Bishop and Welch), hence not presented in detail. However, some significant mathematical steps of EKF algorithm are enumerated here briefly.

Extended Kalman Filter

Step 1: State and measurement equations shown in (C.1) and (C.2) can be represented in discretized form as :

$$\begin{aligned}\mathbf{x}_k &= \mathbf{x}_{k-1} + f(\mathbf{x}_{k-1}, \mathbf{u}_{k-1}, \mathbf{w}_{k-1}) \cdot \nabla t \\ \mathbf{y}_k &= h(\mathbf{x}_k, \mathbf{u}_k, \mathbf{v}_k) \\ \mathbf{w}_k &\approx (0, \mathbf{Q}) \text{ and } \mathbf{v} \approx (0, \mathbf{R})\end{aligned}\tag{C.4}$$

where \mathbf{Q} is process noise covariance matrix and \mathbf{R} is covariance matrix for measurement noise.

Step 2: Initialization of filter is given by,

$$\begin{aligned}\hat{\mathbf{x}}_0^+ &= E(\mathbf{x}_0) \\ \mathbf{P}_0^+ &= E[(\mathbf{x} - \hat{\mathbf{x}}_0^+)(\mathbf{x} - \hat{\mathbf{x}}_0^+)^T]\end{aligned}\tag{C.5}$$

where $\hat{\mathbf{x}}_0^+$ is initial estimate of state matrix and \mathbf{P}_0^+ represents initial state error covariance matrix. E is expected value.

Step 3: Transition matrices for state as well as measurement vector, necessary for time update, are,

$$\mathbf{F}_{k-1} = \left(\frac{\partial \mathbf{f}_{k-1}}{\partial \mathbf{x}} \right)_{\hat{\mathbf{x}}_{k-1}^+} \text{ and } \mathbf{L}_{k-1} = \left(\frac{\partial \mathbf{f}_{k-1}}{\partial \mathbf{w}} \right)_{\hat{\mathbf{x}}_{k-1}^+}\tag{C.6}$$

\mathbf{F}_{k-1} and \mathbf{L}_{k-1} are the Jacobian of partial derivative of \mathbf{f} with respect to \mathbf{x} and \mathbf{w} , respectively. $\hat{\mathbf{x}}_{k-1}^+$ represents *posteriori* state estimate at instant $k - 1$.

Time update and measurement update steps repeated for every instant k are given below.

Step 4: Time update - Time update of state and error covariance matrix is done by,

$$\begin{aligned}\mathbf{P}_k^- &= \mathbf{F}_{k-1} \mathbf{P}_{k-1}^+ \mathbf{F}_{k-1}^T + \mathbf{L}_{k-1} \mathbf{Q}_{k-1}^+ \mathbf{L}_{k-1}^T \\ \hat{\mathbf{x}}_k^- &= f(\hat{\mathbf{x}}_{k-1}^+, \mathbf{u}_{k-1}, 0)\end{aligned}\tag{C.7}$$

Step 5: Transition matrices for measurement update are,

$$\mathbf{H}_k = \left(\frac{\partial \mathbf{h}_k}{\partial \mathbf{x}} \right)_{\hat{\mathbf{x}}_k^-} \text{ and } \mathbf{M}_k = \left(\frac{\partial \mathbf{h}_k}{\partial \mathbf{v}} \right)_{\hat{\mathbf{x}}_k^-}\tag{C.8}$$

\mathbf{H}_k and \mathbf{M}_k are Jacobian of partial derivatives of \mathbf{h} with respect to \mathbf{x} and \mathbf{v} , respectively.

Step 6: Measurement Update - Measurement update of state and state error covariance matrix are done by ,

$$\begin{aligned}
 \mathbf{K}_k &= \mathbf{P}_k^- \mathbf{H}_k^T (\mathbf{H}_k \mathbf{P}_k^- \mathbf{H}_k^T + \mathbf{M}_k \mathbf{R}_k \mathbf{M}_k^T)^{-1} \\
 \hat{\mathbf{x}}_k^+ &= \hat{\mathbf{x}}_k^- + \mathbf{K}_k (\mathbf{y}_k - h(\mathbf{x}_k, \mathbf{v}_k)) \\
 \mathbf{P}_k^+ &= (\mathbf{I} - \mathbf{K}_k \mathbf{H}_k) \mathbf{P}_k^-
 \end{aligned} \tag{C.9}$$

where \mathbf{K}_k is Kalman gain, $\hat{\mathbf{x}}_k^+$ is vector of updated state estimate and \mathbf{P}_k^+ is updated state error covariance matrix.

Appendix D

Unscented Kalman Filter (UKF)

Algorithm

UKF is based on concept of UT which was first proposed in (Julier, Uhlmann, and Durrant-Whyte). Although mathematical formulation and description of UKF based on UT is described in literature (Julier, Uhlmann, and Durrant-Whyte Valverde and Terzija Wang, Gao, and Meliopoulos Simon), only necessary mathematical steps for UKF based DSE are reproduced here for completeness.

First two steps, mathematical presentation and initialization of filter (*i.e.* states and state error covariance matrix) are done in same manner as shown in **Appendix C** - (C.1) to (C.3). In case of UKF, time update and measurement update are carried out as described below :

Step 3 : Time update - State vector and state error covariance matrix use following steps for transition from one time instant to another.

(a) Sigma points $\tilde{\mathbf{x}}^{(r)}$ (where $r = 1, 2, 3 \dots 2c$) are derived as shown in (D.1).

$$\begin{aligned}\tilde{\mathbf{x}}^{(r1)} &= \left(\sqrt{(r + \lambda) \mathbf{P}_{k-1}^+} \right)_{r1}^T \\ \tilde{\mathbf{x}}^{(r1+c)} &= - \left(\sqrt{(r + \lambda) \mathbf{P}_{k-1}^+} \right)_{r1}^T\end{aligned}\tag{D.1}$$

$r1 = 1, 2, 3, \dots c$

The variable $2c$ represents total number of sigma points. The parameter λ is a scaling parameter and is defined by $\lambda = \alpha^2(a + \kappa) - a$. Value of α , that determines the spread of the sigma points around $\hat{\mathbf{x}}_{k-1}^+$, lies between $10^{-4} \leq \alpha \leq 1$ and second

scaling parameter $\kappa = 3 - c$ or $\kappa = 0$ is preferred. Square root matrix can be approximated by $\mathbf{P} = \mathbf{A}\mathbf{A}^T$, where \mathbf{A} is lower triangular matrix obtained from the Cholesky factorization of \mathbf{P} (Julier, Uhlmann, and Durrant-Whyte Valverde and Terzija).

Addition of sigma points $\tilde{\mathbf{x}}^{(r)}$ to recently updated *posteriori* estimate $\hat{\mathbf{x}}_{k-1}^+$ results in $\hat{\mathbf{x}}_{k-1}^r$ sigma points as shown in (D.2).

$$\hat{\mathbf{x}}_{k-1}^r = \hat{\mathbf{x}}_{k-1}^+ + \tilde{\mathbf{x}}^{(r)} \quad (\text{D.2})$$

These sigma points are necessary for transition from $(k-1)^{th}$ instant to k^{th} instant.

(b) Non-linear function f is used to transform these sigma points to get vector $\hat{\mathbf{x}}_k^r$ from $\hat{\mathbf{x}}_{k-1}^r$, so

$$\hat{\mathbf{x}}_k^{(r)} = f(\hat{\mathbf{x}}_{k-1}^{(r)}, \mathbf{u}_k, t_k) \quad (\text{D.3})$$

\mathbf{u}_k is driving function and t_k is time at instant k .

(c) Obtain *priori* estimate $\hat{\mathbf{x}}_k^-$, combine all $\hat{\mathbf{x}}_k^r$ using following equation,

$$\hat{\mathbf{x}}_k^- = \frac{1}{2c} \sum_{r=1}^{2c} \hat{\mathbf{x}}_k^{(r)} \quad (\text{D.4})$$

(d) To evaluate *priori* state error covariance considering effect of process noise \mathbf{Q}_{k-1} using

$$\hat{\mathbf{P}}_k^- = \frac{1}{2c} \sum_{r=1}^{2c} (\hat{\mathbf{x}}_k^{(r)} - \hat{\mathbf{x}}_k^-)(\hat{\mathbf{x}}_k^{(r)} - \hat{\mathbf{x}}_k^-)^T + \mathbf{Q}_{k-1} \quad (\text{D.5})$$

Step 4 : Measurement Update

(a) Utilize latest time updated $\hat{\mathbf{x}}_k^-$ and $\hat{\mathbf{P}}_k^-$ to find optimum sigma points $\hat{\mathbf{x}}_k^{(r)}$ with help of following equations,

$$\begin{aligned} \hat{\mathbf{x}}_k^r &= \hat{\mathbf{x}}_k^- + \tilde{\mathbf{x}}^{(r)} \\ \tilde{\mathbf{x}}^{(r1)} &= \left(\sqrt{(n+\lambda)\mathbf{P}_k^-} \right)_{r1}^T \\ \tilde{\mathbf{x}}^{(r1+c)} &= - \left(\sqrt{(n+\lambda)\mathbf{P}_k^-} \right)_{r1}^T \end{aligned} \quad (\text{D.6})$$

(b) Similar to time update step, for measurement update non-linear function h is used to transform these sigma points to get vector $\hat{\mathbf{y}}_k^r$ from $\hat{\mathbf{x}}_k^r$ such that

$$\hat{\mathbf{y}}_k^{(r)} = h(\hat{\mathbf{x}}_k^{(r)}, t_k) \quad (\text{D.7})$$

(c) Obtain predicted measurement $\hat{\mathbf{y}}_k$ by combining all $\hat{\mathbf{y}}_k^r$ using following equation,

$$\hat{\mathbf{y}}_k = \frac{1}{2c} \sum_{r=1}^{2c} \hat{\mathbf{y}}_k^{(r)} \quad (\text{D.8})$$

(d) To derive measurement error covariance with effect of measurement noise \mathbf{R}_k at instant k using

$$\hat{\mathbf{P}}_y^- = \frac{1}{2c} \sum_{i=1}^{2c} (\hat{\mathbf{y}}_k^{(i)} - \hat{\mathbf{y}}_k)(\hat{\mathbf{y}}_k^{(i)} - \hat{\mathbf{y}}_k)^T + \mathbf{R}_k \quad (\text{D.9})$$

(e) Find cross covariance $\hat{\mathbf{P}}_{xy}^-$ with the help of,

$$\hat{\mathbf{P}}_{xy}^- = \frac{1}{2a} \sum_{r=1}^{2c} (\hat{\mathbf{x}}_k^{(r)} - \hat{\mathbf{x}}_k^-)(\hat{\mathbf{y}}_k^{(r)} - \hat{\mathbf{y}}_k)^T \quad (\text{D.10})$$

(f) Finally updated state estimate $\hat{\mathbf{x}}_k^+$ and state error covariance \mathbf{P}_k^+ are achieved using (D.11).

$$\begin{aligned} \mathbf{K}_k &= \mathbf{P}_{xy}^- \mathbf{P}_y^- \\ \hat{\mathbf{x}}_k^+ &= \hat{\mathbf{x}}_k^- + \mathbf{K}_k(\mathbf{y}_k - \hat{\mathbf{y}}_k) \\ \mathbf{P}_k^+ &= \hat{\mathbf{P}}_k^- - (\mathbf{K}_k \mathbf{P}_y \mathbf{K}_k^T) \end{aligned} \quad (\text{D.11})$$

where \mathbf{K}_k is Kalman gain and $\mathbf{y}_k = h(\mathbf{x}_k, \mathbf{v}_k)$.

Appendix E

Improved Coalesced Model of Synchronous Generator and DFIG

In Chapter # 2 coalesced model of synchronous generator and DFIG is presented using SMIB system. Unification of SG and DFIG is presented using current source model. Base model of DFIG is used to derive the current source state space model of SG with minor modifications as suggested in Table 2.1. Results of MATLAB/Simulink platform is compared with results of similar model created on standard software platform PSCAD/EMTDC during transient condition. Except minor differences due to limited order of modelling, resemblance between results of both platforms endorses unification approach (Fig. 2.2).

Further improvement in modelling is done to proposed model. Using suggested current source state space model approach for DFIG and SG, modified WSCC 3-generator 9-bus system is created. To emulate higher penetration of wind energy sources, modification to standard WSCC system is done as suggested in Section 3.1.2, Chapter # 3. State space model implementation on MATLAB/Simulink platform is simulated as shown in Fig. 3.3, Chapter # 3. Analogous model of modified WSCC system is created on PSCAD/EMTDC platform as presented in Fig. 3.4.

The highlighting feature of improved proposed model is consideration fault MVA and fault feeding capacity of each generator during fault. Each generator is feeding fault according to its fault feeding capacity considering fault MVA and by observ-

ing typical X/R ratio during fault duration. With proposed improvement, during transient condition (3-phase to ground fault at bus #7 and fault clearance by auto reclosure), variation in output currents i_{abc} , i_{ds} and i_{qs} is observed for DFIG (Gen.# 2). Change in output currents is observed on both platforms *viz.* MATLAB and PSCAD as presented in Fig. E.1. The intermediate transient condition for period between 9.8 s and after 10.2 s for Gen.# 2 is presented for both the platforms.

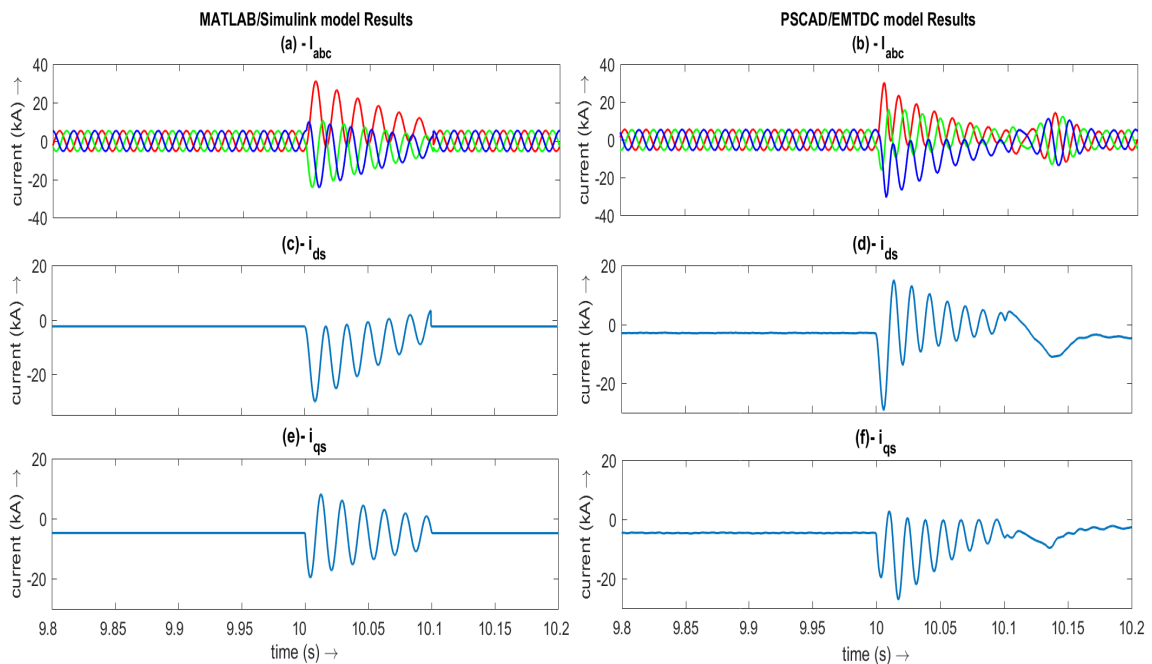


Figure E.1: Instantaneous currents of DFIG (Gen.# 2) (a)–(b) i_{abc} , (b)–(c) stator direct axis current – i_{ds} , (c)–(d) stator quadrature axis current – i_{qs}

To approve unification and current source model representation of SG, in second case DFIG (Gen.#2) is replaced with SG of similar rating, created using current source state space model, on MATLAB/Simulink platform. Alike to previous case, same WSCC model with similar rating of generators is simulated on PSCAD/EMTDC platform with SG as shown in Fig. E.2.

Results of both platforms are observed for the case of WSCC with SG as Gen.# 2. Comparative plot for i_{abc} , i_{ds} and i_{qs} is presented in Fig. E.3.

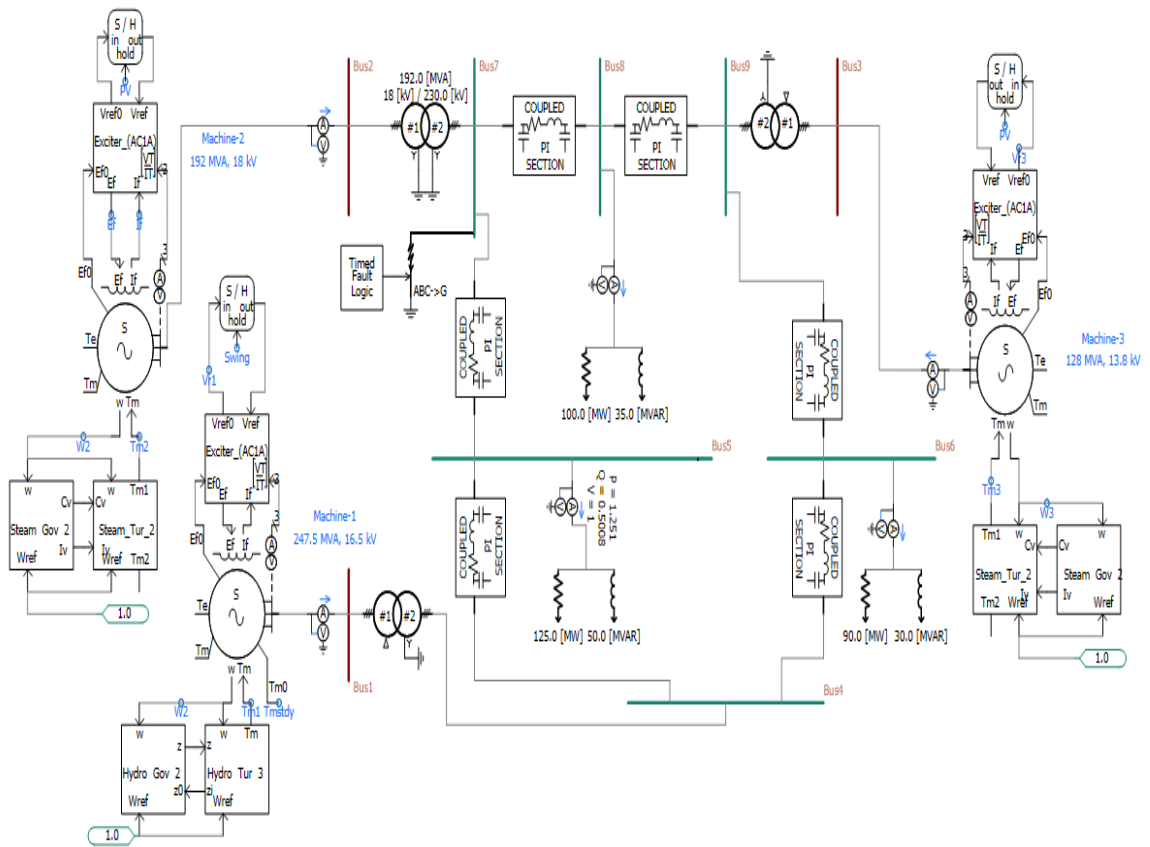


Figure E.2: WSCC 3-gen. 9-bus system with SG (Gen. #2) on PSCAD/EMTDC platform

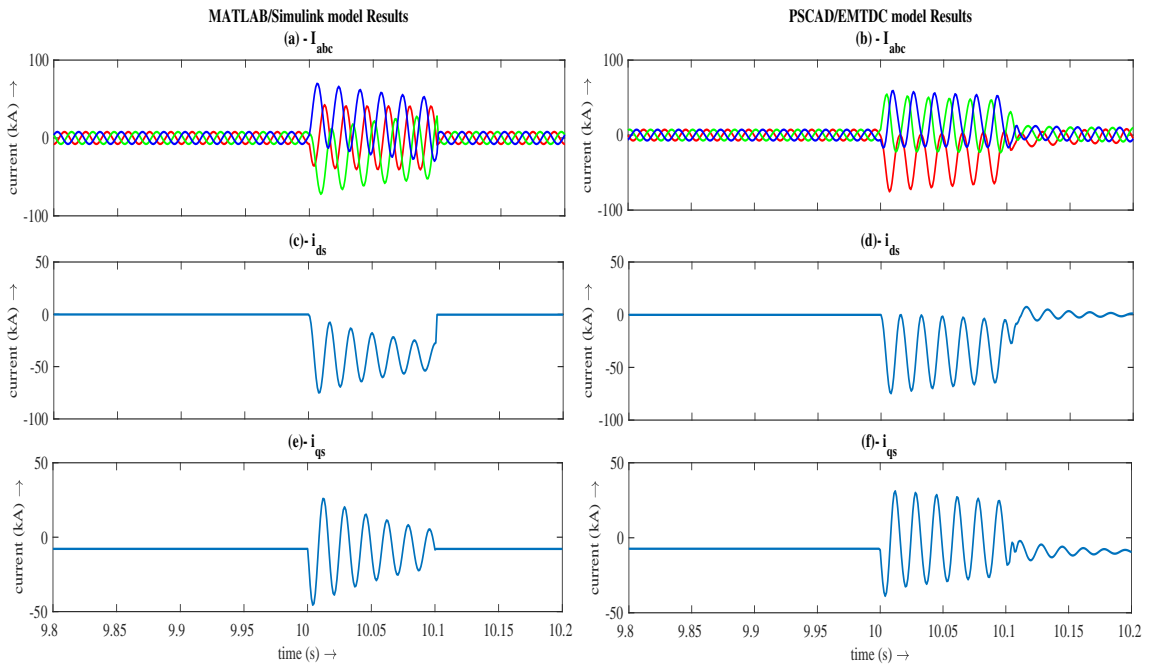


Figure E.3: Instantaneous currents of SG (Gen.# 2) (a)–(b) i_{abc} , (b)–(c) stator direct axis current – i_{ds} , (c)–(d) stator quadrature axis current – i_{qs}

Results shown in Fig.E.1 and Fig. E.3 enforces the model unification approach using current source model. Modification employed considering fault MVA and fault feeding capacity approves model unification approach with thrust.

List of Publications

Journal/ Conference Publications

- **Dishang D. Trivedi** and Santosh C. Vora. *Performance Assessment of EKF and UKF based Dynamic State Estimators for Intermittent Measurement Data in Power System*, International Journal of Advanced Research in Engineering and Technology (IJARET) - IAEME, Volume 8, Issue 2, March 2017, pp. 24-41.
- **Dishang D. Trivedi**, Urmil B. Bhatt and Santosh C. Vora. *Application of EKF Based Dynamic State Estimation for DFIG Rotor Power Control under Faulty Current Sensor Measurement*, International Journal of Advanced Research in Engineering and Technology - IEAME, Volume 8, Issue 4, August 2017, pp. 95-110.
- **Dishang D. Trivedi** and Santosh C. Vora. *A Review of Dynamic State Estimation Techniques in Power System using Synchrophasors As One Aspect of Smart Grid*, at National conference on Power system protection and automation , Society of Power Engineers, School of Technology, Pandit Deendayal Petrouelum University, 7-8 June 2013, pp.128–134 .
- **Dishang D. Trivedi**, Santosh C. Vora and Meera Karamta. *Analysis of Extended Kalman Filter based Dynamic State Estimator's performance under Anomalous Measurement Conditions for Power System*, Proceedings of IEEE-International Conference on Electrical Power and Energy Systems (ICEPES-2016), 14-16 December 2016, pp. 557-563.
- Jigar Patel, Dhaivat Desai, Vaibhav Patel, **Dishang D. Trivedi** and Santosh C. Vora. *Analysing Effect of Bad Measurement Data on Load Flow and State*

Estimation in power system, at Nirma University International Conference on Engineering, Proceeding of NUiCONE 2015, 26-28 November 2015, pp. 1-6.

Journal(Manuscript under review)

- **Dishang D. Trivedi**, Urmil B. Bhatt, Chintan R. Mehta and Santosh C. Vora. *EKF based Centralized Concurrent Dynamic State Estimation in Multi-Machine Power System Employing Current Source Models of DFIG and Synchronous Generators*, Electrical Power System Research (Elsevier).(Submitted on September 2, 2017 and 2nd revision status is “under review” since March 28, 2018)

Journal(Research paper under modification)

- Urmil B. Bhatt,**Dishang D. Trivedi**, Chintan R. Mehta and Santosh C. Vora. *A Unified State Model of Synchronous and Asynchronous Generators*, Journal of Renewable energy (Elsevier).

Works Cited

- Abdelhafidh, Moualdia, et al. “Modeling and control of a wind power conversion system based on the double-fed asynchronous generator.” *International Journal of Renewable Energy Research (IJRER)* 2.2 (2012): 300–306.
- Abdelrahem, M., C. Hackl, and R. Kennel. “Application of extended Kalman filter to parameter estimation of doubly-fed induction generators in variable-speed wind turbine systems.” *2015 International Conference on Clean Electrical Power (ICCEP)*. 2015. 226–233.
- Aminifar, F., et al. “Power System Dynamic State Estimation With Synchronized Phasor Measurements.” *IEEE Transactions on Instrumentation and Measurement* 63.2 (2014): 352–363.
- Anderson, Paul M and Aziz A Fouad. *Power system control and stability*. John Wiley & Sons, 2008.
- Baldick, R., et al. “Implementing nonquadratic objective functions for state estimation and bad data rejection.” *IEEE Transactions on Power Systems* 12.1 (1997): 376–382.
- BELFEDAL, Cheikh, Tayeb ALLAOUI, Belkacem BELABBAS, et al. “Speed-Sensorless DFIG Wind Turbine for Power Optimization Using Fuzzy Sliding Mode Observer.” *International Journal of Renewable Energy Research (IJRER)* 7.2 (2017): 613–621.
- Bila, Cem. “Power system dynamic state estimation and load modelling.” Diss. 2014.
- Bishop, Gary and Greg Welch. “An introduction to the kalman filter.” *Proc of SIG-GRAPH, Course 8.27599-23175* (2001): 41.
- Blood, E. A., B. H. Krogh, and M. D. Ilic. “Electric power system static state estimation through Kalman filtering and load forecasting.” *2008 IEEE Power and*

Energy Society General Meeting - Conversion and Delivery of Electrical Energy in the 21st Century. 2008. 1–6.

Bourdoulis, M. K. and A. T. Alexandridis. “Direct Power Control of DFIG Wind Systems Based on Nonlinear Modeling and Analysis.” *IEEE Journal of Emerging and Selected Topics in Power Electronics* 2.4 (2014): 764–775.

Brown, M., et al. “Characterizing and quantifying noise in PMU data.” *2016 IEEE Power and Energy Society General Meeting (PESGM)*. 2016. 1–5.

CERTS. “Advanced concepts FAQ.” *Measurement*. 2013. <https://www.phasor-rtdms.com/phasorconcepts/phasor_adv_faq.htm>.

Chen, C., et al. “PMU Uncertainty Quantification in Voltage Stability Analysis.” *IEEE Transactions on Power Systems* 30.4 (2015): 2196–2197.

Christie, R. “Power system test archive.” *University of Washington* (1999).

Da Silva, A. M. Leite, M. B. Do Coutto Filho, and J. F. de Queiroz. “State forecasting in electric power systems.” *IEE Proceedings C - Generation, Transmission and Distribution* 130.5 (1983): 237–244.

Debs, A. S. and R. E. Larson. “A Dynamic Estimator for Tracking the State of a Power System.” *IEEE Transactions on Power Apparatus and Systems* PAS-89.7 (1970): 1670–1678.

Deshmukh, S., B. Natarajan, and A. Pahwa. “Stochastic state estimation for smart grids in the presence of intermittent measurements.” *2012 IEEE Latin-America Conference on Communications*. 2012. 1–6.

Ekanayake, J.B., L. Holdsworth, and N. Jenkins. “Comparison of 5th order and 3rd order machine models for doubly fed induction generator (DFIG) wind turbines.” *Electric Power Systems Research* 67.3 (2003): 207–215. <<http://www.sciencedirect.com/science/article/pii/S0378779603001093>>.

EL-Hagry, M. T. and M. N. Eskander. “Estimation of Rotor Voltage Vector on the Double Excited Induction Machine used in WECS.” *Electric Machines & Power Systems* 25.8 (1997): 839–850. <<http://dx.doi.org/10.1080/07313569708955779>>.

Falcao, D. M. and M. A. Arias. “State estimation and observability analysis based on echelon forms of the linearized measurement models.” *IEEE Transactions on Power Systems* 9.2 (1994): 979–987.

- Fan, Lingling and Yasser Wehbe. “Extended Kalman filtering based real-time dynamic state and parameter estimation using PMU data.” *Electric Power Systems Research* 103.Supplement C (2013): 168 –177. <<http://www.sciencedirect.com/science/article/pii/S0378779613001442>>.
- Fan, Rui, et al. “Dynamic state estimation and parameter calibration of a DFIG using the ensemble Kalman filter.” *2015 IEEE Power Energy Society General Meeting*. 2015. 1–5.
- Feijo, Andrs, Jos Cidrs, and Camilo Carrillo. “A third order model for the doubly-fed induction machine.” *Electric Power Systems Research* 56.2 (2000): 121. <<http://www.sciencedirect.com/science/article/pii/S0378779600001036>>.
- Force, U-CPSOT. “Final report on the august 14th blackout in the united states and canada.” *Department of Energy and National Resources Canada* (2004).
- Ghahremani, E. and I. Kamwa. “Dynamic State Estimation in Power System by Applying the Extended Kalman Filter With Unknown Inputs to Phasor Measurements.” *IEEE Transactions on Power Systems* 26.4 (2011): 2556–2566.
- . “Local and Wide-Area PMU-Based Decentralized Dynamic State Estimation in Multi-Machine Power Systems.” *IEEE Transactions on Power Systems* 31.1 (2016): 547–562.
- Giaourakis, Dimitrios G, Athanasios N Safacas, and Savvas N Tsotoulidis. “Dynamic behaviour of a wind energy conversion system including doubly-fed induction generator in fault conditions.” *International Journal of Renewable Energy Research (IJRER)* 2.2 (2012): 227–235.
- Grainger, John J Stevenson, William D John J Grainger, and William D Stevenson. *Power system analysis*. 1994.
- Gu, C. and P. Jirutitijaroen. “Dynamic State Estimation Under Communication Failure Using Kriging Based Bus Load Forecasting.” *IEEE Transactions on Power Systems* 30.6 (2015): 2831–2840.
- Huang, Miao, Wenyuan Li, and Wei Yan. “Estimating parameters of synchronous generators using square-root unscented Kalman filter.” *Electric Power Systems Research* 80.9 (2010): 1137 –1144. <<http://www.sciencedirect.com/science/article/pii/S0378779610000660>>.

- Huang, Z., et al. “Estimating power system dynamic states using extended Kalman Filter.” *2014 IEEE PES General Meeting — Conference Exposition*. 2014. 1–5.
- Huang, Z., et al. “Generator dynamic model validation and parameter calibration using phasor measurements at the point of connection.” *IEEE Transactions on Power Systems* 28.2 (2013): 1939–1949.
- Huang, Zhenyu, K. Schneider, and J. Nieplocha. “Feasibility studies of applying Kalman Filter techniques to power system dynamic state estimation.” *2007 International Power Engineering Conference (IPEC 2007)*. 2007. 376–382.
- “IEEE Recommended Practice for Monitoring Electric Power Quality.” *IEEE Std 1159-2009 (Revision of IEEE Std 1159-1995)* (2009): c1–81.
- Jain, A. and N. R. Shivakumar. “Impact of PMU in dynamic state estimation of power systems.” *2008 40th North American Power Symposium*. 2008. 1–8.
- . “Power system tracking and dynamic state estimation.” *2009 IEEE/PES Power Systems Conference and Exposition*. 2009. 1–8.
- Jiang, Hao, et al. “Comparisons on state space models of doubly fed induction generators (DFIG) for power system research.” *2016 IEEE PES Asia-Pacific Power and Energy Engineering Conference (APPEEC)*. 2016. 895–900.
- Julier, S. J., J. K. Uhlmann, and H. F. Durrant-Whyte. “A new approach for filtering nonlinear systems.” *American Control Conference, Proceedings of the 1995*. 1995. 1628–1632 vol.3.
- Karimi, S., et al. “Current Sensor Fault-Tolerant Control for WECS With DFIG.” *IEEE Transactions on Industrial Electronics* 56.11 (2009): 4660–4670.
- Khedher, Adel, Nihel Khemiri, and Mohamed Faouzi Mimouni. “Wind energy conversion system using DFIG controlled by backstepping and sliding mode strategies.” *International journal of renewable energy research* 2.3 (2012): 421–430.
- Kim, D. J., Y. H. Moon, and H. K. Nam. “A New Simplified Doubly Fed Induction Generator Model for Transient Stability Studies.” *IEEE Transactions on Energy Conversion* 30.3 (2015): 1030–1042.
- Kumar, Ashwani, Biswarup Das, and Jaydev Sharma. “Robust dynamic state estimation of power system harmonics.” *International Journal of Electrical Power & Energy Systems* 28.1 (2006): 65 –74. <<http://www.sciencedirect.com/science/article/pii/S0142061505001298>>.

- Kundur, Prabha, Neal J Balu, and Mark G Lauby. *Power system stability and control*. Vol. 7. McGraw-hill New York, 1994.
- Li, H., et al. “Fault-tolerant control for current sensors of doubly fed induction generators based on an improved fault detection method.” *Measurement* 47.Supplement C (2014): 929 –937. <<http://www.sciencedirect.com/science/article/pii/S0263224113005204>>.
- Malakar, M. K., P. Tripathy, and S. Krishnaswamy. “State estimation of DFIG using an Extended Kalman Filter with an augmented state model.” *2014 Eighteenth National Power Systems Conference (NPSC)*. 2014. 1–6.
- Mandal, J. K., A. K. Sinha, and L. Roy. “Incorporating nonlinearities of measurement function in power system dynamic state estimation.” *IEE Proceedings - Generation, Transmission and Distribution* 142.3 (1995): 289–296.
- Meliopoulos, A. P. S., et al. “Dynamic State Estimation-Based Protection: Status and Promise.” *IEEE Transactions on Power Delivery* 32.1 (2017): 320–330.
- Miller, W. and J. Lewis. “Dynamic state estimation in power systems.” *IEEE Transactions on Automatic Control* 16.6 (1971): 841–846.
- Mishra, Y., et al. “Small-Signal Stability Analysis of a DFIG-Based Wind Power System Under Different Modes of Operation.” *IEEE Transactions on Energy Conversion* 24.4 (2009): 972–982.
- Nguyen, Phuong H., et al. “Dynamic state estimation for distribution networks with renewable energy integration.” *International journal of smart grid and clean energy* 2.3 (2013): 307315.
- Nishiya, K., J. Hasegawa, and T. Koike. “Dynamic state estimation including anomaly detection and identification for power systems.” *IEE Proceedings C - Generation, Transmission and Distribution* 129.5 (1982): 192–198.
- Pai, MA and Dheeman Chatterjee. *Computer techniques in power system analysis*. McGraw-Hill Education (India), 2014.
- Rothenhagen, K. and F. W. Fuchs. “Doubly Fed Induction Generator Model-Based Sensor Fault Detection and Control Loop Reconfiguration.” *IEEE Transactions on Industrial Electronics* 56.10 (2009): 4229–4238.

- S. Yu, Realization of state. “Realization of State-Estimation-Based DFIG Wind Turbine Control Design in Hybrid Power Systems Using Stochastic Filtering Approaches.” *IEEE Transactions on Industrial Informatics* 12.3 (2016): 1084–1092.
- S. Yu, State estimation of. “State Estimation of Doubly Fed Induction Generator Wind Turbine in Complex Power Systems.” *IEEE Transactions on Power Systems* 31.6 (2016): 4935–4944.
- Sauer, Peter W, Mangalore A Pai, and Joe H Chow. *Power System Dynamics and Stability: With Synchrophasor Measurement and Power System Toolbox*. John Wiley & Sons, 2017.
- Schweppe, F. C. “Power System Static-State Estimation, Part III: Implementation.” *IEEE Transactions on Power Apparatus and Systems* PAS-89.1 (1970): 130–135.
- Schweppe, F. C. and D. B. Rom. “Power System Static-State Estimation, Part II: Approximate Model.” *IEEE Transactions on Power Apparatus and Systems* PAS-89.1 (1970): 125–130.
- Schweppe, F. C. and J. Wildes. “Power System Static-State Estimation, Part I: Exact Model.” *IEEE Transactions on Power Apparatus and Systems* PAS-89.1 (1970): 120–125.
- Senjyu, T., et al. “Transient current analysis of induction generator for wind power generating system.” *IEEE/PES Transmission and Distribution Conference and Exhibition*. 2002. 1647–1652 vol.3.
- Shahriari, Sayyed Ali Akbar, et al. “Dynamic state estimation of a doubly fed induction generator based on a comprehensive nonlinear model.” *Simulation Modelling Practice and Theory* 69.Supplement C (2016): 92 –112. <<http://www.sciencedirect.com/science/article/pii/S1569190X15302185>>.
- Shi, D., D. J. Tylavsky, and N. Logic. “An Adaptive Method for Detection and Correction of Errors in PMU Measurements.” *IEEE Transactions on Smart Grid* 3.4 (2012): 1575–1583.
- Simon, Dan. *Optimal state estimation : Kalman, H [infinity] and nonlinear approaches*. Hoboken, N.J: Wiley-Interscience, 2006.
- Singh, A. K. and B. C. Pal. “Decentralized Dynamic State Estimation in Power Systems Using Unscented Transformation.” *IEEE Transactions on Power Systems* 29.2 (2014): 794–804.

- Singh, Bharat and S.N. Singh. "Wind Power Interconnection into the Power System: A Review of Grid Code Requirements." *The Electricity Journal* 22.5 (2009): 54–63. <<http://www.sciencedirect.com/science/article/pii/S1040619009001249>>.
- Sinha, A. K. and J. K. Mandal. "Hierarchical dynamic state estimator using ANN-based dynamic load prediction." *IEE Proceedings - Generation, Transmission and Distribution* 146.6 (1999): 541–549.
- Smith, M. M., et al. "Robust algorithm for state estimation in electrical networks." *IEE Proceedings C - Generation, Transmission and Distribution* 138.4 (1991): 283–288.
- Subudhi, B., et al. "A comparative study on different power system frequency estimation techniques." *International Journal of Automation and Control* 3.2-3 (2009): 202–215. <<http://www.inderscienceonline.com/doi/abs/10.1504/IJAAC.2009.025242>>.
- Tebianian, Hamed and Benjamin Jeyasurya. "Dynamic state estimation in power systems: Modeling, and challenges." *Electric Power Systems Research* 121.Supplement C (2015): 109–114. <<http://www.sciencedirect.com/science/article/pii/S0378779614004441>>.
- Tripathy, P., S. C. Srivastava, and S. N. Singh. "A Divide-by-Difference-Filter Based Algorithm for Estimation of Generator Rotor Angle Utilizing Synchrophasor Measurements." *IEEE Transactions on Instrumentation and Measurement* 59.6 (2010): 1562–1570.
- Ugalde-Loo, C. E., J. B. Ekanayake, and N. Jenkins. "State-Space Modeling of Wind Turbine Generators for Power System Studies." *IEEE Transactions on Industry Applications* 49.1 (2013): 223–232.
- Vahidnia, Arash, et al. "Dynamic equivalent state estimation for multi-area power systems with synchronized phasor measurement units." *Electric Power Systems Research* 96.Supplement C (2013): 170–176. <<http://www.sciencedirect.com/science/article/pii/S0378779612003392>>.
- Valverde, G. and V. Terzija. "Unscented kalman filter for power system dynamic state estimation." *IET Generation, Transmission Distribution* 5.1 (2011): 29–37.

- Wang, S., W. Gao, and A. P. S. Meliopoulos. “An Alternative Method for Power System Dynamic State Estimation Based on Unscented Transform.” *IEEE Transactions on Power Systems* 27.2 (2012): 942–950.
- Wu, F., et al. “Decentralized Nonlinear Control of Wind Turbine With Doubly Fed Induction Generator.” *IEEE Transactions on Power Systems* 23.2 (2008): 613–621.
- Wu, F., et al. “Small signal stability analysis and optimal control of a wind turbine with doubly fed induction generator.” *IET Generation, Transmission Distribution* 1.5 (2007): 751–760.
- Yang, L., et al. “Advanced Control Strategy of DFIG Wind Turbines for Power System Fault Ride Through.” *IEEE Transactions on Power Systems* 27.2 (2012): 713–722.
- Yang, L., et al. “Oscillatory Stability and Eigenvalue Sensitivity Analysis of A DFIG Wind Turbine System.” *IEEE Transactions on Energy Conversion* 26.1 (2011): 328–339.
- Zhou, N. “A Cross-Coherence Method for Detecting Oscillations.” *IEEE Transactions on Power Systems* 31.1 (2016): 623–631.
- Zhou, N., et al. “Dynamic State Estimation of a Synchronous Machine Using PMU Data: A Comparative Study.” *IEEE Transactions on Smart Grid* 6.1 (2015): 450–460.